ulm university universität ulm

Increasing the Bandwidth Efficiency of OFDM-MFSK

DISSERTATION

zur Erlangung des akademischen Grades eines

DOKTOR-INGENIEURS
(DR.-ING.)

der Fakultät für Ingenieurwissenschaften
und Informatik der Universität Ulm

von

EVA DOROTHEA PEIKER-FEIL
AUS REUTLINGEN

Gutachter:	Prof. Dr.-Ing. Jürgen Lindner
	Prof. Dr.-Ing. Andreas Czylwik
Amtierende Dekanin:	Prof. Dr. phil. Tina Seufert

Ulm, 12. Dezember 2014

To Valentina,
Christa,
Karl-Heinz,
Veronika
and Amelie.

And to each of whom I owe more,
than I can possibly express.

Acknowledgements

The work, presented within this dissertation, contains the results of most of the research I did during my years at the Institute of Information Technology and at the Institute of Communications Engineering at Ulm University. Many people have contributed to my dissertation - directly or indirectly - and therefore I would like to thank them.

Thank you Prof. Lindner for the opportunity to do my thesis under your supervision and trusting in my abilities. Thank you for giving me the freedom I needed to work and for your experience in guiding me through my research work. Thank you for all the interesting discussions and your always constructive feedback, your advice and your support.

Thank you Prof. Czylwik for acting as second examiner of my dissertation.

Dr. Werner G. Teich, I thank you for a very good time at the institute with lots of interesting experiences. Thank you for always having time for discussions, your continuous support and contributions to my work, your advice, for proofreading all my publications and for proofreading my complete thesis.

Thank you George Yammine for starting your personal adventure in science with me! It was a great pleasure for me, that you first worked as a HiWi

with me together and that I was allowed to supervise your outstanding master thesis. Thank you for all our good discussions, tea breaks, proofreading my thesis and the time together at the institute. All the best for your own dissertation.

I also would like to thank all my other colleagues for always having a good time together at the institute, for interesting discussions, for their feedback, for being room mates, for good breaks, for help, when there were questions, just to mention a few of the good things. Thank you Mohamad Mostafa and Thanawat Thiasiriphet, Matthias Wetz, Doris Yacoub, Zoran Utkovski, Alexander Schmitt, Petra-Maria Strauß, Alexander Linduska, Christian Pietsch, Rui Zhan, Florian Nothdurft, Stefan Ultes, Ksenya Zablotskaya, Sergey Zablotskiy, Antonia Wachter-Zeh, Alex Zeh, Susanne Sparrer, Mostafa Mohamed and all the other ones. And thank you Werner Birkle and Werner Hack.

I would also like to thank all the students, who did their diploma thesis, master thesis or their Studienarbeit with me.

Thank you all my friends for understanding during and supporting me the last years. Special thanks to you, Verena and your family, for always being there and your open ear. Special thanks to you, Jochen, for being friend and mentor.

Heartfelt thanks to you, Veronika and Amelie for being always on my side and for the good times together. Thank you Freddy, for always kidding around with Valentina!

To Mom and Dad - heartfelt thanks and deep gratitude for all your long-lasting support and being with me. Thank you so much for taking care of my daughter Valentina.

Finally, thank you my dear Valentina!

Eva Peiker
January 2015

Contents

Chapter 1

Introduction

STARTING with the publication of Hochwald and Marzetta [19], noncoherent communication based on subspaces has become a topic of interest in the recent years. These transmission schemes use subspaces for transmission and are commonly discussed in the context of MIMO (multiple-input multiple-output). They offer the potential to be detected without any channel state information in the receiver, i.e. noncoherent detection is possible. This benefit is useful, if the channel is fast time-variant and frequency selective. Amongst others, Hochwald and Marzetta, Zheng and Tse and Utkovski in [19], [47], and [41] made proposals in the context of MIMO for transmission methods based on subspaces.

OFDM-MFSK (orthogonal frequency division multiplexing M-ary frequency shift keying) and its multitone variant (OFDM multitone FSK), proposed by Wetz et al. in [45], [44] and by Linduska et al. in [25], can also be detected noncoherently in the receiver. Moreover, the combination of OFDM and MFSK offers in the case of fast time-varying frequency selective fading channels the advantage of a very robust transmission scheme. OFDM can cope with the frequency selective behaviour of the channel, whereas the FSK part can be detected without the need of any knowledge of the channel. However, the drawback of OFDM-MFSK is its bad bandwidth efficiency.

We show within this thesis, that there exists a close connection between the noncoherent communication based on subspaces in the MIMO context and noncoherent OFDM-MFSK and its multitone variant. The first central point of this thesis is to work out this connection between both types of noncoherent communication and to show, that OFDM-MFSK and its multitone variant can be regarded as a special case of a transmission based on subspaces. Besides a better theoretical understanding and a tight connection to the definition of spaces in the mathematical sense, this new point of view for OFDM-MFSK and its multitone variant offers the possibility to improve the bandwidth efficiency remarkably. In general, the subspace based transmissions make use of subspaces of the same dimension. In contrast to this, we show for OFDM-MFSK, that it is possible to use the available total space in a more efficient way. We combine subspaces of different dimensions. This approach allows us to increase the bandwidth efficiency to approach the upper bound of 1 $\frac{\text{bit/s}}{\text{Hz}}$.

On top of the new combined MFSK alphabet, we propose channel coding with extended mapping and an iterative receiver (see [17] and [8]) to gain one extra bit, which can be used for either increasing the data rate or the redundancy used for channel coding. For the extended mapping, we compare two possible schemes: symmetric extended mapping and non-symmetric extended mapping. For symmetric mapping, for each transmit "symbol" of the combined alphabet there are two possible bit labels leading to ambiguity. Contrary to this, for non-symmetric mapping for the new combined FSK alphabet, it is possible to reduce the ambiguity.

The outline of this thesis is as follows: In Chapter 2, a brief introduction to the fundamentals needed for this thesis is given. This includes the mathematical description of the OFDM transmission model, followed by a brief description of the channel models of interest, the Rayleigh block fading channel and the Rayleigh frequency selective fading channel. We present our transmission model of interest, OFDM-MFSK and its multitone variant and we shortly address its noncoherent detection part. This is followed by the introduction of the coded transmission model. Afterwards an outlook to the capacity of multipath fading channels, as proposed by Telatar in [38], is given and we relate it directly to OFDM-MFSK. We describe the idea of a noncoherent transmission based on subspaces, as proposed by Hochwald and Marzetta in [19] and briefly explain the maximum-likelihood (ML) detection rule, which is derived from a matrix variate normal distribution.

Chapter 3 contains our derivation of the connection of how OFDM-MFSK and its multitone variant can be regarded as a special case of a noncoherent communication based on subspaces. The vector-valued transmission model for OFDM-MFSK is adapted to the matrix-valued transmission model, which is common for the subspace based transmission methods. With the ability to describe OFDM-MFSK and its multitone variant as a special case of noncoherent communication based on subspaces, we are able to develop the idea of how to combine subspaces of different dimensions. The combination of subspaces of different dimensions for OFDM-MFSK and its multitone variant allows us to use the total available mathematical space in a more efficient way. We analyze, that this implicates an increase of the bandwidth efficiency of OFDM-MFSK in general and name the resulting system OFDM-COM-N/MFSK (OFDM combined MFSK). We derive the ML matrix variate probability density function (PDF) for the Rayleigh block fading channel and the Rayleigh frequency selective fading channel. Where possible, we simplify it to an ML detection rule. We discuss the distance criterion, provide a mapping algorithm for Gray mapping and define an upper bound, up to which dimension the subspaces should be combined. To complete this chapter, we explain how to go back from the subspaces to the FSK vectors.

In Chapter 4, detailed simulation results for an uncoded transmission over

the AWGN channel, the Rayleigh block fading channel, and the Rayleigh frequency selective fading channel are discussed. We also show simulation results for a coded transmission over the Rayleigh block fading channel, using an iterative receiver.

In Chapter 5, we address the possibility of extended mapping, to gain an additional bit for increasing the data rate or redundancy for our new proposed transmission scheme OFDM-COM-N/MFSK. Besides the existing approach of extended mapping, we propose a non-symmetric mapping scheme for the combined FSK alphabet, which offers the advantage, that the ambiguity for the mapping can be reduced.

A list of frequently used acronyms, operators and symbols is given at the end of this thesis. All entries of this list are introduced at their first appearance. General notations, used throughout this thesis, are the following: Vectors and matrices are written in bold lower and upper case letters, e.g. $\mathbf{x}$ and $\mathbf{X}$. ^{T} and ^{H} denote the transpose and the hermitian of a vector or a matrix and * denotes the complex conjugate of a scalar.

The main contributions and key ideas of this thesis are contained in Chapter 3, 4 and 5. Parts of them have already been published in [29], [28] and [46].

Chapter 2

Fundamentals

A BASIC model for a digital transmission is shown in Fig. 2.1, where a digital source $\mathcal{Q}$, produces a bit sequence $q(k)$, which is transmitted to the digital sink $\mathcal{S}$. Within the block COD, the bit sequence $q(k)$ is encoded with a channel code and interleaved, resulting in $c(k)$, which is passed to the digital modulation device (MOD). Within this block, the coded data sequence is mapped to the transmit sequence $s(k)$ with a dirac-delta sampler. After an interpolation lowpass filter (IP-LP) the continuous-time transmit signal $s(t)$ is obtained and transmitted over the channel. On the receiving side, the received signal $g(t)$ is obtained and band limited by an anti-aliasing lowpass filter (AA-LP). After dirac-delta sampling, the digital received sequence $g(k)$

is handed over to the detector (DET), resulting in the received bit sequence $\hat{q}(k)$ at the digital sink $\mathcal{S}$.
In case of orthogonal frequency division multiplexing (OFDM) [42], the block MOD and DET contain the OFDM modulation and demodulation.

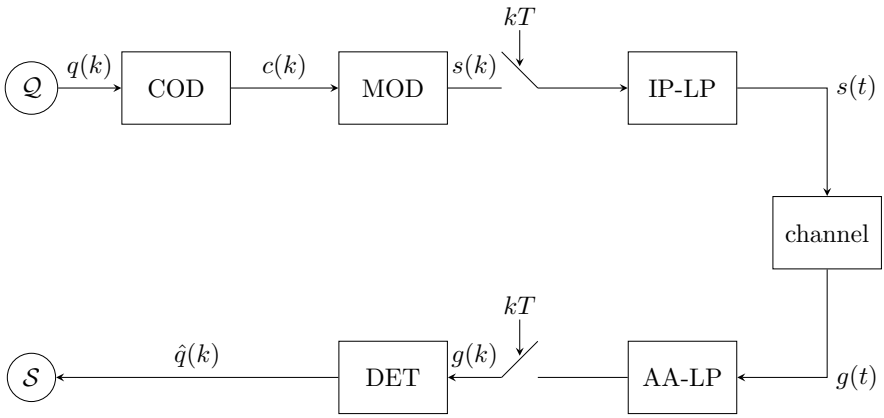

Figure 2.1: Digital transmission model [24]. $\mathcal{Q}$: digital source, COD: encoding and interleaving, MOD: digital modulation device, kT: dirac delta sampling, IP-LP: interpolation lowpass filter, AA-LP: anti-aliasing lowpass filter, DET: detector, $\mathcal{S}$: digital sink.

In the following, the fundamentals for this thesis are discussed. After introducing the vector-valued OFDM transmission model [11], [24], the definition of the assumed channel models is given. We introduce OFDM-MFSK and its multitone variant, as proposed by Wetz et al. in [45] and [44] and by Linduska et al. in [25]. This also includes the maximum-likelihood detection rule for the AWGN (additive white Gaussian noise) channel, the Rayleigh block fading channel and the transmission model for bit-interleaved coded modulation with iterative detection. In the following a brief introduction to the capacity of frequency selective fading channels is given. Since we focus on a transmission based on subspaces, we also explain the principles of a transmission with subspaces.

2.1 OFDM

OFDM is a special case of frequency division multiplexing (FDM). It is widely used in wireless communication systems because of its high spectral efficiency, small realization effort and its flexibility. OFDM is deployed in many wireless communication standards such as LTE, WLAN, DAB and DVB-T, to mention some of them. In the following, a short introduction of OFDM is given, based on the literature of [4], [24], [32], [33] and [42], which are all recommended for further reading on OFDM.

The idea of OFDM is to divide the available frequency band into a large enough number of orthogonal subchannels, also named subcarriers. The subcarriers are transmitted in parallel and a large enough number of orthogonal subcarriers leads to small spaces between neighbouring frequencies.

The setup of an OFDM system is the following. The modulation and demodulation is done by making use of the inverse discrete Fourier transform (IDFT) and the discrete Fourier transform (DFT). This approach, as proposed by Weinstein and Ebert in 1971 [43], allows the usage of efficient fast Fourier transform (FFT) algorithms.

The basic waveforms in the low pass domain used for a transmission with OFDM are time limited complex exponential functions, i.e.

$$e_{T_k}(t) = \text{rect}\left(\frac{t}{T}\right) e^{j2\pi f_k t},\ k = 1, \ldots, N_f,$$

where T is the symbol duration. f_k is the k-th subcarrier frequency and N_f denoting the total number of subcarriers. To maintain orthogonality, the frequencies f_k have to be chosen in the following way

$$f_k = f_c + \frac{k}{T},$$

with f_c being the carrier frequency. The transmit signal is

$$s_{T_k}(t) = \sum_i x_k(i) e_{T_k}(t - iT),\ k = 1, \ldots, N_f.$$

Due to the fact that the basic waveforms $e_{T_k}(t)$, $k = 1, \ldots, N_f$ are time-limited by rect $\left(\frac{t}{T}\right)$, intersymbol interference (ISI) occurs, if the channel is linearly distorting. Therefore, a cyclic prefix of duration T_G was introduced by Peled and Ruiz in 1980 [30] to overcome ISI. The cyclic prefix is the repetition of the last part of an OFDM symbol, which is put at the beginning of the transmit signal. Thus, the OFDM transmit signal becomes

$$s_T(t) = \sum_{k=1}^{N_f} \sum_{i} x_k(i) e_{T_k}(t - iT_s),$$

where $T_s = T + T_G$ is the sum of the symbol duration T plus the guard interval T_G. To make sure that no ISI occurs, the duration of the guard interval has to be at least the maximum expected length of the channel impulse response. However, the application of a cyclic prefix leads to an increase of the transmit power, which looses its influence, if the OFDM symbol duration is sufficiently long enough compared to the length of the cyclic prefix.

Mathematical Description of OFDM

To describe the underlying discrete-time OFDM system model, we use the mathematical description of a vector-valued model, as shown in Fig. 2.2, see [11] and [24]. Fig. 2.2 is based on Fig. 2.1 and includes the OFDM modulation and demodulation.

The OFDM transmission model on symbol basis [11], [24] is defined by

$$\mathbf{y} = \mathbf{H}\mathbf{x} + \mathbf{n}, \tag{2.1}$$

where $\mathbf{x}$ represents a column vector containing the transmit symbols and $\mathbf{y}$ is the corresponding vector at the receiving side before equalization and detection. The OFDM channel matrix is assumed to be diagonal and is denoted by $\mathbf{H}$, where the entries on the main diagonal of $\mathbf{H}$ are the values of the transfer function of the channel at the corresponding subcarrier frequencies. The column vector $\mathbf{n}$ models the additive white Gaussian noise. For this model an OFDM guard interval in frequency domain of the length N_g, being longer than

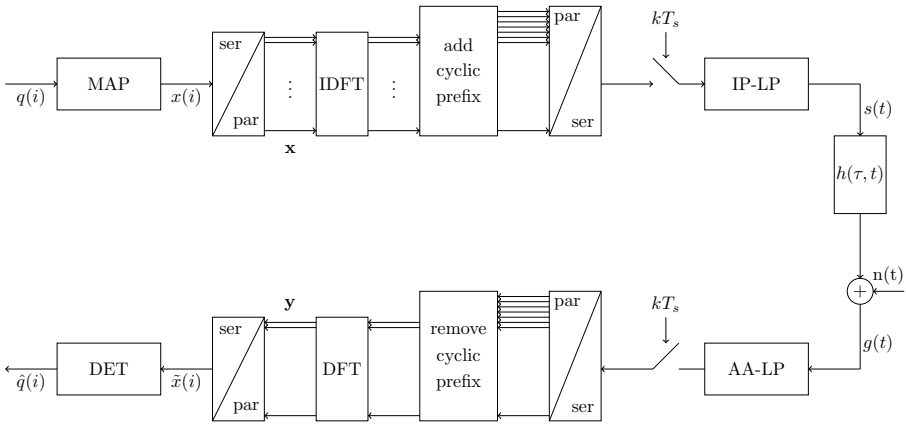

Figure 2.2: Mathematical description of an uncoded vector-valued OFDM system model.
$\mathbf{x}$: transmit vector, containing one OFDM block, $\mathbf{y}$: receive vector, MAP: mapping, ser/par: serial-to-parallel conversion, IDFT: inverse discrete Fourier transform, par/ser: parallel-to-serial conversion, IP-LP: interpolation low pass filter, $h(\tau, t)$: channel impulse response, AA-LP: anti-aliasing low pass filter, DFT: discrete Fourier transform, DET: detection.

the channel impulse response, is assumed. The $(N_f \times 1)$-dimensional vectors $\mathbf{y}$, $\mathbf{x}$ and $\mathbf{n}$ (see Fig. 2.2) are also called blocks, since each vector represents entries of a complete OFDM block.

If a time-variant channel with channel impulse response $h(\tau, t)$ is assumed, there are two scenarios to distinguish: slow time-variant channels and fast time-variant channels. In the first case, there occur no variations within one block, i.e. the variation occurs block by block or after a random number of subsequent OFDM blocks, and the model in Eq. (2.1) remains valid. However, in case of time-variant channels, non-zero entries on the off-diagonal entries of the channel matrix $\mathbf{H}$ occur. They occur due to a loss of orthogonality of the subcarriers, i.e. the time-variance of the channel causes intersubchannel interference. We assume perfect synchronization. To be able to apply the

OFDM transmission model, given in Eq. (2.1), it is possible to model the intersubchannel interference as additional additive noise, which is assumed to be Gaussian for a large enough number of subcarriers N_f, as shown by Russel and Stüber in [34]. We make use of this assumption to model the intersubchannel interference as additional noise and apply the OFDM transmission model on symbol basis, Eq. (2.1).

2.2 Channel Models

In this work, we use a stochastic channel model in the frequency domain, the discrete-time Rayleigh block fading channel model and the discrete-time Rayleigh frequency selective fading channel model. As shown in Eq. (2.1), we assume an OFDM transmission model on symbol basis in frequency domain $\mathbf{y} = \mathbf{H}\mathbf{x} + \mathbf{n}$.

2.2.1 Rayleigh Frequency Selective Fading Channel

For a frequency selective fading channel, one possible realization of the channel matrix for the stochastic process is

$$\mathbf{H} = \begin{bmatrix} h_{11} & 0 & \cdots & 0 \\ 0 & h_{22} & 0 & \vdots \\ \vdots & \cdots & \ddots & \vdots \\ 0 & \cdots & \cdots & h_{N_f N_f} \end{bmatrix} \tag{2.2}$$

with h_{ll}, $l = 1, \ldots, N_f$ being complex-valued zero mean unit variance fading coefficients on the main diagonal of the channel matrix $\mathbf{H}$, i.e. the mean value of the fading coefficients $\mu_h = 0$ and the variance $\sigma_h^2 = 1$. The side-entries remain 0, i.e. no intersubchannel interference is assumed. The channel is time-invariant and full frequency selective, since the fading coefficients are different for every single subcarrier of the whole OFDM block. The fading coefficients are assumed to be completely uncorrelated. Therefore the channel covariance matrix becomes $\mathbf{\Lambda}_h = \sigma_h^2 \mathbf{I}$, where $\mathbf{I}$ is the $N_f \times N_f$ identity matrix. The

definition of $\mathbf{\Lambda}_h$ is given by Eq. (2.11).

2.2.2 Rayleigh Block Fading Channel

In case of a Rayleigh block fading channel, the OFDM block, consisting of N_f subcarriers, is divided into subblocks of size M. Note, that N_f has to be an integer multiple of M. This results in $\frac{N_f}{M}$ channel submatrices $\mathbf{H}_i$, $i = 1, \ldots, \frac{N_f}{M}$ of dimension $M \times M$. The channel matrix for one OFDM block is

$$\mathbf{H} = \begin{bmatrix} \mathbf{H}_1 & 0 & \cdots & 0 \\ 0 & \mathbf{H}_2 & 0 & \vdots \\ \vdots & \cdots & \ddots & \vdots \\ 0 & \cdots & \cdots & \mathbf{H}_{\frac{N_f}{M}} \end{bmatrix}. \tag{2.3}$$

In the following, one channel submatrix $\mathbf{H}_i$ of dimension $M \times M$ is considered

$$\mathbf{H}_i = h\,\mathbf{I}_{M\times M} = \begin{bmatrix} h & 0 & \cdots & 0 \\ 0 & h & 0 & \vdots \\ \vdots & \cdots & \ddots & \vdots \\ 0 & \cdots & \cdots & h \end{bmatrix}_{M\times M}, \tag{2.4}$$

where h is a complex-valued fading coefficient with zero mean and unit variance, i.e. $\mu_h = 0$, $\sigma_h^2 = 1$. This is equivalent to the fact, that the entries on the main diagonal of the channel submatrix $\mathbf{H}_i$ are all the same for a subblock of M subcarriers. For the subsequent block of size M a new independent fading coefficient is obtained. Consequently, the channel matrix for the whole OFDM block is frequency selective, but within each subblock it is constant. The off-diagonal entries of the channel submatrices $\mathbf{H}_i$ are also 0. Since the channel coefficients for a Rayleigh block fading channel are fully correlated, the channel covariance matrix $\mathbf{\Lambda}_{h_i} = \sigma_h^2 \mathbf{1}_{M\times M}$. $\mathbf{1}$ denotes the $M \times M$ all ones matrix.

2.3 OFDM-MFSK and OFDM Multitone FSK

OFDM-MFSK, a combination of OFDM and M-ary frequency shift keying (MFSK), was introduced by Wetz et al. in [45] and [44]. The benefit of this combination is, that the OFDM part is able to cope with the frequency selective behaviour of the channel and the FSK part (see [24] and [32]) can be detected noncoherently in the receiver, i.e. without the need of channel state information (CSI). This makes OFDM-MFSK attractive for transmission over fast time-variant fading channels, because it is difficult or nearly impossible to obtain a reliable channel estimate in the receiver, since it is outdated very fast. An example for the practical application of OFDM-MFSK is frequency hopping, where for each FSK block a jumping on a new set of frequencies has to be made.

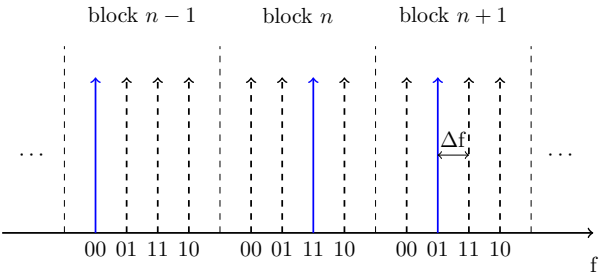

Figure 2.3: Basic principle of an OFDM-4FSK modulation, [45] and [44].
Blue solid line: power on the subcarrier, dashed black line: empty subcarrier, i.e. no power, Δf: subcarrier spacing.

For OFDM-MFSK an OFDM block, which consists of N_f subcarriers, is divided into subblocks of size M, i.e. each subblock consists of M subcarriers. After M subcarriers a new subblock of M subcarriers begins and in total $\frac{N_f}{M}$ subblocks are obtained. These blocks are modulated with MFSK and are therefore called FSK blocks. For OFDM-MFSK one out of M subcarriers within the corresponding FSK block is chosen for transmitting information, whereas the other $M-1$ subcarriers remain empty. With each FSK block of

size M it is possible to transmit $m = \log_2 M$ bits. Fig. 2.3 illustrates in an example for $M = 4$ the basic idea of an OFDM-4FSK modulation scheme, where the total number of the available subcarriers has to be a multiple of $M = 4$ and is divided into FSK blocks of $M = 4$ subcarriers. Each of the resulting FSK blocks is then modulated with 4FSK. This leads to subcarriers, which are used for transmission (solid blue line in Fig. 2.3), i.e. energy is allocated, and frequency positions, which remain empty (dashed black lines in Fig. 2.3). Between the bits and the subcarriers, a Gray mapping is used.

In a conventional OFDM transmission scheme, where for example QAM (quadrature amplitude modulation) is used for modulation, complex-valued transmit symbols are obtained. In comparison, for OFDM-MFSK real-valued vectors, consisting of $M - 1$ "0"s and one "1", result. Therefore, the nomenclature in case of OFDM-MFSK is the following: transmit vectors, selected from a transmit vector alphabet A, consisting of M orthogonal transmit column vectors $\mathbf{x}_k$, $k = 1, \ldots, M$ are chosen for transmission. For OFDM-4FSK this leads to a transmit vector alphabet of

$$A_{\text{4FSK}} = \left\{ \begin{bmatrix} 0 \\ 0 \\ 0 \\ 1 \end{bmatrix}, \begin{bmatrix} 0 \\ 0 \\ 1 \\ 0 \end{bmatrix}, \begin{bmatrix} 0 \\ 1 \\ 0 \\ 0 \end{bmatrix}, \begin{bmatrix} 1 \\ 0 \\ 0 \\ 0 \end{bmatrix} \right\}$$

As described in Sec. 2.1, the channel matrix $\mathbf{H}$ in frequency domain for the OFDM transmission model is a diagonal matrix of size $N_f \times N_f$

$$\mathbf{H} = \begin{bmatrix} h_{11} & 0 & \cdots & 0 \\ 0 & h_{22} & \ddots & \vdots \\ \vdots & \ddots & \ddots & \vdots \\ 0 & \ldots & \ldots & h_{N_f N_f} \end{bmatrix},$$

since the cross talk caused by the time-variance of the channel is modeled as additional noise. A diagonal channel matrix $\mathbf{H}$ leads in case of OFDM-MFSK to the possibility, that each FSK block of size M can be detected separately. This is equivalent to say, that only the corresponding part of the channel matrix $\mathbf{H}$ for the underlying FSK block is needed for detection. This part of

the channel matrix is of size $M \times M$, with M entries on its main diagonal:

$$\mathbf{H} = \begin{bmatrix} h_{11} & 0 & \cdots & 0 \\ 0 & h_{22} & \ddots & \vdots \\ \vdots & \ddots & \ddots & \vdots \\ 0 & ... & ... & h_{MM} \end{bmatrix},$$

In Sec. 2.2 the channel models of interest for this thesis have been introduced. For the Rayleigh frequency selective fading channel it is directly possible to regard the corresponding submatrices of dimension $M \times M$ of the channel matrix $\mathbf{H}$ and to do the FSK block wise detection. For the Rayleigh block fading channel, it is assumed, that the block size M for the submatrices $\mathbf{H}_i$ of the channel matrix $\mathbf{H}$ corresponds to the FSK block size, also abbreviated with M. This means, that for each FSK block of size M and its corresponding submatrix $\mathbf{H}_i$ of the channel matrix $\mathbf{H}$, the fading coefficient remains constant.

With an increasing size of M, the capacity of the Gaussian channel with infinite bandwidth can be approached. However, the disadvantage is, that the bandwidth efficiency η tends to 0 for $M \to \infty$ [24]. For OFDM-MFSK the upper bound for the bandwidth efficiency, i.e. the guard bands as well as the cyclic prefix are neglected, is

$$\eta_{\mathrm{MFSK}} = \frac{\log_2 M}{M}, \tag{2.5}$$

where $\log_2 M$ is the number of bits m, which are assigned to one FSK block of size M. Compared to the logarithmic growth of the numerator, the denominator, i.e. the bandwidth itself, grows linearly. As a result, the bandwidth efficiency decreases with increasing M. Eq. (2.5) shows, that for OFDM-MFSK the maximum achievable value for the bandwidth efficiency is 0.5 $\frac{\mathrm{bit/s}}{\mathrm{Hz}}$ either for OFDM-2FSK or OFDM-4FSK. For an increased number of subcarriers per FSK block of size M, $M > 4$, the bandwidth efficiency η gets smaller. Because of its better power efficiency compared to OFDM-2FSK, OFDM-4FSK is preferred.

To overcome the loss in bandwidth efficiency, Linduska et al. modified in [25] the approach of OFDM-MFSK to OFDM multitone FSK. Instead of using

one single tone out of M tones per FSK block of size M, N subcarriers out of M subcarriers within one FSK block are chosen. This offers the possibility to transmit $m = \lfloor \log_2 \binom{M}{N} \rfloor$ bits per OFDM multitone FSK vector. An abbreviation of OFDM multitone FSK is OFDM-N/MFSK and it is also suitable for conventional OFDM-MFSK, which is OFDM-1/MFSK.

Considering the transmit vector alphabet A for a FSK block size of $M = 4$ and $N = 2$ active subcarriers

$$A_{2/4\mathrm{FSK}} = \left\{ \begin{bmatrix} 0 \\ 0 \\ 1 \\ 1 \end{bmatrix}, \begin{bmatrix} 0 \\ 1 \\ 0 \\ 1 \end{bmatrix}, \begin{bmatrix} 0 \\ 1 \\ 1 \\ 0 \end{bmatrix}, \begin{bmatrix} 1 \\ 0 \\ 0 \\ 1 \end{bmatrix}, \begin{bmatrix} 1 \\ 0 \\ 1 \\ 0 \end{bmatrix}, \begin{bmatrix} 1 \\ 1 \\ 0 \\ 0 \end{bmatrix} \right\}$$

is obtained.

Compared to OFDM-1/MFSK, the bandwidth efficiency is now

$$\eta_{\mathrm{N/MFSK}} = \frac{\left\lfloor \log_2 \binom{M}{N} \right\rfloor}{M}. \tag{2.6}$$

For OFDM-4/8FSK a bandwidth efficiency of $0.75 \frac{\mathrm{bit/s}}{\mathrm{Hz}}$ is obtained and it is possible to transmit six bits within an FSK block consisting of eight subcarriers. This increase is remarkable, since for OFDM-8FSK it is only possible to transmit three bits per FSK block of size $M = 8$ and the bandwidth efficiency is $0.375 \frac{\mathrm{bit/s}}{\mathrm{Hz}}$.

2.3.1 Noncoherent Detection

The maximum-likelihood (ML) detection of the transmitted vector, given the received vector, is based on maximizing the probability density function (PDF), conditioned on the transmitted vector. The PDF is always dependent on the underlying channel and the transmit vector alphabet. In some cases, it is possible to simplify the PDF in a way, that a detection metric results. The noncoherent detection metrics for OFDM-MFSK for transmission over the AWGN channel or the Rayleigh block fading channel were derived in [44].

Since it is a noncoherent detection metric, no channel state information goes into the calculation.

A block diagram of the assumed transmission model $\mathbf{y} = \mathbf{H}\mathbf{x}+\mathbf{n}$ is shown in Fig. 2.4, where $\mathbf{x}$ denotes the transmit vector, $\mathbf{y}$ the corresponding vector on the receiving side and $\mathbf{n}$ the contributions of the additive noise. The channel matrix $\mathbf{H}$ can be reduced to $h = |h_0|e^{j\varphi} = e^{j\varphi}$, with $|h_0| = 1$ for an AWGN channel, whereas for a block fading channel $|h_0| \neq 1$. φ is a random variable and characterizes the unknown phase of the channel and it is assumed to be common for all subcarriers within one FSK block of size M.

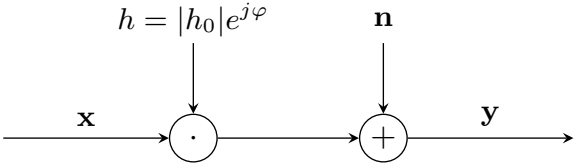

Figure 2.4: Channel model

Wetz et. al have shown in [45] and [44], that a blockwise detection for OFDM-N/MFSK is possible, according to the vector-valued transmission model in Eq. (2.1). For deriving the detection metric, it is necessary to model the intersubchannel interference as additional noise, so that the channel matrix $\mathbf{H}$ remains diagonal. The multivariate conditional probability density function (PDF) for the received vector $\mathbf{y}$, given the transmitted vector $\mathbf{x}$, is based on the derivations in [9] and the definition in [21] and is

$$p(\mathbf{y}|\mathbf{x},\varphi) = \frac{1}{\pi^M \det(\mathbf{\Lambda})} \exp\left(-(\mathbf{y} - E[\mathbf{y}])^H \mathbf{\Lambda}^{-1} (\mathbf{y} - E[\mathbf{y}])\right), \tag{2.7}$$

where $\mathbf{x}$ and $\mathbf{y}$ denote again the transmit and receive vector respectively. φ characterizes the unknown phase of the channel and is assumed to be common for all subcarriers within one MFSK block of size M and $\det(\mathbf{\Lambda})$ denotes the determinant of the covariance matrix

$$\mathbf{\Lambda} = E\left\{(\mathbf{y} - E[\mathbf{y}])(\mathbf{y} - E[\mathbf{y}])^H\right\}. \tag{2.8}$$

$E[\mathbf{y}]$ denotes the expected value of the received vector, i.e. its mean value, respectively. Setting the values of $\mathbf{y}$ and $E[\mathbf{y}]$ into the definition of the covariance matrix $\mathbf{\Lambda}$, we solve the problems to calculate the entries of $\mathbf{\Lambda}$,

$$[\mathbf{\Lambda}]_{ij} = [\mathbf{x}]_i [\mathbf{x}]_j^* \; E\left[\left([\mathbf{H}]_{ii} - E[\mathbf{H}]_{ii} \right) \left([\mathbf{H}]_{jj} - E[\mathbf{H}]_{jj} \right)^* \right] + \sigma_n^2 \delta_{ij}, \tag{2.9}$$

where

$$\delta_{ij} = \begin{cases} 1 & \text{for } i = j \\ 0 & \text{for } i \neq j \end{cases} \tag{2.10}$$

is the Kronecker delta. $[\mathbf{H}]_{ii}$ denotes the values of the channel transfer function at the corresponding subcarrier frequencies on the main diagonal of the channel matrix $\mathbf{H}$ and $E[\mathbf{H}]_{ii}$ denotes the values on the main diagonal of the mean channel matrix $E[\mathbf{H}]$. σ_n^2 is the variance of the noise. The channel covariance matrix $\mathbf{\Lambda}_h$ is componentwise defined by

$$[\mathbf{\Lambda}_h]_{ij} = E\left[\left([\mathbf{H}]_{ii} - E[\mathbf{H}]_{ii} \right) \left([\mathbf{H}]_{jj} - E[\mathbf{H}]_{jj} \right)^* \right]. \tag{2.11}$$

With this definition, it is possible to rewrite Eq. (2.9) by

$$\mathbf{\Lambda} = \mathrm{diag}(\mathbf{x}) \mathbf{\Lambda}_H \mathrm{diag}(\mathbf{x}^H) + \sigma_n^2 \mathbf{I}, \tag{2.12}$$

where $\mathbf{I}$ denotes the $M \times M$ identity matrix. $\mathrm{diag}(\mathbf{x})$ transforms the column vector $\mathbf{x}$ into a diagonal matrix $\mathbf{X}$. The entries on the main diagonal of $\mathbf{X}$ are the elements of the column vector $\mathbf{x}$. In [44], Wetz made use of the derivation in [9] and the conditional PDF, where φ is integrated out, was obtained

$$\begin{aligned} p(\mathbf{y}|\mathbf{x}) &= \int_{-\pi}^{\pi} \frac{1}{2\pi} p(\mathbf{y}|\mathbf{x}, \varphi) \, d\varphi \\ &= \frac{1}{\pi^M \det \mathbf{\Lambda}} \exp\left(-\mathbf{y}^H \mathbf{\Lambda}^{-1} \mathbf{y} - \mathbf{x}^H E\left[\mathbf{H}^H\right] \mathbf{\Lambda}^{-1} E[\mathbf{H}] \mathbf{x} \right) \\ &\quad I_0\left(2 \left| \mathbf{y}^H \mathbf{\Lambda}^{-1} E[\mathbf{H}] \mathbf{x} \right| \right). \end{aligned} \tag{2.13}$$

I_0 is the zero order modified Bessel function of the first kind. After specifying the channel conditions for AWGN and Rayleigh block fading channels and the

assumption of equiprobable bits, the same detection rule for OFDM-MFSK results for both channel models

$$\hat{\mathbf{x}} = \underset{\mathbf{x}_k \in \{\mathbf{x}_1, \cdots, \mathbf{x}_K\}}{\operatorname{argmax}} |\mathbf{y}^H \mathbf{x}_k|^2, \tag{2.14}$$

which is the squared scalar product between the received vector $\mathbf{y}$ and all possible transmit vectors $\mathbf{x}_k$.

The ML detection rule is based on the smallest angle, i.e. the principal angle, between the received vector $\mathbf{y}$ and any of the transmit vectors $\mathbf{x}_k$. The definition of the angle, see [6], between any pair of two vectors $\mathbf{y}$ and $\mathbf{x}$ is

$$\cos_{\mathbf{y},\mathbf{x}_k} \alpha = \frac{|\mathbf{y}^H \mathbf{x}|}{\|\mathbf{y}\| \|\mathbf{x}\|}, \tag{2.15}$$

where $\mathbf{y}^H \mathbf{x}$ denotes the scalar product and $\|\cdot\|$ the norm of the corresponding vector.

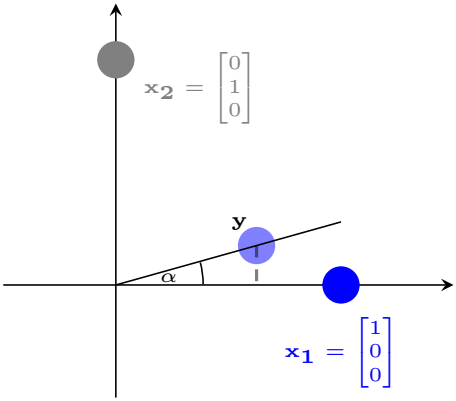

Figure 2.5: Projection of a received FSK vector for a transmission over a Rayleigh block fading channel.

Fig. 2.5 shows a visualizing example for a transmission of a 3FSK vector over a Rayleigh block fading channel. The FSK vector $\mathbf{x_1}$ has been transmit-

ted. The corresponding received vector $\mathbf{y}$ was scaled by the fading coefficient and the additive noise lead to a shift into the space. By calculating the principal angle with the possible transmit vectors $\mathbf{x}_1$ and $\mathbf{x}_2$, the received vector $\mathbf{y}$ is projected on both axes. The decision is made in favour of the minimum principal angle. Note, that for an AWGN channel, there is no scaling of the transmit vector along its corresponding axis. Simply noise is added. As a consequence, for an AWGN channel, it would be possible to apply amplitude shift keying (ASK).

2.3.2 Bit-Interleaved Coded Modulation

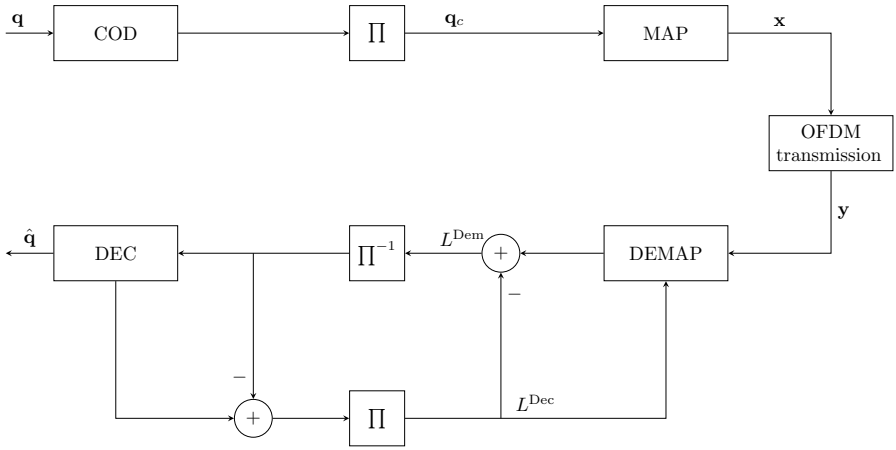

Figure 2.6: BIC-OFDM transmission model with an iterative receiver.

Channel coding adds in the transmitter redundancy, allowing the receiver to detect and/or correct errors. Therefore, channel coding is used to improve the performance of digital transmissions. We assume bit-interleaved coded modulation [7] with iterative detection (BICM-ID) for our system. Fig. 2.6 shows the corresponding vector-valued transmission model from Eq. (2.1) for a coded transmission with an iterative receiver. The source bit vector $\mathbf{q}$, i.e. one

information block vector, is convolutionally encoded in the block "COD" with a terminated convolutional code with rate $r = \frac{k}{n_c}$ [5]. k denotes the length of the information sequence and n_c the length of the code word sequence. Since convolutional codes are sensitive to burst errors, an interleaver (block $\prod$) is used and afterwards the coded vector $\mathbf{q}_c$ is mapped onto the OFDM-N/MFSK vectors $\mathbf{x}_k,\ k = 1, \ldots, \frac{N_f}{M}$, resulting in $\mathbf{x} = [\mathbf{x}_1\ \cdots\ \mathbf{x}_{\frac{N_f}{M}}]^T$. In the next step the transmit vector $\mathbf{x}$ are transmitted over the vector-valued OFDM transmission model, described in Sec. 2.1. In the receiver, the received vector $\mathbf{y} = [\mathbf{y}_1\ \cdots\ \mathbf{y}_{\frac{N_f}{M}}]^T$ contains one complete code block of OFDM-MFSK vectors and it is processed by an iterative receiver, as suggested by Li and Ritcey in [23] and then the received information block vector $\hat{\mathbf{q}}$ is obtained. Another point of view for iterative demapping and decoding in the receiver, as it can be seen in Fig. 2.6, is to treat the mapping as an inner code with code rate $r = 1$, since no redundancy is added for the mapping, and the channel code is regarded as an outer code.

Because of the special structure of the OFDM-N/MFSK blocks, it is possible to fragment the received vector $\mathbf{y}$ into subvectors $\mathbf{y}_k$ of size $M \times 1$, i.e. the MFSK block size, as it has already been shown for the detection metric. These subvectors $\mathbf{y}_k$ are demapped and the iterative process is running as described above. In the following the block indizes k are neglected for the purpose of keeping the notation simple.

Demapping and decoding within an iterative receiver (c.f. Fig. 2.6) are performed independently of each other, therefore the iterative receiver becomes a suboptimum receiver. The demapper (DEMAP) calculates reliability information for each bit of the received vectors $\mathbf{y}$. The reliability information is deinterleaved within the block $\prod^{-1}$ and passed to the decoder (DEC). Within the decoder, the reliability for each code bit is improved. Demapper and decoder are able to exchange information about the reliability within iterations. Only extrinsic information, i.e. information gained within the demapper or decoder is exchanged and therefore the input information is subtracted from the gained reliability information.

For defining the reliability, log-likelihood ratios (LLR) [16] or L-values are

a very useful measure. The idea of LLR is a mapping from probability space to log-likelihood ratios. In [44], it has been shown, that the LLR of one code bit c_j, under the condition, that the vector $\mathbf{y}$ has been received, is defined by

$$L(c_j|\mathbf{y}) = \ln\left(\frac{\sum_{\mathbf{a}_i \in S_j^0} p(\mathbf{y}|\mathbf{x}=\mathbf{a_i})P(\mathbf{x}=\mathbf{a}_i)}{\sum_{\mathbf{a}_i \in S_j^1} p(\mathbf{y}|\mathbf{x}=\mathbf{a_i})P(\mathbf{x}=\mathbf{a}_i)}\right), \tag{2.16}$$

where $p(\mathbf{y}|\mathbf{x}=\mathbf{a_i})$ denotes the PDF of the received vector $\mathbf{y}$ under the assumption that the vector $\mathbf{a}_i$ was transmitted. The PDF depends on the channel and can be evaluated for the received vector $\mathbf{y}$. $P(\mathbf{x}=\mathbf{a}_i)$ defines the a-priori probability, that the vector $\mathbf{a}_i$ has been transmitted and is derived with the extrinsic feedback from the previous decoding steps

$$P(\mathbf{x}=\mathbf{a}_i) = \prod_k P(c_k = c_{k_{\mathbf{a}_i}}) \tag{2.17}$$

with $c_{k_{\mathbf{a}_i}}$ being the bits of the vector $\mathbf{a}_i$ at position k. Since these bits are independently from each other, their probabilities can be multiplied.

$$\begin{aligned} P(c_k=0) &= \frac{\exp(\mathbf{L}_k^{\mathrm{Dec}})}{1+\exp(\mathbf{L}_k^{\mathrm{Dec}})} \\ P(c_k=1) &= \frac{1}{1+\exp(\mathbf{L}_k^{\mathrm{Dec}})} \end{aligned} \tag{2.18}$$

specify the probabilities that the bits $c_{k_{\mathbf{a}_i}}$ according to the vectors $\mathbf{a}_i$ have been transmitted. The L-values derived by the channel decoder in the previous iteration are represented with the vector $\mathbf{L}^{\mathrm{Dec}}$ (c.f. Fig. 2.6). It is obvious, that no feedback information $\mathbf{L}^{\mathrm{Dec}}$ is available for the first iteration. Therefore the a-priori probability for all symbols is assumed to be equal. After subtraction of the a-priori information, it is now possible to obtain the extrinsic L-values of all bits in the demapper. This results in $\mathbf{L}^{\mathrm{Dem}}$, the vector of extrinsic L-values.

The decoder works with the BCJR algorithm, which has been introduced by Bahl et al. in [3]. It is possible to investigate and especially to visualize the convergence behaviour of iterative decoding schemes in the receiver by making use of extrinsic information transfer (EXIT) charts, as proposed by Ten Brink in [39] and [40].

2.4 Capacity of Multipath Fading Channels

The capacity and mutual information of frequency selective fading channels without channel state information in the receiver has been discussed in [38] by Telatar and Tse. The following main results were obtained.

- For an increasing bandwidth, the capacity of a frequency selective fading channel approaches the capacity of the infinite bandwidth AWGN channel. Furthermore, it has been shown, that for "spread-spectrum" like signals, for example code division multiple access (CDMA), the mutual information approaches zero for an increasing bandwidth. This result was confirmed by Medard et al. in [26].

- It is argued, that the input signals, which can achieve capacity, have to be "peaky" in time or in frequency. Telatar et al. [38] also state, that this is achieved by applying FSK and noncoherent detection.

These results are of high interest with respect to OFDM-MFSK and its multitone variant. OFDM-MFSK signals are "peaky" by definition and we are interested in noncoherent detection for frequency selective fading channels, wherefore we expect OFDM-MFSK to be a very good candidate to approach the maximum mutual information for frequency selective fading channels, as proposed in [38].

2.5 Principles of Subspaces for Transmission

Unitary space-time modulation, as proposed by Hochwald and Marzetta in [18] and [19], is a transmission scheme for MIMO channels based on subspaces and can be noncoherently detected for Rayleigh flat fading channels. In the following, we discuss the basic principles of a transmission based on subspaces on the basis of the work by Hochwald and Marzetta for unitary space-time modulation.

There also exists a transmission model on symbol basis, as already given for a single-input single-output (SISO) OFDM transmission in Sec. 2.1, Eq. (2.1),

and it is described by

$$\mathbf{Y} = \mathbf{H}\,\mathbf{X} + \mathbf{N}. \tag{2.19}$$

$\mathbf{X}$ is the transmit matrix of dimension $M_{\text{tx}} \times T$, where M_{tx} denotes the number of transmit antennas and T denotes the number of time-slots. $\mathbf{X}$ is taken from a set of transmit matrices of a transmit matrix alphabet A, whereby

$$\mathbf{X} \in A = \{\mathbf{X}_1, \ldots, \mathbf{X}_n\}.$$

$\mathbf{Y}$ is the corresponding $N_{\text{rx}} \times T$ matrix at the receiving side, where N_{rx} denotes the number of receive antennas. The MIMO channel matrix $\mathbf{H}$ of size $M_{\text{tx}} \times N_{\text{rx}}$ comprises complex Gaussian distributed fading coefficients with zero mean and unit variance, which are assumed to be constant over T time-slots, before they change to new independent realizations. The additive noise, modeled by the matrix $\mathbf{N}$, incorporates the noise contributions in $\mathbf{Y}$ and it is white Gaussian noise with two-sided noise power spectral density of $\frac{N_0}{2}$.

In the following, the description of how the unitary space time modulation signaling scheme could be regarded as a transmission based on subspaces, is given. An illustrative example for transmitting 2-dimensional subspaces of the 3-dimensional space is given for a MIMO transmission. Without loss of generality, it can be extended to higher dimensional spaces.

For a 2×2 MIMO transmission model, i.e. two transmit antennas ($M_{\text{tx}} = 2$) and two receive antennas ($N_{\text{rx}} = 2$), respectively, and constant fading coefficients over $T = 3$ symbol periods, the following MIMO transmission model on symbol basis, as proposed in Eq. (2.19), is obtained:

$$\mathbf{Y} = \begin{bmatrix} h_{11} & h_{12} \\ h_{21} & h_{22} \end{bmatrix} \begin{bmatrix} x_{11} & x_{12} & x_{13} \\ x_{21} & x_{22} & x_{23} \end{bmatrix} + \begin{bmatrix} n_{11} & n_{12} & n_{13} \\ n_{21} & n_{22} & n_{23} \end{bmatrix} \tag{2.20}$$

The first important condition for transmitting subspaces is $T > M_{\text{tx}}$, i.e. the number of time-slots T has to be larger than the number of transmit antennas M_{tx}, since T defines the dimension of the space and M_{tx} defines the dimension of the subspace. In the example of Eq. (2.20) the dimension of the space is $T = 3$ (the number of the columns) and the dimension of the subspace is $M_{\text{tx}} = 2$ (the number of the rows). The second condition is, that the

row vectors of the transmit matrix $\mathbf{X}$, i.e. the $1 \times T$-dimensional row vectors $\mathbf{x}_1 = \begin{bmatrix} x_{11} & x_{12} & x_{13} \end{bmatrix}$ and $\mathbf{x}_2 = \begin{bmatrix} x_{21} & x_{22} & x_{23} \end{bmatrix}$, have to be linearly independent to span a M_{tx}-dimensional subspace of the T-dimensional space. If the row vectors are orthogonal to each other, they can be interpreted as basis vectors of the M_{tx}-dimensional subspace. Hochwald and Marzetta [19] assumed orthonormal complex-valued vectors, i.e. the length of the $1 \times T$-dimensional row vectors is normed to 1 and unitary transmit matrices (matrices with orthonormal row vectors) are obtained. The transmit matrix $\mathbf{X}$ of Eq. (2.20) could now be rewritten by $\mathbf{X} = \begin{bmatrix} \mathbf{x}_1 \\ \mathbf{x}_2 \end{bmatrix}$. Inserted in Eq. (2.20), this leads to

$$\begin{bmatrix} \mathbf{y}_1 \\ \mathbf{y}_2 \end{bmatrix} = \begin{bmatrix} h_{11} & h_{12} \\ h_{21} & h_{22} \end{bmatrix} \begin{bmatrix} \mathbf{x}_1 \\ \mathbf{x}_2 \end{bmatrix} + \begin{bmatrix} \mathbf{n}_1 \\ \mathbf{n}_2 \end{bmatrix}, \tag{2.21}$$

where the received matrix $\mathbf{Y} = \begin{bmatrix} \mathbf{y}_1 \\ \mathbf{y}_2 \end{bmatrix}$ as well as the noise matrix $\mathbf{N} = \begin{bmatrix} \mathbf{n}_1 \\ \mathbf{n}_2 \end{bmatrix}$ have also been replaced.

In the receiver, no knowledge of the channel matrix $\mathbf{H}$ is required and it is therefore called noncoherent. In the noise-free case, i.e. for $\mathbf{N} = \mathbf{0}$, Eq. (2.21) reduces to two received row vectors $\mathbf{y}_1$ and $\mathbf{y}_2$ of the received matrix $\mathbf{Y}$, which are a linear combination of both of the transmitted row vectors $\mathbf{x}_1$ and $\mathbf{x}_2$ of the transmit matrix $\mathbf{X}$, scaled by the channel fading coefficients h_{kl}, $k = 1, \ldots, N_{rx}$, $l = 1 \ldots, M_{tx}$.

$$\begin{aligned} \mathbf{y}_1 &= h_{11}\,\mathbf{x}_1 + h_{12}\,\mathbf{x}_2 \\ \mathbf{y}_2 &= h_{21}\,\mathbf{x}_1 + h_{22}\,\mathbf{x}_2 \end{aligned} \tag{2.22}$$

Fig. 2.7 illustrates this for the xy-plane in $\mathbb{R}^3$, where a 2-dimensional subspace, spanned by the orthonormal basis vectors $\mathbf{x}_1 = \begin{bmatrix} 1 & 0 & 0 \end{bmatrix}$ and $\mathbf{x}_2 = \begin{bmatrix} 0 & 1 & 0 \end{bmatrix}$, is shown. For illustrating purposes the fading coefficients $h_{kl}, k = 1, N_{\text{rx}} = 2, l = 1, M_{\text{tx}} = 2$ are assumed to be real valued. Each fading coefficient scales one of the orthonormal basis vectors. The resulting vectors $\mathbf{y}_1 = h_{11}\mathbf{x}_1 + h_{12}\mathbf{x}_2$ and $\mathbf{y}_2 = h_{21}\mathbf{x}_1 + h_{22}\mathbf{x}_2$ are both still located in the xy-plane. This is equivalent to the fact, that the transmitted subspace has not been changed by the channel matrix $\mathbf{H}$. Going back to Eq. (2.22), it becomes obvious, that $\mathbf{y}_1$ and $\mathbf{y}_2$ are linear combinations of $\mathbf{x}_1$ and $\mathbf{x}_2$,

in which $\mathbf{x}_1$ and $\mathbf{x}_2$ are just scaled by the channel fading coefficients h_{kl}, $k = 1, \ldots, N_{\text{rx}}$, $l = 1, \ldots, M_{\text{tx}}$. It is clear, that the received matrix $\mathbf{Y}$ is the same subspace as the transmit matrix $\mathbf{X}$, i.e. the channel matrix $\mathbf{H}$ cannot change the transmitted subspace $\mathbf{X}$. There are two cases, for the noise-free case for which the original transmitted plane is lost and a correct decision is not possible anymore: First of all, if one of the fading coefficients is 0 and secondly, if both resulting vectors $\mathbf{y}_1$ and $\mathbf{y}_2$ are pointing in the same direction. However, the probability for the second event could be neglected compared to the probability of having fading coefficients near zero. For both cases one dimension is lost.

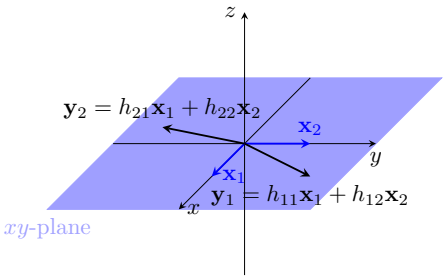

Figure 2.7: Illustration how the orthonormal basis vectors $\mathbf{x}_1$ and $\mathbf{x}_2$, which span a 2-dimensional subspace (a plane) in the 3-dimensional space, are scaled and rotated by different fading coefficients $h_{kl}, k = 1, N_{\text{rx}} = 2, l = 1, M_{\text{tx}} = 2$.

We have seen so far, that the channel does not change the transmitted subspace. However, the contributions from the row vectors of the noise matrix $\mathbf{N}$ are present in any component of the T-dimensional space. This means, that the noise changes the transmitted subspace, i.e. the subspace is rotated out. Fig. 2.8 shows this effect for the example of transmitting a plane in $\mathbb{R}^3$. The corresponding noise components result in the vectors $\mathbf{y}_1 = h_{11}\mathbf{x}_1 + h_{12}\mathbf{x}_2 + \mathbf{n}_1$ and $\mathbf{y}_2 = h_{21}\mathbf{x}_1 + h_{22}\mathbf{x}_2 + \mathbf{n}_2$, which could be located outside of the xy-plane. The received plane, which is spanned by $\mathbf{y}_1$ and $\mathbf{y}_2$, is rotated out of the xy-plane.

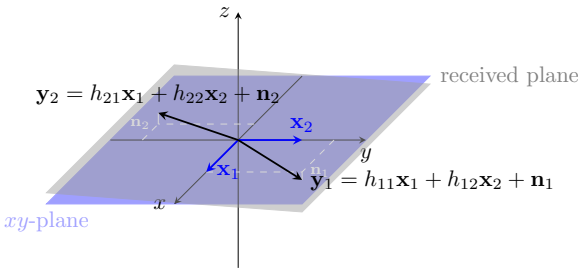

Figure 2.8: Illustration how the orthonormal basis vectors $\mathbf{x}_1$ and $\mathbf{x}_2$, which span a 2-dimensional subspace (a plane) in the 3-dimensional space, are scaled and rotated by different fading coefficients $h_{kl}, k = 1, N_{\text{rx}} = 2, l = 1, M_{\text{tx}} = 2$. The noise components $\mathbf{n}_1$ and $\mathbf{n}_2$ cause a rotation of the transmitted subspace out in the 3-dimensional space.

It is clear, why the fading coefficients of the channel matrix $\mathbf{H}$ for the MIMO scenario have to be constant for a duration over T time-slots. T defines the dimension of the space and the $1 \times T$ dimensional row vectors $\mathbf{x}_l$, $l = 1, \ldots, M_{\text{tx}}$, which have to be linearly independent, span the M_{tx}-dimensional subspace. Therefore the row vectors are not allowed to change within T time-slots, because otherwise the underlying subspace would be changed. After T time slots, the channel coefficients change to new independent realizations, which also have to be constant for the upcoming T time-slots.

Note, that in case of different numbers of transmit and receive antennas, the following two cases arise: For $M_{\text{tx}} < N_{\text{rx}}$ the rows of the receive matrix $\mathbf{Y}$ become linearly dependent, whereas for $M_{\text{tx}} > N_{\text{rx}}$ the received subspace $\mathbf{Y}$ becomes a subspace of lower dimension of the transmitted subspace $\mathbf{X}$.

In [19], Hochwald and Marzetta are assuming unitary transmit matrices $\mathbf{\Phi}_l$ of dimension $M_{\text{tx}} \times T$

$$\mathbf{\Phi}_l \mathbf{\Phi}_l^H = \mathbf{I}, \tag{2.23}$$

where T denotes the number of time-slots and M_{tx} denotes the number of

transmit antennas. The resulting identity matrix $\mathbf{I}$ is of dimension $T \times T$. The row vectors of the unitary transmit matrices $\mathbf{\Phi}_l$ are assumed to be linearly independent from each other. Note, that Hochwald and Marzetta originally used the matrix-valued transmission model $\mathbf{Y} = \mathbf{XH} + \mathbf{N}$. For this case, the transmit matrices $\mathbf{\Phi}_l$ are of dimension $T \times M_{\text{tx}}$ and orthonormal column vectors occur. Since we use the matrix-valued transmission model from Eq. 2.19, we adapted the original system of Hochwald and Marzetta.

In [19] the conditional matrix variate probability density function of the received matrix $\mathbf{Y}$, under the condition, that $\mathbf{\Phi}_l$ has been transmitted, was used and it is defined by

$$p(\mathbf{Y}|\mathbf{\Phi}_l) = \frac{\exp\left(-\text{tr}\left\{\mathbf{\Lambda}^{-1}\mathbf{Y}^H\mathbf{Y}\right\}\right)}{\pi^{TN_{\text{rx}}}\det^{N_{\text{rx}}}\mathbf{\Lambda}}, \tag{2.24}$$

where $\mathbf{Y}$ is of size $N_{\text{rx}} \times T$, $\text{tr}(\mathbf{A})$ denotes the trace of the matrix $\mathbf{A}$ and $\det \mathbf{\Lambda}$ is the determinant of $\mathbf{\Lambda}$. $\mathbf{\Lambda}$ is the $T \times T$ covariance matrix

$$\mathbf{\Lambda} = \mathbf{I} + \frac{\rho}{M_{\text{tx}}}\mathbf{\Phi}_l^H\mathbf{\Phi}_l. \tag{2.25}$$

$\mathbf{I}$ denotes the $T \times T$ identity matrix and ρ the expected signal-to-noise ratio (SNR) at each receiver antenna, independently of the number of transmit antennas. Furthermore, it is assumed that the channel matrix $\mathbf{H}$ is neither known by the transmitter nor by the receiver. Therefore no channel state information is available for the detection of the transmitted matrices $\mathbf{\Phi}_l$ in the receiver and the receiver itself is called noncoherent.

The maximum-likelihood (ML) decision rule for the transmission of unitary

subspace based matrices, as defined in [19], is

$$\begin{aligned}
\hat{\mathbf{\Phi}}_l &= \underset{\mathbf{\Phi}_l \in \{\mathbf{\Phi}_1, \cdots, \mathbf{\Phi}_L\}}{\operatorname{argmax}} p\left(\mathbf{Y}|\mathbf{\Phi}_l\right) \\
&= \underset{\mathbf{\Phi}_l \in \{\mathbf{\Phi}_1, \cdots, \mathbf{\Phi}_L\}}{\operatorname{argmax}} \frac{\exp\left(-\operatorname{tr}\left\{\left[\mathbf{I} + \frac{\rho T}{M_{\mathrm{tx}}} \mathbf{\Phi}_l^H \mathbf{\Phi}_l\right]^{-1} \mathbf{Y}^H \mathbf{Y}\right\}\right)}{\pi^{TN} \det^{N_{\mathrm{rx}}}\left[\mathbf{I} + \frac{\rho T}{M_{\mathrm{tx}}} \mathbf{\Phi}_l^H \mathbf{\Phi}_l\right]} \qquad (2.26) \\
&= \underset{\mathbf{\Phi}_l \in \{\mathbf{\Phi}_1, \cdots, \mathbf{\Phi}_L\}}{\operatorname{argmax}} \operatorname{tr}\{\mathbf{Y} \mathbf{\Phi}_l^H \mathbf{\Phi}_l \mathbf{Y}^H\}. \qquad (2.27) \\
&= \underset{\mathbf{\Phi}_l \in \{\mathbf{\Phi}_1, \cdots, \mathbf{\Phi}_L\}}{\operatorname{argmax}} \|\mathbf{Y} \mathbf{\Phi}_l^H\|_F^2, \qquad (2.28)
\end{aligned}$$

where $\|\cdot\|_F^2$ is the squared Frobenius norm. It projects the received subspace $\mathbf{Y}$ back to the tested subspaces $\mathbf{\Phi}_l$. The decision is made in favour of the maximum received value. A detailed explanation of the derivation of the ML decision rule is given within Appendix A.

2.6 Chapter Summary

The basic essentials, which build the foundation for this thesis, have been introduced within this chapter. An overview of OFDM and the vector-valued transmission model for OFDM, as proposed by [24] and [11] has been given. This section was followed by the definition of the assumed channel models, the Rayleigh block fading channel model as well as the Rayleigh frequency selective fading channel model. OFDM-MFSK and OFDM multitone FSK, which is the transmission technique of interest, have been explained. The drawback, its bad bandwidth efficiency, has been worked out. The derivation of the detection metric has been discussed. Afterwards the transmission model for bit-interleaved coded modulation with iterative detection for OFDM-MFSK and its multitone variant has been addressed. We gave a brief introduction on the capacity of frequency selective fading channels, as proposed within the work of [38] and [26]. To achieve capacity of frequency selective fading channels, "peaky" signals, which can be noncoherently detected, should be used. This is

true for OFDM-MFSK and its multitone variant. We expect OFDM-MFSK to be a very good candidate to achieve capacity within frequency selective fading channels. Last, the principles of subspaces for transmission have been discussed and visualized with examples.

Chapter 3

OFDM-MFSK and Transmissions Based on Subspaces

NONCOHERENT transmission based on subspaces in the MIMO context were proposed by Hochwald and Marzetta in [19], c.f. Sec. 2.5. OFDM-MFSK and its multitone variant is also called noncoherent and there seems to be a connection between OFDM-MFSK and those subspace based transmission methods. In the following we will show, that OFDM-MFSK and its multitone variant are special cases of a noncoherent communication based on subspaces as shown for MIMO systems in Sec. 2.5.

The key idea of this thesis is to combine subspaces of different dimensions in terms of OFDM-MFSK to exploit the total available mathematical space in a more efficient way. The possibility of having orthogonal subspaces, as it is the case for 1/MFSK is lost. However, we will show, that a combination of subspaces of different dimensions in case of OFDM-MFSK and its multitone variant offers the advantage of increasing the bandwidth efficiency of OFDM-MFSK significantly and the upper bound of 1 $\frac{\text{bit/s}}{\text{Hz}}$ can be approached. This is without a substantial increase in complexity.

Because of the transmission based on subspaces and the combination of subspaces of different dimensions, an ML detection rule, based on the matrix variate complex-valued normal distribution will be derived. We will study the matrix variate probability density function for complex-valued receive matrices for the Rayleigh block fading channel, the AWGN channel and the Rayleigh frequency selective fading channel, and we will simplify it to an ML detection rule, where possible.

We will provide a criterion up to which dimension it is useful to combine subspaces of different dimensions and show an algorithm for a Gray mapping of the subspaces. Therefore, we briefly describe the distance criterion, which is the principal angle between any pair of subspaces.

The connection between the combined subspaces and the FSK vectors will be illustrated. The matrix variate PDF and the bivariate PDF are compared for this purpose. The shape of the multivariate PDF for a line and a plane is shown in a descriptive example.

Parts of this work have been published in [29] and [28].

3.1 OFDM-MFSK as a Subspace Based Transmission

The basis for the derivation of the connection between OFDM-N/MFSK and the noncoherent MIMO subspace transmission was laid in the work of Wetz in [44] and further developed in our work, presented in [29].

In Sec. 2.1, Eq. (2.1), a vector-valued transmission model in the frequency domain for a conventional OFDM transmission scheme is introduced where column vectors $\mathbf{x}$ are transmitted. As shown in Sec. 2.5, for a noncoherent detection in the receiver based on subspaces, transmit matrices $\mathbf{X}$ are required. To reach this goal, i.e. the representation of a transmit vector $\mathbf{x}$ of a conventional OFDM system as a transmit matrix $\mathbf{X}$, each column vector will be represented by a diagonal matrix.

$$\mathbf{X} = \begin{bmatrix} x_1 & 0 & \dots & 0 \\ 0 & x_2 & \dots & 0 \\ \dots & \dots & \dots & \dots \\ 0 & 0 & \dots & x_{N_f} \end{bmatrix},$$

where N_f represents the number of OFDM subcarriers and x_l, $l = 1, \dots, N_f$ are taken from a transmit symbol alphabet. Consequentially, the transmit vector alphabet changes to a transmit matrix alphabet consisting of a set of transmit matrices $\mathbf{X}_l = \mathrm{diag}(\mathbf{x}_l)$, where $\mathrm{diag}(\mathbf{x}_l)$ is the function, which transforms the transmit vector $\mathbf{x}_l$ to a diagonal transmit matrix $\mathbf{X}$. It is now possible to rewrite the vector-valued transmission model for a conventional OFDM transmission (c.f. Eq. (2.1))

$$\mathbf{y} = \mathbf{H}\mathbf{x} + \mathbf{n}$$

with matrices, resulting in

$$\mathbf{Y} = \mathbf{H}\mathbf{X} + \mathbf{N}.$$

It is important to notice, that $\mathbf{X}$, $\mathbf{Y}$ and $\mathbf{N}$ have become diagonal matrices of dimension $N_f \times N_f$. The resulting matrix-valued transmission model corresponds to Eq. (2.19), on which the subspace based transmission, explained in Sec. 2.5, is built upon. The channel matrix $\mathbf{H}$ remains unchanged. For the

special case of OFDM-N/MFSK, it is here also possible, to regard the FSK block matrices of size $M \times M$ independently from each other

$$\begin{bmatrix} x_1 & 0 & \cdots & 0 \\ 0 & \ddots & & \vdots \\ \vdots & & \ddots & 0 \\ 0 & 0 & 0 & x_M \end{bmatrix},$$

instead of taking the matrix for the whole OFDM block of dimension $N_f \times N_f$ into account. In Sec. 2.3, it was shown, that OFDM-1/MFSK and its multitone variant OFDM-N/MFSK are based on transmitting column vectors. In case of OFDM-1/4FSK, the transmit vectors $\mathbf{x}_l$, $l = 1, \ldots, M = 4$ are chosen from the transmit vector alphabet

$$A_{1/4\text{FSK}} = \left\{ \begin{bmatrix} 0 \\ 0 \\ 0 \\ 1 \end{bmatrix}, \begin{bmatrix} 0 \\ 0 \\ 1 \\ 0 \end{bmatrix}, \begin{bmatrix} 0 \\ 1 \\ 0 \\ 0 \end{bmatrix}, \begin{bmatrix} 1 \\ 0 \\ 0 \\ 0 \end{bmatrix} \right\}.$$

For the subspace based representation of OFDM-N/MFSK, transmit matrices $\mathbf{X}_l$ and their corresponding receive matrices $\mathbf{Y}_l$, as well as noise matrices $\mathbf{N}$ are needed. In the case of OFDM-N/MFSK these matrices are $M \times M$-dimensional matrices, since M defines the number of subcarriers within one FSK block and M also defines the dimension of the space. In case of OFDM-1/4FSK, the new transmit matrix alphabet is

$$A_{1/4_{\text{FSK}}} = \left\{ \begin{bmatrix} 0 & 0 & 0 & 0 \\ 0 & 0 & 0 & 0 \\ 0 & 0 & 0 & 0 \\ 0 & 0 & 0 & 1 \end{bmatrix}, \begin{bmatrix} 0 & 0 & 0 & 0 \\ 0 & 0 & 0 & 0 \\ 0 & 0 & 1 & 0 \\ 0 & 0 & 0 & 0 \end{bmatrix}, \begin{bmatrix} 0 & 0 & 0 & 0 \\ 0 & 1 & 0 & 0 \\ 0 & 0 & 0 & 0 \\ 0 & 0 & 0 & 0 \end{bmatrix}, \begin{bmatrix} 1 & 0 & 0 & 0 \\ 0 & 0 & 0 & 0 \\ 0 & 0 & 0 & 0 \\ 0 & 0 & 0 & 0 \end{bmatrix} \right\}.$$

Obviously, the frequencies are now on the main diagonal of the transmit matrices $\mathbf{X}_l$, $l = 1, \ldots, \binom{M}{N}$. For illustrating purposes, the frequency positions are colored in blue. The frequencies of the OFDM subcarriers of the FSK block of size M are now represented by the scalar entries x_{ll}, $l = 1, \ldots, M$ on the main diagonal of the corresponding matrix. In general, the transmit

matrix alphabet could be created by

$$A = \left\{ \mathrm{diag}(\mathbf{x}_l) \,|\, \mathbf{x}_l \in A_{\mathrm{N/MFSK}},\, l = 1, \ldots, \binom{M}{N} \right\}.$$

$\mathrm{diag}(\mathbf{x})$ is the function, which transforms a vector $\mathbf{x}$ to a diagonal matrix $\mathbf{X}$, with the subcarrier frequencies on the main diagonal of the matrix $\mathbf{X}$. One important condition for transmitting subspaces within the MIMO context is, that the number of the transmit antennas M_{tx}, defining the dimension of the subspace, has to be smaller than the number of time-slots T, defining the dimension of the space. For the vector-valued OFDM-N/MFSK transmission model it is obvious, that if rewriting the transmit vectors to transmit matrices, this necessary condition is not fulfilled. From now on, we restrict ourselves to the case of pure OFDM-1/MFSK and its multitone variant, where M defines the dimension of the space and $M \times M$ transmit matrices $\mathbf{X}_l$, $l = 1, \ldots, \binom{M}{N}$ are used. To transmit subspaces, at least one row has to be zero or linearly dependent of the other $M - 1$ rows (c.f. Sec. 2.5). For OFDM-N/MFSK this is always true, since at most $M - 1$ subcarriers out of M subcarriers per FSK block could be chosen for transmission, c.f. Sec. 2.3. By transforming the transmit vectors $\mathbf{x}_l$ into diagonal matrices $\mathbf{X}_l$, an artificial degree of freedom is added. The OFDM subcarriers are on the main diagonal, whereas the off-diagonal entries are zero. These off-diagonal zeros are "artificial", since they do not exist within the OFDM transmission model. For any OFDM-N/MFSK transmit matrix alphabet, subspaces, i.e. lines or planes are obtained, since N of the row vectors are linearly independent and define a basis of a N-dimensional subspace. Since $M - N$ rows are the $\mathbf{0}$ vector of dimension $1 \times M$, they are linearly dependent. In the case of OFDM-N/MFSK, the resulting row vectors within the matrices are always orthogonal vectors. An example is the following matrix

$$\begin{bmatrix} 1 & 0 & 0 & 0 \\ 0 & 0 & 0 & 0 \\ 0 & 0 & 1 & 0 \\ 0 & 0 & 0 & 0 \end{bmatrix},$$

which represents the column vector $\begin{bmatrix} 1 & 0 & 1 & 0 \end{bmatrix}^T$ of the OFDM-2/4FSK alphabet and which represents now a $N = 2$–dimensional subspace of the

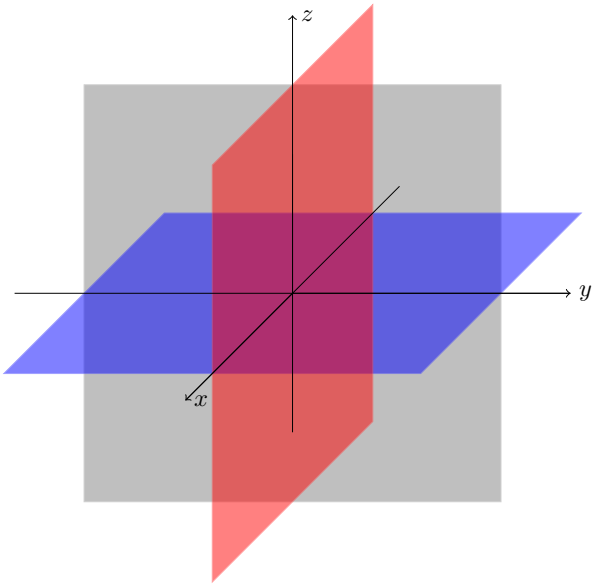

Figure 3.1: Illustrating example: OFDM-2/3FSK. Three 2-dimensional subspaces of the 3-dimensional real-valued space $\mathbb{R}^3$ are shown.

$M = 4$–dimensional space.

Fig. 3.1 illustrates an example of 2-dimensional subspaces of the 3-dimensional real-valued vector space $\mathbb{R}^3$. This corresponds to an OFDM-2/3FSK alphabet, where $N = 2$ out of $M = 3$ subcarriers are selected. Note, that this is just an example to visualize the subspace based representation of OFDM-N/MFSK.

The transmit matrix alphabet is

$$A_{2/3\text{FSK}} = \left\{ \begin{bmatrix} 1 & 0 & 0 \\ 0 & 1 & 0 \\ 0 & 0 & 0 \end{bmatrix}, \begin{bmatrix} 1 & 0 & 0 \\ 0 & 0 & 0 \\ 0 & 0 & 1 \end{bmatrix}, \begin{bmatrix} 0 & 0 & 0 \\ 0 & 1 & 0 \\ 0 & 0 & 1 \end{bmatrix} \right\}$$

and represents three orthogonal, 2-dimensional planes of the 3-dimensional

space. Note, that the three planes are orthogonal in the sense, that they form a right angle, but they are not orthogonal subspaces, since they intersect in more points than the origin [6], [20], [36].

3.2 Combining Subspaces of Different Dimensions

So far, we have shown in the previous section, that pure OFDM-1/MFSK and OFDM multitone FSK are special cases of the more general approach for MIMO systems based on subspaces. For the MIMO transmission scenarios, there usually exist two assumptions: All the subspaces have the same dimension and their corresponding complex-valued matrices are in general assumed to be unitary, see Hochwald and Marzetta, as well as Ashikhmin et al. in [19] and in [2] for example. There exists one obvious reason for this restriction, since every subspace of a lower dimension is included within a subspace of higher dimension. Fig. 3.2 illustrates in an example a plane, which is a 2-dimensional subspace of the 3-dimensional space, and two lines, which are 1-dimensional subspaces of the 3-dimensional space and which are also a subspace of the plane.

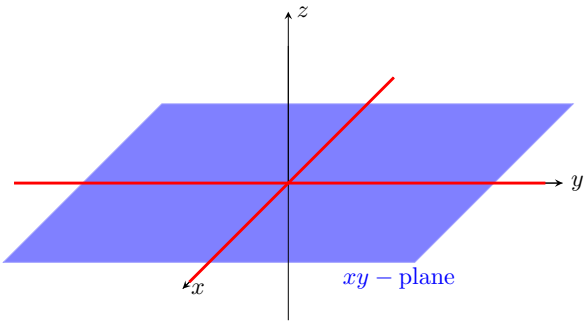

Figure 3.2: Subspaces of different dimensions in the 3-dimensional space.

A possibility of combining subspaces of different dimensions would be ap-

preciable to exploit the available total mathematical space in a better way. In the following, we will show how to combine subspaces of different dimensions in case of OFDM-N/MFSK. This scheme is called combined OFDM-N/MFSK, in short OFDM-COM-N/MFSK.

A combination of subspaces of different dimensions results in an increase in the size of the transmit matrix alphabet A. For different combinations of OFDM-N/MFSK the new transmit matrix alphabet becomes

$$A = \bigcup_{N=1}^{M/2} A_{\mathrm{N/MFSK}}, \tag{3.1}$$

i.e. the union of the transmit alphabets $A_{1/\mathrm{MFSK}}$ up to $A_{\frac{\mathrm{M}}{2}/\mathrm{MFSK}}$ is the new set of transmit matrices. It is of course possible to combine the subspaces beyond $\frac{M}{2}$. However, there exist drawbacks, which we work out at the end of Sec. 3.5. If not stated otherwise, we will use the expression OFDM-COM-N/MFSK for $\bigcup_{N=1}^{M/2} \mathrm{OFDM-N/MFSK}$, i.e. subspaces of different dimensions are combined up to the dimension $\frac{M}{2}$.

Fig. 3.3 shows an example for the purpose of illustration of subspaces in the 3-dimensional space. Neglecting the fact, that we have an odd dimension of three, three one-dimensional lines and three two-dimensional planes are obtained. The transmit matrix alphabet consists now of six different matrices, which could be chosen for transmission. The new transmit matrix alphabet becomes

$$A_{1/3\mathrm{FSK}\cup 2/3\mathrm{FSK}} = \left\{ \begin{bmatrix} 1 & 0 & 0 \\ 0 & 0 & 0 \\ 0 & 0 & 0 \end{bmatrix}, \begin{bmatrix} 0 & 0 & 0 \\ 0 & 1 & 0 \\ 0 & 0 & 0 \end{bmatrix}, \begin{bmatrix} 0 & 0 & 0 \\ 0 & 0 & 0 \\ 0 & 0 & 1 \end{bmatrix}, \begin{bmatrix} 1 & 0 & 0 \\ 0 & 1 & 0 \\ 0 & 0 & 0 \end{bmatrix}, \begin{bmatrix} 1 & 0 & 0 \\ 0 & 0 & 0 \\ 0 & 0 & 1 \end{bmatrix}, \begin{bmatrix} 0 & 0 & 0 \\ 0 & 1 & 0 \\ 0 & 0 & 1 \end{bmatrix} \right\}.$$

The lines and the planes are spanned by a set of three row vectors, which are the basis vectors of the 3-dimensional space $\left\{ \begin{bmatrix} 1 & 0 & 0 \end{bmatrix}, \begin{bmatrix} 0 & 1 & 0 \end{bmatrix}, \begin{bmatrix} 0 & 0 & 1 \end{bmatrix} \right\}$.

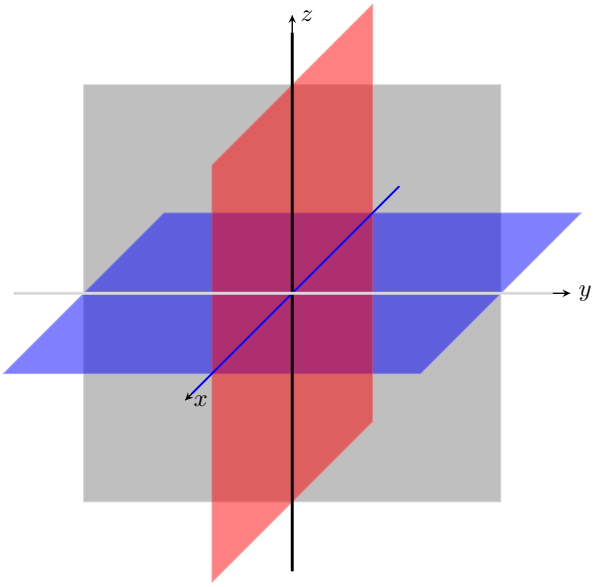

Figure 3.3: Subspaces of different dimensions in the 3-dimensional space. The x-,y- and z-axis of the 3-dimensional space, colored in blue, gray and black represent three lines, i.e. 1-dimensional subspaces. The planes, colored in light blue, light gray and light red are the 2-dimensional subspaces of the 3-dimensional space.

Compared to pure OFDM-1/MFSK or OFDM multitone FSK, the modulation principle in frequency domain, as shown in Fig. 2.3 does not change significantly. Instead of choosing one or N subcarriers respectively for each FSK block of size M for transmission, different amounts of subcarriers per FSK block are now chosen for transmission. The number of selected subcarriers corresponds to the dimension of the subspace. In the case of a FSK block size of $M = 4$, Fig. 3.4 shows this in an example for the COM-N/4FSK alphabet.

The corresponding transmit matrix alphabet for OFDM-COM-N/4FSK with-

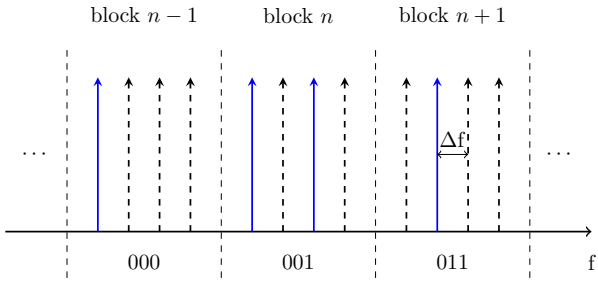

Figure 3.4: Basic principle of OFDM-COM-N/4FSK modulation. Blue solid line: power on the subcarrier, black dashed line: empty subcarrier, Δf: subcarrier spacing.

out any energy normalization is

$$
\begin{aligned}
A_{\mathrm{COM-N/4FSK}} = \Bigg\{ & \begin{bmatrix} 1&0&0&0\\0&0&0&0\\0&0&0&0\\0&0&0&0 \end{bmatrix}, \begin{bmatrix} 0&0&0&0\\0&1&0&0\\0&0&0&0\\0&0&0&0 \end{bmatrix}, \begin{bmatrix} 0&0&0&0\\0&0&0&0\\0&0&1&0\\0&0&0&0 \end{bmatrix}, \\
& \begin{bmatrix} 0&0&0&0\\0&0&0&0\\0&0&0&0\\0&0&0&1 \end{bmatrix}, \begin{bmatrix} 1&0&0&0\\0&1&0&0\\0&0&0&0\\0&0&0&0 \end{bmatrix}, \begin{bmatrix} 1&0&0&0\\0&0&0&0\\0&0&1&0\\0&0&0&0 \end{bmatrix}, \\
& \begin{bmatrix} 1&0&0&0\\0&0&0&0\\0&0&0&0\\0&0&0&1 \end{bmatrix}, \begin{bmatrix} 0&0&0&0\\0&1&0&0\\0&0&1&0\\0&0&0&0 \end{bmatrix} \begin{bmatrix} 0&0&0&0\\0&1&0&0\\0&0&0&0\\0&0&0&1 \end{bmatrix}, \\
& \begin{bmatrix} 0&0&0&0\\0&0&0&0\\0&0&1&0\\0&0&0&1 \end{bmatrix} \Bigg\}.
\end{aligned}
$$

For comparison, the transmit vector alphabet is

$$A_{\mathrm{COM-N/4FSK}} = \left\{ \begin{bmatrix}1\\0\\0\\0\end{bmatrix}, \begin{bmatrix}0\\1\\0\\0\end{bmatrix}, \begin{bmatrix}0\\0\\1\\0\end{bmatrix}, \begin{bmatrix}0\\0\\0\\1\end{bmatrix}, \begin{bmatrix}1\\1\\0\\0\end{bmatrix}, \begin{bmatrix}1\\0\\1\\0\end{bmatrix}, \begin{bmatrix}1\\0\\0\\1\end{bmatrix}, \begin{bmatrix}0\\1\\1\\0\end{bmatrix}, \begin{bmatrix}0\\1\\0\\1\end{bmatrix}, \begin{bmatrix}0\\0\\1\\1\end{bmatrix} \right\}.$$

It is obvious, that there are now ten subspaces and eight out of ten have to be chosen for transmitting $m = \log_2 8 = 3$ bits per FSK block of size $M = 4$. The question now is: Which subspaces should be chosen for transmission? We will address this topic within Sec. 3.5.

3.3 Increased Bandwidth Efficiency of Combined OFDM-N/MFSK

The possibility of combining subspaces of different dimensions leads to an increased bandwidth efficiency of OFDM-COM-N/MFSK and is the main contribution of this thesis. The number of bits per subspace is

$$\left\lfloor \log_2 \left[\sum_{N=1}^{\frac{M}{2}} \binom{M}{N} \right] \right\rfloor = M - 1. \tag{3.2}$$

In Sec. 2.3, the upper bound for the bandwidth efficiency $\eta_{1/\mathrm{MFSK}}$ of pure OFDM-1/MFSK, Eq. (2.5), is

$$\eta_{1/\mathrm{MFSK}} = \frac{\log_2 M}{M}$$

and for OFDM multitone FSK, $N > 1$, c.f. Eq. (2.6), the upper bound becomes

$$\eta_{\mathrm{N/MFSK}} = \frac{\left\lfloor \log_2 \binom{M}{N} \right\rfloor}{M}.$$

For OFDM-COM-N/MFSK, the bandwidth efficiency $\eta_{\mathrm{COM-N/MFSK}}$ is defined by

$$\eta_{\mathrm{COM-N/MFSK}} = \frac{\left\lfloor \log_2 \left[\sum_{N=1}^{M/2} \binom{M}{N} \right] \right\rfloor}{M} = \frac{M-1}{M}. \tag{3.3}$$

Eq. 3.3 shows, that by combining different alphabets up to the dimension $\frac{M}{2}$, the bandwidth efficiency $\eta_{\mathrm{COM-N/MFSK}}$ increases remarkably, since the numerator now increases linearly with the dimension M. It is of course possible to combine subspaces beyond $\frac{M}{2}$, however it turned out, that the combination up to $\frac{M}{2}$ is an effective way of combining subspaces, c.f. Sec. 3.5. It can be also observed, that for an increasing FSK block size M, i.e. for an increasing dimension of the space, the upper bound of the bandwidth efficiency of 1 $\frac{\mathrm{bit/s}}{\mathrm{Hz}}$ is approached.

Table 3.1 shows the increased bandwidth efficiency for different OFDM-N/MFSK and OFDM-COM-N/MFSK schemes. The modulation schemes are ordered according to the increase in bandwidth efficiency. In the column "Number of vectors/matrices" of Table 3.1 the set of the total available amount of vectors/subspaces is presented. However, for calculating the bandwidth efficiency in the last column of Table 3.1, only 2^{M-1} vectors/subspaces out of the set of the available vectors/subspaces are used, since this number corresponds to the effectively number of used vectors/subspaces for transmission. This means, that the bandwidth efficiency is round down.

We also added COM-N/4FSK/15, where all subspaces of the $M = 4$-dimensional space, including the 4-dimensional space itself and excluding the null space, i.e. the all zero matrix, are used. This is indicated by the writing "/15", since 15 subspaces are obtained. It can be seen, that 3.9069 bits per FSK block of size $M = 4$ can be transmitted and a bandwidth efficiency of 0.9767 $\frac{\mathrm{bit/s}}{\mathrm{Hz}}$ is achieved. The upper bound in bandwidth efficiency for OFDM-MFSK in general is 1 $\frac{\mathrm{bit/s}}{\mathrm{Hz}}$.

It is obvious, that for OFDM-COM-N/4FSK, a remarkable increase in bandwidth efficiency is obtained. Since 8 out of 10 vectors/subspaces are used, three bits per FSK block of size $M = 4$ can be transmitted, leading to a bandwidth efficiency of 0.75 $\frac{\mathrm{bit/s}}{\mathrm{Hz}}$. A bandwidth efficiency of 0.75 $\frac{\mathrm{bit/s}}{\mathrm{Hz}}$ is also achieved for OFDM-4/8FSK, but with a higher effort, since from 70 available subspaces, $2^6 = 64$ subspaces have to be chosen. It is obvious, that the complexity of COM-N/4FSK is less, compared to 4/8FSK, since only eight out of ten subspaces are needed to achieve the same bandwidth efficiency.

If OFDM-7/16FSK, which has a bandwidth efficiency of $0.8125\,\frac{\text{bit/s}}{\text{Hz}}$, is compared to OFDM-COM-N/8FSK, which has a bandwidth efficiency of $0.875\,\frac{\text{bit/s}}{\text{Hz}}$, we can see, that OFDM-COM-N/8FSK has the higher spectral efficiency for less effort, since 7 bits are transmitted per FSK block of size $M = 8$ and therefore only 128 subspaces (from 162 available subspaces) are needed. For OFDM-7/16FSK $8196 = 2^{13}$ subspaces out of 11440 available subspaces have to be chosen to achieve a lower bandwidth efficiency with a much higher realization effort.

Our proposal of combined subspaces turns out to be an efficient possibility to increase the bandwidth efficiency of OFDM-MFSK remarkably, without a noteworthy increase in the complexity of the system. To achieve the same bandwidth efficiency with multitone FSK, which uses subspaces of the same dimension, more subspaces are needed, as it can be seen in Tab. 3.1.

Furthermore, it can be seen, that for an increased FSK block size, the combined alphabet tends to reach an upper bound of $1\,\frac{\text{bit/s}}{\text{Hz}}$. Detailed simulation results for the AWGN channel, the Rayleigh block fading channel and the Rayleigh frequency selective fading channel will be shown in Chapter 4.

Table 3.1: Comparison of the number of transmitted bits per FSK block and the bandwidth efficiency in $\frac{\text{bit/s}}{\text{Hz}}$ for different OFDM-N/MFSK and OFDM-COM-N/MFSK modulation schemes.

Modulation scheme	Number of vectors/matrices	Bits per FSK block $\left\lfloor \log_2 \left[\sum_{N=1}^{M/2} \binom{M}{N} \right] \right\rfloor$	Bandwidth efficiency
1/16FSK	16	4	0.25
1/8FSK	8	3	0.375
2/16FSK	120	6	0.375
1/4FSK	4	2	0.5
2/4FSK	6	2	0.5

Table 3.1: Comparison of the number of transmitted bits per FSK block and the bandwidth efficiency in $\frac{\text{bit/s}}{\text{Hz}}$ for different OFDM-N/MFSK and OFDM-COM-N/MFSK modulation schemes.

Modulation scheme	Number of vectors/matrices	Bits per FSK block $\left\lfloor \log_2 \left[\sum_{N=1}^{M/2} \binom{M}{N} \right] \right\rfloor$	Bandwidth efficiency
2/8FSK	28	4	0.5
3/16FSK	560	9	0.5625
3/8FSK	56	5	0.625
4/16FSK	1820	10	0.625
COM-N/4FSK	10	3	0.75
4/8FSK	70	6	0.75
5/16FSK	4368	12	0.75
6/16FSK	8008	12	0.75
7/16FSK	11440	13	0.8125
8/16FSK	12870	13	0.8125
COM-N/8FSK	162	7	0.875
COM-N/16FSK	39202	15	0.9375
COM-N/32FSK	$\sum_{N=1}^{16} \binom{32}{N}$	31	0.9688
COM-N/4FSK/15	15	3.9069	0.9767
COM-N/64FSK	$\sum_{N=1}^{32} \binom{64}{N}$	63	0.9844

3.4 Detection of Subspaces

So far we have shown, that it is also possible to combine different OFDM-N/MFSK alphabets, mathematically resulting in a combination of subspaces

of different dimensions. The matrix-valued transmission model

$$\mathbf{Y} = \mathbf{H}\mathbf{X} + \mathbf{N} \tag{3.4}$$

is our transmission model of interest. To derive an ML detection rule for a transmission based on subspaces, a matrix variate normal distribution is needed, which builds the starting point. This involves both cases, the subspaces of the same dimension as well as the combination of subspaces of different dimensions. The matrix variate Θ distribution of a matrix $\mathbf{Y}$ is defined by Gupta and Nagar in [14] and [15]

$$\begin{aligned} f(\mathbf{Y}) &= \frac{1}{\left(2\Gamma\left(1+\frac{1}{\Theta}\right)\right)^{MM}\det(\mathbf{A})^{M}\det(\mathbf{B})^{M}} \\ &\quad \exp\left\{-\sum_{i=1}^{M}\sum_{j=1}^{M}\left|\sum_{k=1}^{M}\sum_{l=1}^{M}A_{ik}^{-1}(Y_{kl}-E\left[Y_{kl}\right])B_{lj}^{-1}\right|^{\Theta}\right\}. \end{aligned} \tag{3.5}$$

$\mathbf{Y}$ is the $M \times M$ receive matrix and $\mathbf{A}$ and $\mathbf{B}$ are constant and nonsingular $M \times M$ matrices. The stepwise derivation of the PDF is presented in the Appendix B.

For $\Theta = 2$, the PDF in Eq. (B.1) is then the matrix variate normal distribution and [15] states for this case, that

$$\Gamma\left(1+\frac{1}{2}\right) = \frac{1}{2}\sqrt{\pi}. \tag{3.6}$$

The conditional matrix variate PDF for maximum-likelihood detection for a received matrix $\mathbf{Y}$, given a transmitted matrix $\mathbf{X}$, is

$$p(\mathbf{Y}|\mathbf{X}) = \frac{1}{(\pi)^{\frac{MM}{2}}\det(\mathbf{\Sigma})^{\frac{M}{2}}\det(\mathbf{\Phi})^{\frac{M}{2}}}\exp\left\{-\mathrm{tr}\left[\mathbf{Y}^{H}\mathbf{\Sigma}^{-1}\mathbf{Y}\mathbf{\Phi}^{-1}\right]\right\} \tag{3.7}$$

where $\mathbf{\Sigma}$ and $\mathbf{\Phi}$ are the among row covariance matrix and the among column covariance matrix, c.f. [10]. All matrices are square $M \times M$ matrices and

equiprobable transmit matrices $\mathbf{X}_k$ are assumed. It is possible to calculate $\mathbf{\Sigma}$ by

$$\begin{aligned}\mathbf{\Sigma} &= E\left[(\mathbf{Y}-E[\mathbf{Y}])(\mathbf{Y}-E[\mathbf{Y}])^H\right] \\ &= \left[\frac{E_s}{M}(\sigma_h^2-\mu_h^2)+\sigma_n^2\right]\mathbf{I}, \end{aligned} \tag{3.8}$$

E_s is the symbol energy divided by the FSK block size M. The complex-valued fading coefficients are normal distributed with zero mean ($\mu_h = 0$) and unit variance ($\sigma_h^2 = 1$). The complex-valued additive white Gaussian noise has zero mean and a two sided noise power spectral density of $\frac{N_0}{2}$.

The among column covariance matrix $\mathbf{\Phi}$ is defined by

$$\begin{aligned}\mathbf{\Phi} &= E\left[(\mathbf{Y}-E[\mathbf{Y}])^H(\mathbf{Y}-E[\mathbf{Y}])\right] \\ &= \mathbf{X}^H\mathbf{\Lambda}_h\mathbf{X}+\sigma_n^2\mathbf{I}-\mu_h^2\mathbf{X}^H\mathbf{X}, \end{aligned} \tag{3.9}$$

where $\mathbf{\Lambda}_h$ denotes the $M \times M$ covariance matrix of the channel.

In the following, we will derive the detection rules for the Rayleigh block fading channel as well as the Rayleigh frequency selective fading channel, as proposed in Sec. 2.2, for different modulation schemes, i.e. for N/MFSK as well as for COM-N/MFSK. Or in other words, the detection rule for subspaces of the same dimension as well as for subspaces of different dimensions will be derived.

3.4.1 Rayleigh Block Fading Channel

The conditional PDF for a matrix variate Gaussian distribution for a transmission over a Rayleigh block fading channel for detecting OFDM-N/MFSK and OFDM-COM-N/MFSK, is

$$p(\mathbf{Y}|\mathbf{X}) = \frac{1}{(\pi)^{\frac{MM}{2}}\det(\mathbf{\Sigma})^{\frac{M}{2}}\det(\mathbf{\Phi})^{\frac{M}{2}}}\exp\left\{-\sum_{k=1}^{M}\sum_{l=1}^{M}\left[\mathbf{Y}^H\mathbf{\Sigma}^{-1}\mathbf{Y}\mathbf{\Phi}^{-1}\right]\right\} \tag{3.10}$$

with $\mathbf{\Sigma}$ and $\mathbf{\Phi}$, as defined in Eq. (3.8) and Eq. (3.9), respectively. Eq. (3.10) has been slightly modified compared to Eq. (3.7), since the trace has been substituted by the double sum $\sum\sum$, which sums up all entries of the resulting matrix $\mathbf{Y}^H\mathbf{\Sigma}^{-1}\mathbf{Y}\mathbf{\Phi}^{-1}$. We will show in the following, why the entries of the resulting matrix have to be summed up.

For the Rayleigh Block Fading Channel, c.f. Sec. 2.2 the channel matrix $\mathbf{H}$ is defined by (2.4)

$$\mathbf{H} = h\,\mathbf{I}_{M\times M}.$$

The fading coefficient h, constant for one FSK block of size M, has zero mean, i.e. $\mu_h = 0$, and unit variance ($\sigma_h^2 = 1$). Therefore the fading coefficients on the main diagonal of the channel matrix are fully correlated, leading to an $M \times M$ channel covariance matrix $\mathbf{\Lambda}_h = \sigma_h^2\mathbf{1}$, i.e. the all ones matrix. For an energy normalized transmit matrix alphabet A, i.e. $\mathrm{tr}\{\mathbf{X}^H\mathbf{X}\} = 1$, the $M \times M$ among row covariance matrix $\mathbf{\Sigma}$ becomes

$$\mathbf{\Sigma} = \left[\frac{1}{M} + \sigma_n^2\right]\mathbf{I}, \tag{3.11}$$

$$\mathbf{\Sigma}^{-1} = \frac{1}{\frac{1}{M} + \sigma_n^2}\mathbf{I} \tag{3.12}$$

$$\text{and } \det(\mathbf{\Sigma}) = \left[\frac{1}{M} + \sigma_n^2\right]^M. \tag{3.13}$$

The $M \times M$ among column covariance matrix becomes

$$\mathbf{\Phi} = \mathbf{X}^H\mathbf{\Lambda}_h\mathbf{X} + \sigma_n^2\mathbf{I}. \tag{3.14}$$

$\mathbf{\Phi}$ cannot be inverted in general, since the application of the Sherman-Morrison-Woodbury formula [12] or any other inversion lemma leads to no solution. However, since the transmit matrices $\mathbf{X}$ have the special property of being transformed column vectors $\mathbf{x}$,

$$\mathbf{X}^H\mathbf{\Lambda_h}\mathbf{X}$$

is identical to the dyadic product

$$\mathbf{x}\mathbf{x}^H \tag{3.15}$$

of the corresponding column vector $\mathbf{x} = \mathrm{diag}(\mathbf{X})$. Substituting $\mathbf{X}^H \mathbf{\Lambda}_h \mathbf{X}$ by the dyadic product of the vector $\mathbf{x}$ in (3.15), we obtain

$$\mathbf{\Phi} = \mathbf{x}\mathbf{x}^H + \sigma_n^2 \mathbf{I}. \tag{3.16}$$

Note, that the matrix variate normal distribution in general uses the trace instead of the double sum, c.f. [15] and [14]. However, for the Rayleigh block fading channel in Sec. 2.2, this model is no longer valid. Under the trace, if we only consider the part of the among column covariance matrix coming from the channel, information is lost. Therefore, we have to sum over the whole matrix to take into account all available information, which is outside the main diagonal. Since the determinant of $\mathbf{\Lambda}_h$ is zero, it is not invertible and as soon as subspaces of dimension 2 or higher are used, off-diagonal entries for the dyadic product occur. As mentioned before, these entries are needed for the right decision, since we want to maximize over the conditional probability density function and

$$\mathrm{tr}\{\mathbf{X}^H \mathbf{\Lambda}_h \mathbf{X}\} = \mathrm{tr}\{\mathbf{x}\mathbf{x}^H\} \underset{\{N \geq 2\}}{<} \sum_{k=1}^{M} \sum_{l=1}^{M} \mathbf{x}\mathbf{x}^H. \tag{3.17}$$

As shown in [44], it is now possible to apply the Sherman-Morrison-Woodbury formula [12] and

$$\begin{aligned} \mathbf{\Phi}^{-1} &= \left[\mathbf{x}\mathbf{x}^H + \sigma_n^2 \mathbf{I}\right]^{-1} \\ &= \frac{1}{\sigma_n^2}\mathbf{I} - \frac{1}{\sigma_n^2}\mathbf{I}\mathbf{x}\left(\mathbf{I} + \mathbf{x}^H \frac{1}{\sigma_n}^2 \mathbf{I}\mathbf{x}\right)^{-1} \mathbf{x}^H \frac{1}{\sigma_n^2}\mathbf{I} \\ &= \frac{1}{\sigma_n^2}\mathbf{I} - \frac{1}{\sigma_n^4\left(1 + \frac{1}{\sigma_n^2}\mathbf{x}^H\mathbf{x}\right)}\mathbf{x}\mathbf{x}^H \end{aligned} \tag{3.18}$$

The determinant of $\mathbf{\Phi}$ becomes

$$\begin{aligned} \det(\mathbf{\Phi}) &= \det\left(\mathbf{x}\mathbf{x}^H + \sigma_n^2 \mathbf{I}\right) \\ &= \sigma_n^{2M} \det\left(\frac{1}{\sigma_n^2}\mathbf{x}\mathbf{x}^H + \mathbf{I}\right) \\ &= \sigma_n^{2M}\left(1 + \frac{1}{\sigma_n^2}\mathbf{x}^H\mathbf{x}\right). \end{aligned} \tag{3.19}$$

Setting $\mathbf{\Sigma}^{-1}$, $\det \mathbf{\Sigma}$, $\mathbf{\Phi}^{-1}$ and $\det \mathbf{\Phi}$ in Eq. (3.10), results in

$$\begin{aligned} p(\mathbf{Y}|\mathbf{X}) &= \frac{1}{(\pi)^{\frac{MM}{2}} \det(\mathbf{\Sigma})^{\frac{M}{2}} \det(\mathbf{\Phi})^{\frac{M}{2}}} \exp\left\{ -\sum_{k=1}^{M}\sum_{l=1}^{M} \left[\mathbf{Y}^H \mathbf{\Sigma}^{-1} \mathbf{Y} \mathbf{\Phi}^{-1}\right] \right\} \\ &= \frac{1}{(\pi)^{\frac{MM}{2}} \left(\frac{1}{M}+\sigma_n^2\right)^{\frac{MM}{2}} \left(\sigma_n^{2M}(1+\frac{\mathbf{x}^H\mathbf{x}}{\sigma_n^2})\right)^{\frac{M}{2}}} \\ &\quad \exp\left\{ -\sum_{k=1}^{M}\sum_{l=1}^{M} \left[\mathbf{Y}^H \frac{1}{\frac{1}{M}+\sigma_n^2} \mathbf{I} \mathbf{Y} \left(\frac{1}{\sigma_n^2}\mathbf{I} - \frac{1}{\sigma_n^4(1+\frac{\mathbf{x}^H\mathbf{x}}{\sigma_n^2})} \mathbf{x}\mathbf{x}^H \right) \right] \right\}. \end{aligned} \tag{3.20}$$

This can be further simplified

$$\begin{aligned} \hat{\mathbf{x}} &= \underset{\mathbf{x}_p \in \{\mathbf{x}_1,\cdots,\mathbf{x}_P\}}{\operatorname{argmax}} \underbrace{\frac{1}{\frac{1}{M}+\sigma_n^2} \frac{1}{\sigma_n^4(1+\frac{\mathbf{x}_p^H\mathbf{x}_p}{\sigma_n^2})}}_{=c} \sum_{k=1}^{M}\sum_{l=1}^{M} \left[\mathbf{Y}^H \mathbf{Y} \mathbf{x}_p \mathbf{x}_p^H\right]_{k,l} \\ &= \underset{\mathbf{x}_p \in \{\mathbf{x}_1,\cdots,\mathbf{x}_P\}}{\operatorname{argmax}} c \left| \sum_{k=1}^{M}\sum_{l=1}^{M} \left[\underbrace{\mathbf{Y}^H}_{=\operatorname{diag}(\mathbf{y}^H)} \mathbf{x}_p \right]_{k,l} \right|^2 \\ &= \underset{\mathbf{x}_p \in \{\mathbf{x}_1,\cdots,\mathbf{x}_P\}}{\operatorname{argmax}} c \left|\mathbf{y}^H \mathbf{x}_p\right|^2 \\ &= \underset{\mathbf{x}_p \in \{\mathbf{x}_1,\cdots,\mathbf{x}_P\}}{\operatorname{argmax}} \left|\mathbf{y}^H \mathbf{x}_p\right|^2, \end{aligned} \tag{3.21}$$

which is the squared scalar product of the vectors $\mathbf{y}$ and $\mathbf{x}$, and $\hat{\mathbf{x}}$ is the detected transmit vector. This result has been already derived in [44] for pure OFDM-MFSK and has now also become the ML detection rule for transmitting subspaces of the same dimension or of different dimensions for transmission over the Rayleigh block fading channel. We have shown the connection between the transmission based on matrices and the transmission based on vectors and we can conclude now, that it is also possible to use the combined alphabet for the vector-valued transmission model for a transmission over a Rayleigh block fading channel and detect it with the squared scalar product.

AWGN

The ML detection rule for the AWGN channel turns out to be the same as for the block fading channel. This is true, since we assume an unknown phase φ, which is the same for all subcarriers, as defined in [44]. The channel matrix for the whole OFDM block is $\mathbf{H} = \mathbf{I}\exp\{j\varphi\}$. Therefore, the values of the channel covariance matrix $\mathbf{\Lambda}_h$ are fully correlated and $\mathbf{\Lambda}_h = \mathbf{1}$. Consequentially, the derivations, made for the Rayleigh block fading channel in the previous subsection, can be used without any changes.

3.4.2 Rayleigh Frequency Selective Fading Channel

For a Rayleigh frequency selective fading channel, as described in Sec. 2.2, the channel matrix

$$\mathbf{H} = \begin{bmatrix} h_{11} & 0 & \cdots & 0 \\ 0 & h_{22} & 0 & \vdots \\ \vdots & \cdots & \ddots & \vdots \\ 0 & \cdots & \cdots & h_{MM} \end{bmatrix} \tag{3.22}$$

has fading coefficients on its main diagonal with zero mean ($\mu_h = 0$) and unit variance ($\sigma_h^2 = 1$). The fading coefficients are not correlated at all and therefore the $M \times M$ channel covariance matrix is

$$\mathbf{\Lambda}_h = \sigma_h^2 \mathbf{I}.$$

This results for an energy normalized alphabet A in the same among row covariance matrix $\mathbf{\Sigma}$ (c.f. Eq. (3.13)) as for the transmission over a Rayleigh block fading channel. The $M \times M$ among column covariance matrix becomes

$$\mathbf{\Phi} = \mathbf{X}^H \mathbf{I} \mathbf{X} + \sigma_n^2 \mathbf{I}. \tag{3.23}$$

Inverting $\mathbf{\Phi}$ using the Sherman-Morrison-Woodbury formula [12] yields

$$\mathbf{\Phi}^{-1} = \frac{1}{\sigma_n^2}\mathbf{I} - \frac{1}{\sigma_n^2}\mathbf{I}\mathbf{X}\left(\mathbf{I} + \mathbf{X}^H \frac{1}{\sigma_n^2}\mathbf{I}\mathbf{X}\right)^{-1} \mathbf{X}^H \frac{1}{{\sigma_\mathbf{n}}^2}\mathbf{I}$$

$$
\begin{aligned}
&= \frac{1}{\sigma_n^2}\mathbf{I} - \frac{1}{\sigma_n^4}\mathbf{X}\left(\mathbf{I} + \frac{1}{\sigma_n^2}\mathbf{X}^H\mathbf{X}\right)^{-1}\mathbf{X}^H \\
&= \frac{1}{\sigma_n^2}\mathbf{I} - \frac{1}{\sigma_n^4}\mathbf{X}\underbrace{\begin{bmatrix} \frac{1}{1+\frac{1}{\sigma_n^2}x_{11}^* x_{11}} & 0 & \cdots & \cdots & 0 \\ 0 & \frac{1}{1+\frac{1}{\sigma_n^2}x_{22}^* x_{22}} & 0 & \cdots & \vdots \\ \vdots & \ddots & \ddots & \ddots & \vdots \\ 0 & \cdots & \cdots & \cdots & \frac{1}{1+\frac{1}{\sigma_n^2}x_{MM}^* x_{MM}} \end{bmatrix}}_{=\mathbf{C}}\mathbf{X}^H \\
&= \frac{1}{\sigma_n^2}\mathbf{I} - \frac{1}{\sigma_n^4}\mathbf{C}\mathbf{X}\mathbf{X}^H.
\end{aligned}
\tag{3.24}
$$

The matrix $\mathbf{C}$ is an $M \times M$ diagonal matrix, which contains the value 1 for $x_{kk}^* x_{kk} = 0$, i.e. the corresponding frequency is inactive. For an active frequency position k, $[\mathbf{C}]_{kk}$ has the value $\frac{1}{1+\frac{1}{\sigma_n^2}x_{kk}^* x_{kk}}$. The matrices can be permuted, since all matrices are diagonal matrices. The determinant of $\mathbf{\Phi}$ becomes

$$
\begin{aligned}
\det\mathbf{\Phi} &= \det\left(\mathbf{X}\,\mathbf{I}\,\mathbf{X}^H + \sigma_n^2\mathbf{I}\right) \\
&= \left(x_{kk}x_{kk}^* + \sigma_n^2\right)^N \left(\sigma_n^2\right)^{M-N},
\end{aligned}
\tag{3.25}
$$

where the first term consists of the entries for non-zero x_{kk}, i.e. the active subcarriers. M denotes the dimension of the space (the FSK block size) and N denotes the dimension of the subspace, i.e. the number of active subcarriers per FSK block of size M. Inserting $\mathbf{\Sigma}^{-1}$, $\det\mathbf{\Sigma}$, $\mathbf{\Phi}^{-1}$ and $\det\mathbf{\Phi}$ into Eq. (3.7),

$$
\begin{aligned}
p(\mathbf{Y}|\mathbf{X}) &= \frac{1}{(\pi)^{\frac{MM}{2}}\left(\frac{1}{M}+\sigma_n^2\right)^M \left(x_{kk}^* x_{kk} + \sigma_n^2\right)^N \left(\sigma_n^2\right)^{M-N}} \\
&\qquad \exp\left\{-\mathrm{tr}\left[\mathbf{Y}^H\left(\frac{1}{\frac{1}{M}+\sigma_n^2}\right)\mathbf{Y}\left(\frac{1}{\sigma_n^2}\mathbf{I} - \frac{1}{\sigma_n^4}\mathbf{C}\mathbf{X}\mathbf{X}^H\right)\right]\right\}
\end{aligned}
\tag{3.26}
$$

is obtained as the conditional PDF for a Rayleigh frequency selective fading channel. Two cases have to be distinguished now, subspaces of the same di-

mension and the combination of subspaces of different dimensions.

If subspaces of the same dimension are transmitted, the diagonal entries on the matrix $\mathbf{C}$ in Eq. (3.24) can be reduced to the constant $c = \frac{1}{1+\frac{1}{\sigma_n^2} x_{kk}^* x_{kk}}$, $x_{kk} \neq 0$. Since the entries c_{kk} of $\mathbf{C}$ are multiplied on $\mathbf{X}\mathbf{X}^H$, which has N active and $M-N$ inactive frequency positions, only the entries $\frac{1}{1+\frac{1}{\sigma_n^2} x_{kk}^* x_{kk}}$ are contributing. They are the entries multiplied on the active subcarriers and they are all the same. The PDF in (3.26) can now be further simplified to

$$\begin{aligned}
\hat{\mathbf{X}} &= \underset{\mathbf{X}_k \in \{\mathbf{X}_1, \cdots, \mathbf{X}_K\}}{\operatorname{argmax}} \frac{1}{(\pi)^{\frac{MM}{2}} \left(\frac{1}{M} + \sigma_n^2\right)^M \left(x_{kk} x_{kk} + \sigma_n^2\right)^N \left(\sigma_n^2\right)^{M-N}} \\
&\qquad \exp\left\{-\operatorname{tr}\left[\mathbf{Y}^H \left(\frac{1}{\frac{1}{M} + \sigma_n^2}\right) \mathbf{Y} \left(\frac{1}{\sigma_n^2}\mathbf{I} - \frac{1}{\sigma_n^4} c \mathbf{X}\mathbf{X}^H\right)\right]\right\} \\
&= \underset{\mathbf{X}_k \in \{\mathbf{X}_1, \cdots, \mathbf{X}_K\}}{\operatorname{argmax}} \operatorname{tr}\left[\mathbf{Y}^H \mathbf{X}_k \mathbf{X}_k^H \mathbf{Y}\right] \\
&= \underset{\mathbf{X}_k \in \{\mathbf{X}_1, \cdots, \mathbf{X}_K\}}{\operatorname{argmax}} \|\mathbf{Y}^H \mathbf{X}_k\|_F^2, \qquad (3.27)
\end{aligned}$$

the squared Frobenius norm. With this result, we have proven, that it is possible to use multitone FSK, i.e. subspaces of the same dimension, for a transmission over full frequency selective fading channels with noncoherent detection.

In case of the combination of subspaces of different dimensions, no further simplification can be done. The entries $\frac{1}{1+\frac{1}{\sigma_n^2} x_{kk}^* x_{kk}}$ for the active subcarriers are different for every subspace of a different dimension, since the FSK blocks are energy normalized. For the determinant of the among column covariance matrix $\mathbf{\Phi}$, it is the same. It changes with the dimension of the subspace. So far, no simplification of the PDF could be found for the transmission of subspaces of different dimensions.

3.5 Distance Measure

There are two questions open to answer for the combination of subspaces of different dimensions: First of all, which subspaces should be chosen from the transmit matrix alphabet for transmission? And what is an appropriate distance measure between neighboring subspaces?

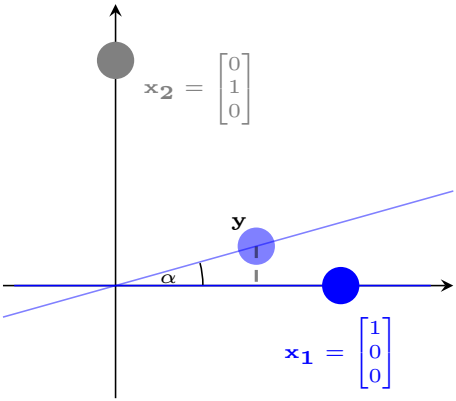

Figure 3.5: Projection of a received one-dimensional subspace for a transmission over a Rayleigh block fading channel.

In Fig. 2.5, Chapter 2 the projection of a received vector $\mathbf{y}$ for a transmission over a Rayleigh block fading channel has been shown. Fig. 3.5 shows the same scenario, when regarding the transmit vector $\mathbf{x}_1$ as a one-dimensional subspace, i.e. a line, for a transmission over a Rayleigh block fading channel. The subspace is scaled by the complex-valued fading coefficient and so far, the subspace remains the same. Through the addition of the noise the subspace is rotated into the space. Calculating the principal angle is the projection of the subspace to all possible transmitted subspaces and is therefore an appropriate measure of distance between the subspaces.

In case of pure OFDM-1/MFSK, both for the vector-valued transmission model and the matrix-valued transmission model, the principal angle between

neighboring subspaces is always 90°. In case of OFDM multitone FSK and OFDM-COM-N/MFSK, different angles between the subspaces occur.

Between any pair of vectors $\mathbf{x}_k$ and $\mathbf{x}_l$, the enclosed angle is computed by Eq. (2.15). In case of the matrix-valued transmission model, the principal angle α between any two matrices $\mathbf{X}_k$ and $\mathbf{X}_l$, i.e. subspaces, is defined by

$$\cos \alpha_{\mathbf{X}_k \mathbf{X}_l} = \frac{\operatorname{tr}\left\{\mathbf{X}_k^H \mathbf{X}_l\right\}}{\|\mathbf{X}_k\|_F \|\mathbf{X}_l\|_F}. \tag{3.28}$$

Both definitions have the same result since

$$\operatorname{tr}\left\{\mathbf{X}_k^H \mathbf{X}_l\right\} \underbrace{=}_{M \times M \text{ diagonal matrices } \mathbf{X}_k, \mathbf{X}_l} \mathbf{x}_k^H \mathbf{x}_l$$

and

$$\begin{aligned} \|\mathbf{X}\|_F &= \sqrt{\sum_{p=1}^{M} \sum_{q=1}^{M} |x_{pq}|^2} \\ &\underbrace{=}_{\text{only diagonal matrices } \mathbf{X}} \sqrt{x_{11}^2 + \cdots + x_{MM}^2} \\ &\underbrace{=}_{x_{pp}=x_p,\, p=1,\ldots,M} \sqrt{x_1^2 + \cdots + x_M^2} \\ &= \|\mathbf{x}\|. \end{aligned}$$

$\|\mathbf{X}\|_F$ is the Frobenius norm of the matrix $\mathbf{X}$ and $\|\mathbf{x}\|$ defines the norm of the vector $\mathbf{x}$. The principal angles are identical for either the subspaces or their corresponding FSK vectors.

We developed an algorithm for the mapping of the subspaces, c.f. Fig. 3.6, where the distance criterion between any pair of subspaces is the principal angle. By having a Gray mapping over the resulting set $\mathcal{B}$, each pair of neighboring subspaces, which encloses the minimum principal angle, differs only by one bit.

procedure FINDMAP($\mathcal{A}$)
  $\mathcal{B} = \emptyset$
  $\mathcal{B} + \mathbf{A}_1 \in \mathcal{A}$
  for all $\mathcal{A} \setminus \mathcal{B}$ **do**
    $\alpha_{\mathbf{A}_i\mathbf{B}} = \arccos\left(\frac{\mathrm{tr}(\mathbf{A}_i\mathbf{B})}{\|\mathbf{A}_i\|_F\|\mathbf{B}\|_F}\right)$
    $\hat{\mathbf{A}} = \underset{\mathbf{A}_i}{\operatorname{argmin}}(\alpha_{\mathbf{A}_i\mathbf{B}}))$
    $\mathcal{B} + \hat{\mathbf{A}}$
  end for
  return $\mathcal{B}$, GRAY($\mathcal{B}$)
end procedure

Figure 3.6: Gray mapping algorithm for COM-N/MFSK, $\mathbf{A}_i \in \mathcal{A}$, $\mathbf{B} \in \mathcal{B}$ [46].

To find the ordered set $\mathcal{B}$ of transmit matrices, which shall be used, the algorithm starts with the ordered set of subspaces $\mathcal{A}$. Ordered set $\mathcal{A}$ means here, that the null space is excluded, since it cannot be used for transmission, and that the subspaces $\mathbf{A}$ are ordered increasingly according to their number in the binary system. The set $\mathcal{B}$ is ordered in the sense of a Gray mapping. The set $\mathcal{A}$ builds the starting point to find the ordered set of transmit matrices $\mathcal{B}$. $\mathcal{B}$ is constructed by taking the first subspace ($\mathbf{A}_1$) from $\mathcal{A}$, i.e. $\mathbf{B} = \mathbf{A}_1 \in \mathcal{A}$. Next, all principal angles, separating each pair of subspaces $\alpha_{\mathbf{A}_i\mathbf{B}}$ are calculated. The smallest $\alpha_{\mathbf{A}_i\mathbf{B}}$, i.e. the subspace $\hat{\mathbf{A}}$ with the smallest principal angle, is then added to the ordered set $\mathcal{B}$. This process is repeated with the last subspace $\mathbf{B}$, added to $\mathcal{B}$, and again all principal angles to the remaining subspaces in the set $\mathcal{A}$ are calculated and compared. The closest neighbor is selected and added to $\mathcal{B}$. If more than one pair of subspaces have the same minimum principal angle, $\alpha_{\mathbf{A}_i\mathbf{B}}$, the first one is selected. The algorithm continues until all subspaces are ordered pairwise according to the minimum principal angle.

In Table 3.2, the distance profile for combined OFDM-N/4FSK based on the angle between the subspaces, is given. Due to simplicity reasons of the

manageable representation of the vectors $\mathbf{x}_k$, compared to their corresponding matrices $\mathbf{X}_k$, the distance profile is calculated according to the enclosed angle between the vectors. Since Gray mapping is wanted, the subspaces

Table 3.2: Distance profile for the enclosed angle for combined OFDM-1/4FSK and OFDM-2/4FSK.

	$\mathbf{x}_1$	$\mathbf{x}_2$	$\mathbf{x}_3$	$\mathbf{x}_4$	$\mathbf{x}_5$	$\mathbf{x}_6$	$\mathbf{x}_7$	$\mathbf{x}_8$	$\mathbf{x}_9$	$\mathbf{x}_{10}$
	$\begin{bmatrix}1\\0\\0\\0\end{bmatrix}$	$\begin{bmatrix}0\\1\\0\\0\end{bmatrix}$	$\begin{bmatrix}0\\0\\1\\0\end{bmatrix}$	$\begin{bmatrix}0\\0\\0\\1\end{bmatrix}$	$\begin{bmatrix}1\\1\\0\\0\end{bmatrix}$	$\begin{bmatrix}1\\0\\1\\0\end{bmatrix}$	$\begin{bmatrix}1\\0\\0\\1\end{bmatrix}$	$\begin{bmatrix}0\\1\\1\\0\end{bmatrix}$	$\begin{bmatrix}0\\1\\0\\1\end{bmatrix}$	$\begin{bmatrix}0\\0\\1\\1\end{bmatrix}$
$\mathbf{x}_1$	0°	90°	90°	90°	45°	45°	45°	90°	90°	90°
$\mathbf{x}_2$		0°	90°	90°	45°	90°	90°	45°	45°	90°
$\mathbf{x}_3$			0°	90°	90°	45°	90°	45°	90°	45°
$\mathbf{x}_4$				0°	90°	90°	45°	90°	45°	45°
$\mathbf{x}_5$					0°	60°	60°	60°	60°	90°
$\mathbf{x}_6$						0°	60°	60°	90°	60°
$\mathbf{x}_7$							0°	90°	60°	60°
$\mathbf{x}_8$								0°	60°	60°
$\mathbf{x}_9$									0°	60°
$\mathbf{x}_{10}$										0°

have to be arranged in a way, that the angle between the directly neighboring subspaces becomes minimum, i.e. 45° in the case of our example. One possible mapping of choosing eight subspaces out of the transmit matrix alphabet $A_{\mathrm{COM-N/4FSK}}$, containing ten matrices, is shown in Fig. 3.7. Due to the simpler representation, we chose the vector representation. The angle between the direct neighboring subspaces is always 45°, i.e. the minimum principal angle.

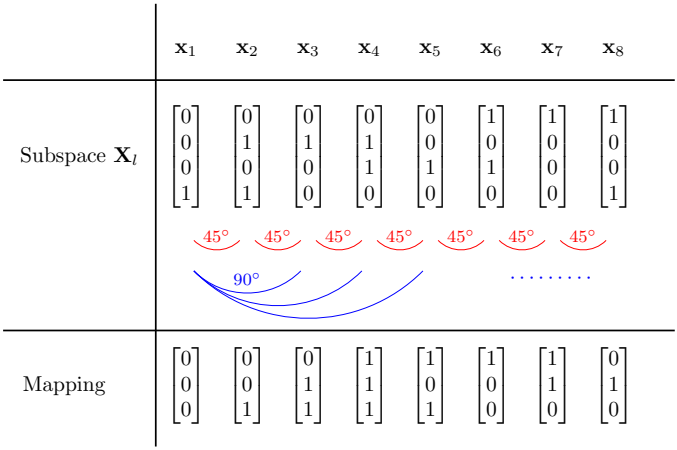

Figure 3.7: Basic principle for Gray mapping of OFDM-COM-N/4FSK.

For comparison reasons, we have a closer look at the second possible combination of subspaces of different dimensions of the $M = 4$-dimensional space. One- and three-dimensional subspaces, i.e. OFDM-1/4FSK and OFDM-3/4FSK, are combined and the resulting transmit matrix alphabet becomes

$$A_{1/4\text{FSK}\cup 3/4\text{FSK}} = \left\{ \begin{bmatrix} 1&0&0&0\\0&0&0&0\\0&0&0&0\\0&0&0&0 \end{bmatrix}, \begin{bmatrix} 0&0&0&0\\0&1&0&0\\0&0&0&0\\0&0&0&0 \end{bmatrix}, \begin{bmatrix} 0&0&0&0\\0&0&0&0\\0&0&1&0\\0&0&0&0 \end{bmatrix}, \right.$$
$$\begin{bmatrix} 0&0&0&0\\0&0&0&0\\0&0&0&0\\0&0&0&1 \end{bmatrix}, \begin{bmatrix} 0&0&0&0\\0&1&0&0\\0&0&1&0\\0&0&0&1 \end{bmatrix}, \begin{bmatrix} 1&0&0&0\\0&0&0&0\\0&0&1&0\\0&0&0&1 \end{bmatrix},$$
$$\left. \begin{bmatrix} 1&0&0&0\\0&1&0&0\\0&0&0&0\\0&0&0&1 \end{bmatrix}, \begin{bmatrix} 1&0&0&0\\0&1&0&0\\0&0&1&0\\0&0&0&0 \end{bmatrix} \right\}.$$

Table 3.3: Distance profile according to the enclosed angle for combined OFDM-1/4FSK ∪ OFDM-3/4FSK.

	$\mathbf{x}_1$	$\mathbf{x}_2$	$\mathbf{x}_3$	$\mathbf{x}_4$	$\mathbf{x}_5$	$\mathbf{x}_6$	$\mathbf{x}_7$	$\mathbf{x}_8$
	$\begin{bmatrix}1\\0\\0\\0\end{bmatrix}$	$\begin{bmatrix}0\\1\\0\\0\end{bmatrix}$	$\begin{bmatrix}0\\0\\1\\0\end{bmatrix}$	$\begin{bmatrix}0\\0\\0\\1\end{bmatrix}$	$\begin{bmatrix}0\\1\\1\\1\end{bmatrix}$	$\begin{bmatrix}1\\0\\1\\1\end{bmatrix}$	$\begin{bmatrix}1\\1\\0\\1\end{bmatrix}$	$\begin{bmatrix}1\\1\\1\\0\end{bmatrix}$
$\mathbf{x}_1$	0°	90°	90°	90°	90°	54.7°	54.7°	54.7°
$\mathbf{x}_2$		0°	90°	90°	54.7°	90°	54.7°	54.7°
$\mathbf{x}_3$			0°	90°	54.7°	54.7°	90°	54.7°
$\mathbf{x}_4$				0°	54.7°	54.7°	54.7°	90°
$\mathbf{x}_5$					0°	48.2°	48.2°	48.2°
$\mathbf{x}_6$						0°	48.2°	48.2°
$\mathbf{x}_7$							0°	48.2°
$\mathbf{x}_8$								0°

In comparison to the combination of COM-N/4FSK, eight possible matrices are obtained for 1/4FSK ∪ 3/4FSK. The matrices of the OFDM-3/4FSK alphabet are the flipped versions with respect to their frequency positions of the matrices obtained for OFDM-1/4FSK. The corresponding distance profile for the principal angles is shown in Table 3.3. Compared to COM-N/4FSK, the minimum angle for combined OFDM-1/4FSK ∪ OFDM-3/4FSK is 54.7° and therefore greater compared to the minimum angle of 45° for COM-N/4FSK. For large additive noise, the alphabet for COM-N/4FSK is more robust against errors, since less frequency positions are active. A false decision for a chosen subcarrier in case of combined OFDM-1/4FSK ∪ OFDM-3/4FSK is more likely, since for OFDM-3/4FSK more subcarriers are active and therefore exposed both to the fading from the channel and the additive noise. Therefore, the subcarriers modulated with OFDM-3/4FSK, contain more errors, as if they were modulated with OFDM-2/4FSK. For the low noise region, this be-

haviour reverses, since the greater minimum angle is the deciding criterion.

Within Sec. 3.2, we mentioned, that only subspaces up to dimension $\frac{M}{2}$ are combined. Since the application area of OFDM-N/MFSK are wireless connections to users moving with high velocities, the mobile communication channel suffers from a fast time-variant multipath propagation and additive noise. Therefore, the receiver has to be capable of coping with the multiplicative noise of the channel and the additive noise. As a consequence, we have decided only to combine subspaces up to the dimension $\frac{M}{2}$, since they are more robust against multiplicative noise as well as large additive noise. There exists a further reason: It is impossible to use the null space, since it is included in every subspace and the space itself. Using methods like bit stuffing in case of the null space is not possible, since the worse channel conditions do not allow a recovery of the bit stuffed positions. Gaining another full bit, when going beyond $\frac{M}{2}$ becomes impossible. Because of this reasons, we restrict ourselves to combine subspaces up to the dimension $\frac{M}{2}$.

3.6 From Subspaces Back to Vectors

It is possible to increase the bandwidth efficiency of OFDM-MFSK by combining subspaces of different dimensions. To complete the topic, we show the connection between the subspace based transmission model and the vector-valued transmission model in the following. This connection can be shown, by analyzing the different ML detection rules for the Rayleigh block fading channel and the Rayleigh frequency selective fading channel.

3.6.1 Rayleigh Block Fading Channel

The multivariate conditional PDF for a received vector $\mathbf{y}$, given the transmitted vector $\mathbf{x}$, for a transmission over a Rayleigh block fading channel, was

given by Wetz in [44]

$$p(\mathbf{y}|\mathbf{x}) = \frac{1}{\pi^M \sigma_n^M \left(1+\frac{\mathbf{x}^H\mathbf{x}}{\sigma_n^2}\right)} \exp\left(-\frac{1}{\sigma_n^2}\mathbf{y}^H\mathbf{y} + \frac{1}{\sigma_n^4\left(1+\frac{\mathbf{x}^H\mathbf{x}}{\sigma_n^2}\right)}\mathbf{y}^H\mathbf{x}\mathbf{x}^H\mathbf{y}\right). \quad (3.29)$$

The derived ML detection rule is

$$\hat{\mathbf{x}} = \underset{\mathbf{x}_k \in \{\mathbf{x}_1,\cdots,\mathbf{x}_K\}}{\operatorname{argmax}} |\mathbf{y}^H\mathbf{x}|^2 \quad (3.30)$$

for energy normalized transmit vector alphabets, i.e. $\mathbf{x}^H\mathbf{x} = 1$.

We derived the conditional matrix variate PDF, c.f. Eq. (3.10), to be

$$p(\mathbf{Y}|\mathbf{X}) = \frac{1}{(\pi)^{\frac{MM}{2}}\left(\frac{1}{M}+\sigma_n^2\right)^{\frac{MM}{2}}\left(\sigma_n^{2M}(1+\frac{\mathbf{x}^H\mathbf{x}}{\sigma_n^2})\right)^{\frac{M}{2}}} \exp\left\{-\sum_{k=1}^{M}\sum_{l=1}^{M}\left[\mathbf{Y}^H\frac{1}{\frac{1}{M}+\sigma_n^2}\mathbf{I}\mathbf{Y}\left(\frac{1}{\sigma_n^2}\mathbf{I} - \frac{1}{\sigma_n^4(1+\frac{\mathbf{x}^H\mathbf{x}}{\sigma_n^2})}\mathbf{x}\mathbf{x}^H\right)\right]\right\}.$$

This PDF is valid for the subspace based transmission for OFDM-N/MFSK as well as OFDM-COM-N/MFSK, if energy normalized transmit matrix alphabets are used. We further simplified the conditional PDF to the squared scalar product, for both OFDM-N/MFSK and the combination of subspaces of different dimensions, c.f. Eq. (3.21). The necessary condition for deriving the squared scalar product as the detection rule are energy normalized subspaces in any case. If a decision based on matrices, i.e. subspaces, is wanted, it is not possible to simplify the PDF, since the covariance matrix $\mathbf{\Phi}$ in Eq. (3.14) cannot be inverted in general, as it has been shown in Sec. 3.4.1. In this case the PDF has to be used.

The connection between the subspaces and the vectors for OFDM-N/MFSK and OFDM-COM-N/MFSK follows directly from the derivation of the ML

detection rule, which is in both cases based on the squared scalar product (Eq. (3.21)). By showing in [29] and in Sec. 3.1, that OFDM-MFSK is a special case of the more general transmission based on subspaces, we developed the idea to combine subspaces of different dimensions, [28], Sec. 3.2. Deriving the ML detection rule for the subspace based transmission in Sec. 3.4.1, brought us back to the vector-valued transmission model, defined in Eq. (2.1). A simplification of the conditional matrix variate normal distribution in Eq. (3.10) was only possible, if the among column covariance matrix $\mathbf{\Phi}$ was inverted by making use of the dyadic product of the transmit vector $\mathbf{x}$, c.f. Eq. (3.18) The conclusion is, that it is also possible to combine different energy normalized transmit vectors and detect them with the squared scalar product. The system complexity remains very low and the gain in bandwidth efficiency is remarkable, as shown within Sec. 3.3.

Finally, the PDF for the multivariate Gaussian distribution,

$$p(\mathbf{y}|\mathbf{x}) = \frac{1}{(2\pi)^{M/2}\det(\mathbf{\Lambda})^{M/2}} \exp\left\{-\frac{1}{2}(\mathbf{y}-E[\mathbf{y}])\mathbf{\Lambda}^{-1}(\mathbf{y}-E[\mathbf{y}])^H\right\},$$

with covariance matrix $\mathbf{\Lambda}$, as defined in Sec. 2.3.1, Eq. (2.12), is visualized for the Rayleigh block fading channel. We chose the bivariate PDF, since it is only possible to visualize the PDF of a two-dimensional real-valued vector. To show the effects of transmit vectors with energy normalization and without energy normalization, two energy normalized vectors

$$\mathbf{x}_1 = \begin{bmatrix}1\\0\end{bmatrix},\ \mathbf{x}_2 = \begin{bmatrix}\frac{1}{\sqrt{2}}\\ \frac{1}{\sqrt{2}}\end{bmatrix}$$

and two vectors without energy normalization

$$\mathbf{x}_1 = \begin{bmatrix}1\\0\end{bmatrix},\ \mathbf{x}_2 = \begin{bmatrix}1\\1\end{bmatrix},$$

are chosen. Both vectors belong to a combined OFDM-1/2FSK $\cup$ OFDM-2/2FSK alphabet. For the illustrative example, the 1-dimensional subspace of the 2-dimensional space ($\mathbf{x}_1$) as well as the 2-dimensional space itself ($\mathbf{x}_2$) are used. It should be noticed, that for illustration purpose only the vectors

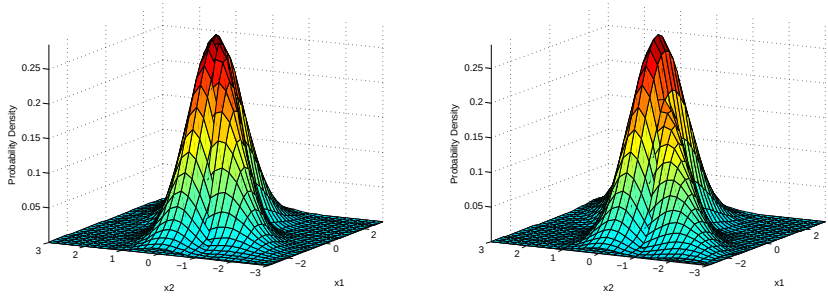

(a) with energy normalization (b) without energy normalization

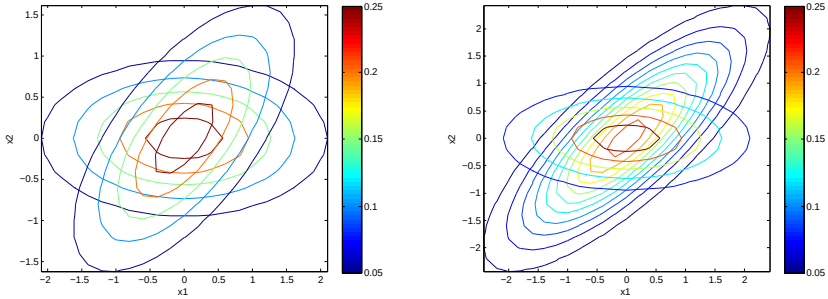

(c) with energy normalization (d) without energy normalization

Figure 3.8: Comparison of the PDFs of the combined OFDM-1/2FSK ∪ OFDM-2/2FSK alphabet with energy normalization and without energy normalization for transmission over the Rayleigh block fading channel, $\sigma_n = 0.5$

could be used. But however, we have shown, that they could also be interpreted as matrices, c.f. Sec. 3.1. Fig. 3.8 shows for large noise the bivariate PDFs for transmission over the Rayleigh block fading channel for transmit alphabets with energy normalization and without energy normalization, i.e. for the transmitted vectors $\mathbf{x}_1$ and $\mathbf{x}_2$. Two PDFs are plotted within Fig. 3.8, the PDF for the 1-dimensional subspace of the 2-dimensional space, i.e. the PDF for transmission of $\mathbf{x}_1$ over a Rayleigh block fading channel with large noise and the PDF for the 2-dimensional space, i.e. the PDF for transmission

of $\mathbf{x}_2$ over a Rayleigh block fading channel with large noise. Fig. 3.8a and Fig. 3.8b show the two plotted PDFs from a side view, whereas Fig. 3.8c and Fig. 3.8d present the top view. Both views are presented to be suggestive of how the PDFs with respect to their width and height look like for subspaces of different dimensions.

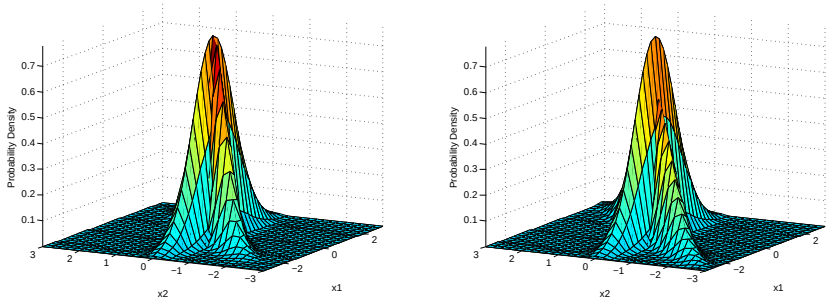

(a) with energy normalization

(b) without energy normalization

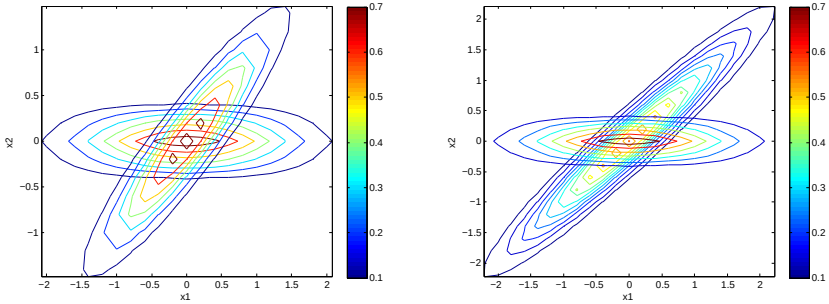

(c) with energy normalization

(d) without energy normalization

Figure 3.9: Comparison of the PDFs of the combined OFDM-1/2FSK ∪ OFDM-2/2FSK alphabet with energy normalization and without energy normalization for transmission over the Rayleigh block fading channel, $\sigma_n = 0.2$

It can be observed, that, in case of the transmit alphabet with energy nor-

malization in Fig. 3.8a and in Fig. 3.8c, the PDFs for both vectors have the shape of a comb and the same height. This shows, that a detection rule exists besides the PDF. In contrary, Fig. 3.8b and Fig. 3.8d show, that without any energy normalization, the PDF for the vector $\mathbf{x}_2$, is higher compared to the PDF for the vector $\mathbf{x}_1$. In the terminology of regarding OFDM-COM-N/MFSK as a noncoherent transmission based on subspaces, it can be seen, that the height of the PDF for the two-dimensional space is much higher compared to the height of the PDF for the one-dimensional subspace. It is impossible to derive a decision in this case with the squared scalar product, as derived in Eq. (3.21). For transmit alphabets without energy normalization the PDF has to be used for detection. It can be also observed, that both vectors and therefore the subspaces are not orthogonal.

Furthermore, the two Gaussian distributions, resulting from the multiplicative channel and the additive white Gaussian noise, can be distinguished well. This can be seen, when comparing Fig. 3.8 for large noise with Fig. 3.9 showing the PDFs for transmit alphabets with energy normalization and without energy normalization for a transmission over the Rayleigh block fading channel with low noise, $\sigma_n = 0.2$. All other observations made with respect to the subspace based transmission for the comparison of the PDFs for a transmission over a Rayleigh block fading channel with energy normalized subspaces and with subspaces without energy normalization within Fig. 3.8 can be also made for Fig. 3.9.

3.6.2 Rayleigh Frequency Selective Fading Channel

In the following, we also show the connection between the multivariate PDF and the matrix variate PDF for a Rayleigh frequency selective fading channel, i.e. the connection between the subspaces and the vectors is also worked out. As shown within Sec. 3.4.2, we derived a detection rule for OFDM multitone FSK, or in terms of subspace terminology, for subspaces with the same dimension for a transmission over a Rayleigh frequency selective fading channel. An ML detection rule for a Rayleigh frequency selective fading channel for OFDM-N/MFSK, based on the vector-valued transmission model, has not been derived in [44]. Therefore, we derive it in the following and afterwards,

the comparison between subspaces and vectors can be done.

Multivariate PDF

In [44] the detection rule, i.e. the squared scalar product, for an AWGN channel and a Rayleigh block fading channel has already been derived. For OFDM-1/MFSK, it is also valid for Rayleigh frequency selective fading channels, since only one subcarrier is active, and therefore the effect of Rayleigh block fading and Rayleigh frequency selective fading is the same. However, for OFDM multitone FSK and OFDM-COM-N/MFSK, it is no longer valid. In the case of a Rayleigh frequency selective fading channel, the fading coefficients h_{kk}, $k = 1, \ldots, M$, are complex Gaussian distributed with zero mean ($\mu_h = 0$) and unit variance ($\sigma_h^2 = 1$) on the main diagonal of the channel matrix $\mathbf{H}$. Since they are completely uncorrelated, the correlation matrix of the channel $\mathbf{\Lambda}_h = \sigma_h \mathbf{I}$. Inserted into the covariance matrix in Eq. (2.12), shown in Sec. 2.3.1, this results in

$$\mathbf{\Lambda} = \mathrm{diag}(\mathbf{x})\mathbf{I}\mathrm{diag}(\mathbf{x}^H) + \sigma_n^2 \mathbf{I}, \tag{3.31}$$

where $\mathrm{diag}(\mathbf{x})$ and $\mathrm{diag}(\mathbf{x}^H)$, are the transformed transmit vectors $\mathbf{x}$ and its transposed. Rewriting Eq. (3.31) leads to

$$\begin{aligned} \mathbf{\Lambda} &= \mathrm{diag}(\mathbf{x})\mathbf{I}\mathrm{diag}(\mathbf{x}^H) + \sigma_n^2 \mathbf{I} \\ &= \mathbf{X}\mathbf{X}^H + \sigma_n^2 \mathbf{I}. \end{aligned}$$

$\mathbf{\Lambda}$ can now be inverted with the Sherman-Morrison-Woodbury formula [12]

$$\begin{aligned} \mathbf{\Lambda}^{-1} &= \frac{1}{\sigma_n^2}\mathbf{I} - \frac{1}{\sigma_n^2}\mathbf{I}\mathbf{X}\left(\mathbf{I} + \mathbf{X}^H \frac{1}{\sigma_n^2}\mathbf{I}\mathbf{X}\right)^{-1} \mathbf{X}^H \frac{1}{{\sigma_\mathbf{n}}^2}\mathbf{I} \\ &= \frac{1}{\sigma_n^2}\mathbf{I} - \frac{1}{\sigma_n^4}\mathbf{X}\left(\mathbf{I} + \frac{1}{\sigma_n^2}\mathbf{X}^H\mathbf{X}\right)^{-1} \mathbf{X}^H \\ &= \frac{1}{\sigma_n^2}\mathbf{I} - \frac{1}{\sigma_n^4}\mathbf{C}\mathbf{X}\mathbf{X}^H. \end{aligned} \tag{3.32}$$

The matrix $\mathbf{C}$ contains the constants $\frac{1}{1+\frac{1}{\sigma_n^2}x_{kk}^* x_{kk}}$ of the corresponding k-th subcarrier on its main diagonal. It is identical to the matrix $\mathbf{C}$ derived within

Sec. 3.4.2. For OFDM multitone FSK, the matrix $\mathbf{C}$ can be reduced to a constant $c = \frac{1}{1+\frac{1}{\sigma_n^2} x_{kk}^* x_{kk}}$, $x_{kk} \neq 0$, which is the same for all vectors $\mathbf{x}_k$ of the transmit vector alphabet, since it only affects the active subcarrier frequencies.

The determinant of the covariance matrix $\mathbf{\Lambda}$ for OFDM-N/MFSK becomes

$$\begin{aligned} \det \mathbf{\Lambda} &= \det\left(\operatorname{diag}(\mathbf{x})\,\mathbf{I}\,\operatorname{diag}(\mathbf{x^H}) + \sigma_n^2\mathbf{I}\right) \\ &= \det\left(\mathbf{X}\,\mathbf{I}\,\mathbf{X^H} + \sigma_n^2\mathbf{I}\right) \\ &= \left(x_{kk}x_{kk}^* + \sigma_n^2\right)^N \left(\sigma_n^2\right)^{M-N}. \end{aligned} \tag{3.33}$$

Inserting Eq. (3.32) and Eq. (3.33) in Eq. (2.12), Sec. 2.3.1, results in

$$\begin{aligned} p(\mathbf{y}|\mathbf{x}) &= \frac{1}{\pi^N \det \mathbf{\Lambda}} \exp\left(-\mathbf{y}^H \mathbf{\Lambda}^{-1}\mathbf{y}\right) \\ &= \frac{1}{\pi^N \left(x_{kk}x_{kk}^* + \sigma_n^2\right)^N \left(\sigma_n^2\right)^{M-N}} \\ &\qquad \exp\left(-\mathbf{y}^H \left[\frac{1}{\sigma_n^2}\mathbf{I} - \frac{1}{\sigma_n^4}\underbrace{\left(\frac{1}{1+\frac{1}{\sigma_n^2}x_{kk}^* x_{kk}}\right)}_{=c}\mathbf{X}\mathbf{X}^H\right]\mathbf{y}\right), \\ &= \frac{1}{\pi^N \left(x_{kk}x_{kk}^* + \sigma_n^2\right)^N \left(\sigma_n^2\right)^{M-N}} \exp\left(-\frac{1}{\sigma_n^2}\mathbf{y}^H\mathbf{y} + \frac{1}{\sigma_n^4}c\mathbf{y}^H\,\mathbf{X}\,\mathbf{X}^H\,\mathbf{y}\right). \end{aligned} \tag{3.34}$$

For transmit vectors with equal energy, we obtain the ML detection rule for OFDM multitone FSK, i.e. OFDM-N/MFSK, $1 \leq N < M$ for a Rayleigh frequency selective fading channel

$$\begin{aligned} \hat{\mathbf{x}} &= \underset{\mathbf{x}_k \in \{\mathbf{x}_1,\cdots,\mathbf{x}_K\}}{\operatorname{argmax}} \mathbf{y}^H \operatorname{diag}(\mathbf{x})\operatorname{diag}(\mathbf{x}^H)\mathbf{y} \\ &= \underset{\mathbf{x}_k \in \{\mathbf{x}_1,\cdots,\mathbf{x}_K\}}{\operatorname{argmax}} \|\mathbf{y}^H\mathbf{X}\|_F^2, \end{aligned} \tag{3.35}$$

is based on the squared Frobenius norm. This directly corresponds to the result obtained in Eq. (3.27), which has been derived for a transmission based

on subspaces of the same dimension.

As already discussed for the combination of subspaces of different dimensions in Sec. 3.4.2, it is not possible to simplify the PDF for the combined alphabet. For the multivariate PDF it is the same, since for a combination of different FSK vectors, the constants within the matrix $\mathbf{C}$ are dependent on the number of active tones per FSK vector. Therefore $[\mathbf{C}]_{kk}$ are not constant and cannot be neglected. The same reason holds for $\det \mathbf{\Lambda}$.

Comparison of the PDFs

The PDF for the vector-valued transmission over a frequency selective fading channel, was derived in (3.34) and for the transmission with a fixed number N out of M subcarriers, i.e. without a combined transmit vector alphabet, it can be further simplified to the squared Frobenius norm as shown in Eq. (3.35). The matrix-valued PDF, Eq. (3.26), is

$$p(\mathbf{Y}|\mathbf{X}) = \frac{1}{(\pi)^{\frac{MM}{2}} \left(\frac{1}{M}+\sigma_n^2\right)^M \left(x_{kk}x_{kk}^*+\sigma_n^2\right)^N \left(\sigma_n^2\right)^{M-N}} \exp\left\{-\mathrm{tr}\left[\mathbf{Y}^H\left(\frac{1}{\frac{1}{M}+\sigma_n^2}\right)\mathbf{Y}\left(\frac{1}{\sigma_n^2}\mathbf{I}-\mathbf{C}\mathbf{X}\mathbf{X}^H\right)\right]\right\}.$$

From both PDFs, the multivariate PDF as well as the matrix variate PDF, it can be observed, that in case of OFDM-COM-N/MFSK, there is no possibility for further simplification of the PDFs, since the factors within the matrix $\mathbf{C}$ and the determinants are dependent on the single elements x_k (for the vector-valued transmission) or x_{kk} in case of the subspace based transmission. x_k and x_{kk} differ because of the different active frequency positions or the different dimensions of the subspaces, respectively. Furthermore, there is no possibility for achieving a constant determinant for the purpose of neglecting it.

However, in the case of a pure multitone FSK alphabet, that is for a constant number N of active subcarriers, or, when regarding the matrix-valued transmission, for a transmission with subspaces of the same dimension N, the determinants become constant and the matrix $\mathbf{C}$ contains a constant factor

$c = \frac{1}{1+\frac{1}{\sigma_n^2} x_{kk}^* x_{kk}}$ on the active frequency positions on its main diagonal and can therefore be reduced to the constant factor c, c.f. Sec. (3.4.2), as well as the underlying section. This results in the squared Frobenius norm.

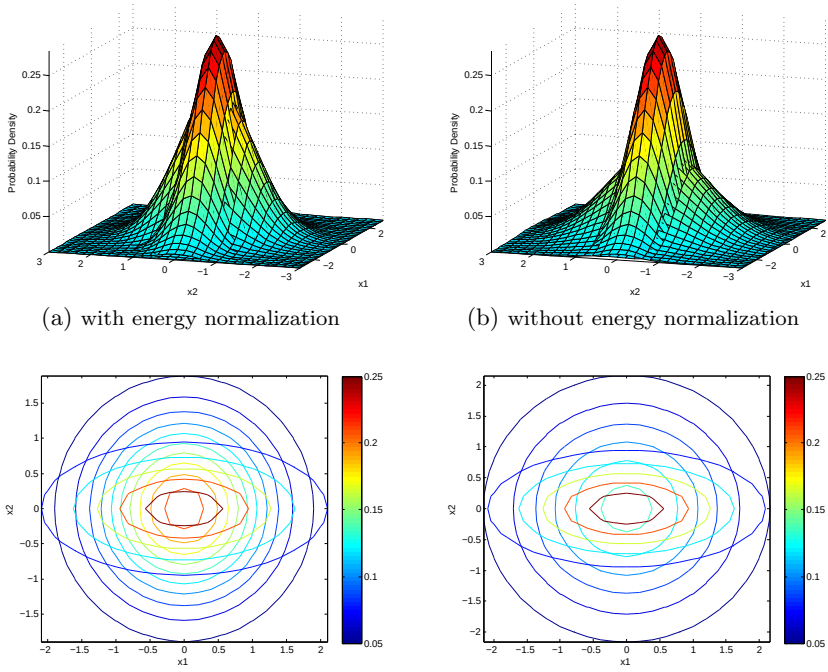

(a) with energy normalization

(b) without energy normalization

(c) with energy normalization

(d) without energy normalization

Figure 3.10: Comparison of the PDFs of the combined OFDM-1/2FSK ∪ OFDM-2/2FSK alphabet with energy normalization and without energy normalization for transmission over the Rayleigh frequency selective fading channel, $\sigma_n = 0.5$

Fig. 3.10 and Fig. 3.11 show the bivariate PDF, evaluated for the vectors $\mathbf{x}_1$ and $\mathbf{x}_2$, defined in Sec. 3.6.1, for transmission over the frequency selective

fading channel for $\sigma_n = 0.5$ and $\sigma_n = 0.2$. We do again the comparison for

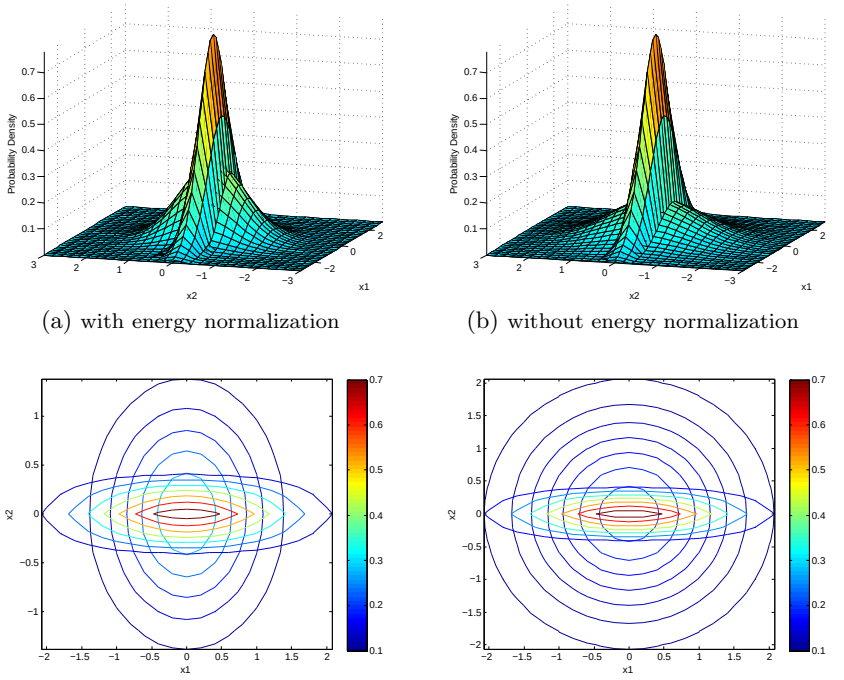

(a) with energy normalization

(b) without energy normalization

(c) with energy normalization

(d) without energy normalization

Figure 3.11: Comparison of the PDFs of the combined OFDM-1/2FSK ∪ OFDM-2/2FSK alphabet with energy normalization and without energy normalization for transmission over the Rayleigh frequency selective fading channel, $\sigma_n = 0.2$

using the vectors or subspaces with energy normalization and without energy normalization. It is stressed again, that two different PDFs are plotted within one of the subfigures to do a direct comparison of the PDFs for 1-dimensional subspaces and the 2-dimensional space itself. Again, a view from the side as well as the top view are presented to see the differences for the PDFs

with respect to the subspaces of different dimensions as well as with respect to energy normalization or no energy normalization for the transmit alphabet.

One important observation can be made: It becomes obvious, that the vector-valued transmission with combined OFDM-N/MFSK can be regarded as a noncoherent transmission based on subspaces. In this case $\mathbf{x}_1$ is regarded as a line and $\mathbf{x}_2$ as a plane, whose basis vectors are rotated independently by different fading coefficients. Therefore, the PDF for the line is shaped like a comb over a line, whereas the PDF for the plane is a cone in the plane. It becomes also obvious, that the line lies within the plane, since the comb is within the cone.

Another point is, that no energy normalization (c.f. Fig. 3.10b, Fig. 3.10d, Fig. 3.11b and Fig. 3.9d leads to a lower height of the PDF for the plane and the diameter of the base area of the cone increases compared to the energy normalized alphabet (c.f. Fig. 3.10a, Fig. 3.10c, Fig. 3.11a and Fig. 3.11c).

It becomes obvious, that it is impossible to derive a detection rule in case of the combined alphabet, since the subspaces of different dimensions cannot be distinguished.

3.7 Chapter Summary

The key idea of this thesis is the increase in bandwidth efficiency of OFDM-MFSK. The starting point established the connection between the subspace based noncoherent transmission schemes for MIMO channels, and OFDM-MFSK and its multitone variant. We derived the connection between both transmission schemes and we have shown, that OFDM-MFSK is s special case of a noncoherent transmission based on subspaces as proposed by Hochwald and Marzetta, Zheng and Tse, and Utkovski in [19], [47] and [41].

We presented the possibility of how to combine subspaces of different dimensions of OFDM-MFSK and its multitone variant. This combination of subspaces of different dimensions is the key step to increase the bandwidth

efficiency of OFDM-MFSK and its multitone variant significantly. For an increasing FSK block size, the upper bound of the bandwidth efficiency approaches 1 $\frac{\text{bit/s}}{\text{Hz}}$. Compared to pure OFDM-1/MFSK, which has an upper bound for the bandwidth efficiency of 0.5 $\frac{\text{bit/s}}{\text{Hz}}$ for OFDM-1/2FSK and OFDM-1/4FSK, OFDM-COM-N/4FSK has an upper bound of 0.75 $\frac{\text{bit/s}}{\text{Hz}}$, which is an increase of 50 %.

First of all, we studied how to combine subspaces of different dimensions to utilize the total available mathematical space in a better way. We have seen, that the combination of subspaces never leads to orthogonal subspaces. In contrary, for unitary space-time modulation unitary transmit matrices are used. However, attention has to be paid to the combination of subspaces of different dimensions, since the bandwidth efficiency of OFDM-MFSK can be increased in a very effective way. The complexity of the system is less compared to the multitone FSK approach, proposed in [25]. We have seen for different FSK modulation schemes, that for our new proposed method COM-N/4FSK a bandwidth efficiency of 0.75 $\frac{\text{bit/s}}{\text{Hz}}$ is obtained. For 4/8FSK the same bandwidth efficiency is obtained, but with the cost of requiring 70 subspaces. For our combined alphabet COM-N/4FSK, we only need eight subspaces to obtain this bandwidth efficiency.

To be able to detect the subspaces, we studied the matrix variate probability density function for complex-valued matrices. We have derived the matrix variate PDF in its most general form and we have taken it as a starting point to derive the conditional matrix variate PDF for the Rayleigh block fading channel, the AWGN channel and the Rayleigh frequency selective fading channel. For the Rayleigh block fading channel, we have shown, that the conditional PDF could be simplified to the squared scalar product for N/MFSK and COM-N/MFSK, if energy normalized subspaces are assumed. This has shown directly the connection between the subspaces and the FSK vectors. For the Rayleigh frequency selective fading channel, the conditional PDF could be simplified for the case, if subspaces of the same dimension are used, i.e. OFDM multitone FSK. In this case, the ML detection rule turned out to be the squared Frobenius norm. In the case of COM-N/MFSK, a simplification of the conditional PDF for the Rayleigh frequency selective fading

channel is not possible.

We analyzed the distance criterion, which turned out to be the principal angle between any pair of subspaces. We concluded, that it is only useful to combine the subspaces up to the dimension of $\frac{M}{2}$. There are several reasons for this bound: First of all, the null space, i.e. the all zero matrix, can never be used, since it is included within all subspaces and the space itself. In a consequence, it is never possible to gain another full bit, when going beyond $\frac{M}{2}$. We have shown for COM-N/4FSK/15, where all possible combinations of subspaces of the $M = 4$-dimensional space and the 4-dimensional space itself, except the null space, have been used, that the bandwidth efficiency of 0.9767 $\frac{\text{bit/s}}{\text{Hz}}$ almost reaches the upper bound of 1 $\frac{\text{bit/s}}{\text{Hz}}$. Since the null space cannot be used for transmission, we omitted it by applying perfect bit stuffing, i.e. we made sure, that four consecutive zeros will never be transmitted. Applying a normal bit stuffing algorithm is not possible, since the worse channel conditions in a Rayleigh block or Rayleigh frequency selective fading environment, lead to the consequence, that bit errors are likely and therefore the bit stuffed positions cannot be recovered completely. A transmission with a reasonable BER performance is therefore impossible. Additional reasons for omitting subspaces with a dimension greater than $\frac{M}{2}$ are, that these subspaces are technically the "bit flipped" versions of the subspaces of lower dimensions. Therefore, more frequency positions are active and the subspaces are more prone to errors, when transmitting over the assumed Rayleigh block fading and Rayleigh frequency selective fading channels.

We have characterized the connection between the subspaces and the vectors by analyzing the different PDFs and showing, that in our special case they can be transformed into each other. Illustrating examples for the multivariate PDF for a COM-N/2FSK alphabet have been given and discussed.

If the resulting PDFs for the Rayleigh block fading channel and for the Rayleigh frequency selective fading channel are compared, the Rayleigh block fading channel leads to two non-orthogonal combs in case of the combined alphabet, crossing in the origin. If the alphabet is with energy normalization, the combs have the same height and the PDF could be further simplified to

the squared scalar product, which is ML, for the vector-valued as well as for the subspace based transmission. For the Rayleigh frequency selective fading channel, the PDFs show, that the subspaces of different dimensions are scaled by the different fading coefficients and rotated within the underlying subspace.

Finally, we want to stress the huge potential of combining subspaces of different dimensions in case of OFDM-MFSK. The increase in bandwidth efficiency is significant and can be achieved without a substantial increase in complexity. We have also shown the connection between the subspaces and the vectors and therefore all results can be directly used with the vector-valued transmission model. The combination of OFDM-MFSK and its multitone variant is one of the main ideas in this work. The key idea has been discussed in Sec. 3.1, where the connection between OFDM-MFSK and a transmission based on subspaces has been derived. The combination of different OFDM-N/MFSK alphabets, or in other words the combination of subspaces of different dimensions and therefore the resulting increase in bandwidth efficiency, makes OFDM-COM-N/MFSK a very attractive transmission scheme for a transmission over fast fading time-variant channels.

Chapter 4

Simulation Results

In the following, simulation results for a transmission over the AWGN channel, the Rayleigh block fading channel and the Rayleigh frequency selective fading channel are discussed. The increase in terms of

- bandwidth efficiency
- power efficiency

is visualized for the bit error rate (BER) over $\frac{E_b}{N_0}$ for an uncoded transmission as well as for a bit-interleaved coded transmission with an iterative receiver, c.f. Sec. 2.3.2.

Table 4.1: Bandwidth efficiency for different N/MFSK and COM-N/MFSK modulation schemes.

Modulation scheme	Bits per FSK block	Number of FSK blocks	Number of subcarriers	Bandwidth efficiency $\left[\frac{\text{bit/s}}{\text{Hz}}\right]$
1/4FSK	2	105	420	0.5
3/8FSK	5	42	336	0.625
COM-N/4FSK	3	70	280	0.75
4/8FSK	6	35	280	0.75
7/16FSK	13	16	256	0.8125
COM-N/8FSK	7	30	240	0.875
COM-N/16FSK	15	14	224	0.9375
COM-N/4FSK/15	3.9069	52	208	0.9767

As reference plots we use 1/4FSK and different multitone FSK alphabets. The modulation alphabets of interest are listed in Tab. 4.1. The setup is done in a way, that the data rate is fixed and a total amount of 210 information bits for 1/4FSK, 3/8FSK, COM-N/4FSK, 4/8FSK, COM-N/8FSK and COM-N/16FSK is transmitted. For 7/16FSK and COM-N/4FSK/15 (introduced in Sec. 3.3) 208 information bits are transmitted in total. We see, that pure OFDM-1/MFSK needs 50 % more subcarriers to transmit the same amount of bits as our proposed COM-N/4FSK alphabet. The simulations were carried out without guard bands and/or guard intervals and therefore we compare the upper bound for the bandwidth efficiency. For each transmission scheme 200 OFDM blocks are used. All alphabets are energy normalized, i.e. the sum energy within one FSK block of size M is one. This means, that with an increasing number of active frequencies, i.e. an increasing dimension of the subspaces, the energy per active subcarrier decreases.

4.1 Uncoded Transmission

Fig. 4.1 shows the bit error rate (BER) over $\frac{E_b}{N_0}$ for an uncoded transmission over an AWGN channel for OFDM-1/4FSK, as proposed in [45] and [44], and for OFDM-3/8FSK, OFDM-4/8FSK and OFDM-7/16FSK, as proposed by [25]. OFDM-1/4FSK shows the best performance. However, it has the worst bandwidth efficiency of 0.5 $\frac{\text{bit/s}}{\text{Hz}}$, c.f. Tab. 3.1. In the high noise region,

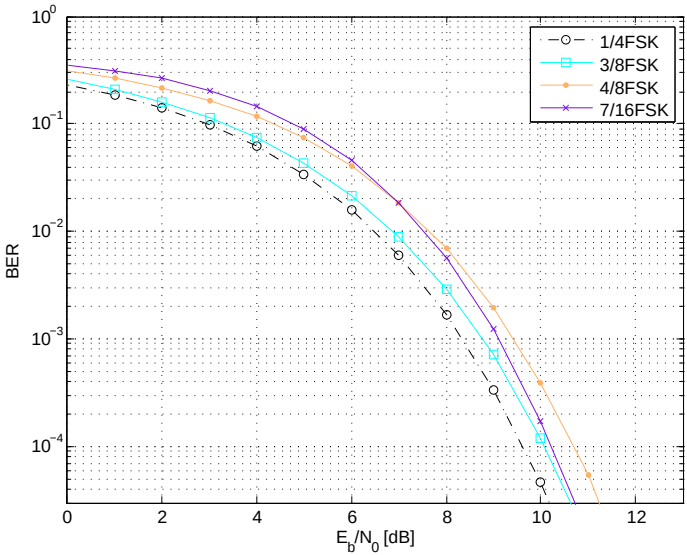

Figure 4.1: Performance comparison (BER vs. $\frac{E_b}{N_0}$) of uncoded OFDM-1/4FSK, OFDM-3/8FSK, OFDM-4/8FSK and OFDM-7/16FSK with noncoherent detection and transmission over the AWGN channel, no cyclic prefix, no guard bands.

we observe, that the alphabets with a smaller FSK block size perform better. At $\frac{E_b}{N_0} = 7$ dB, 4/8FSK and 7/16FSK intersect and 7/16FSK starts to approach 3/8FSK. For the low noise region, the minimum distance, i.e. the principal angle, plays an important role, since the alphabets with a higher

minimum angle, start to perform better. It turns out, that 7/16FSK has a good bandwidth efficiency as well as a good power efficiency but with the cost of an increased complexity, since 8192 subspaces are needed to transmit 13 bits per FSK block and to approach a bandwidth efficiency of 0.8125 $\frac{\text{bit/s}}{\text{Hz}}$.

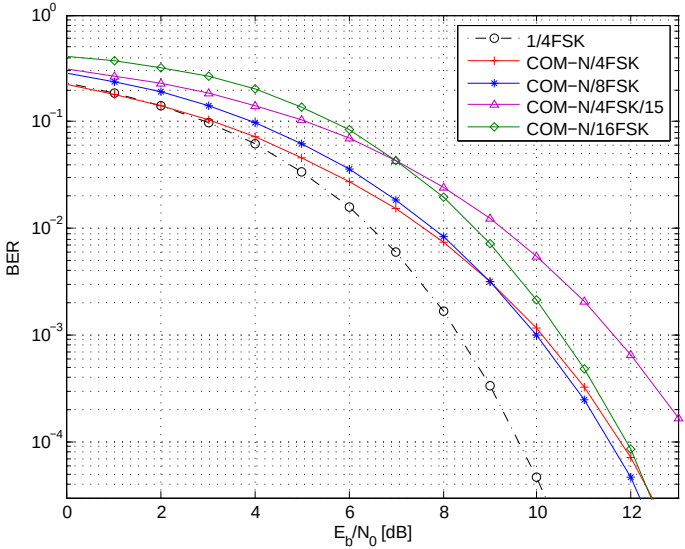

Figure 4.2: Performance comparison (BER vs. $\frac{E_b}{N_0}$) of uncoded OFDM-1/4FSK, OFDM-COM-N/4FSK, OFDM-COM-N/8FSK, OFDM-COM-N/16FSK and OFDM-COM-N/4FSK/15 with noncoherent detection and transmission over the AWGN channel, no cyclic prefix, no guard bands.

Fig. 4.2 shows the performance of 1/4FSK, COM-N/4FSK, COM-N/8FSK, COM-N/16FSK and COM-N/4FSK/15 for an uncoded transmission over the AWGN channel. The detection rule used for all transmission schemes is the squared scalar product.

1/4FSK shows again the best performance having a worse bandwidth ef-

ficiency. For the combined alphabets up to a dimension of $\frac{M}{2}$, we observe the same behaviour as for the multitone alphabets. For the low noise region, the principal angle is the determining factor. The alphabets with a larger minimum principal angle start to perform better compared to the ones with a lower minimum principal angle. They gain in power efficiency.

For COM-N/4FSK/15 all subspaces without the null subspace are used. Therefore the minimum distance, i.e. the principal angle, plays a role from the beginning and it performs worse compared to COM-N/8FSK. At 7 dB, it intersects with COM-N/16FSK. With respect to the minimum distance, we benefit from the point, that for the combined alphabets up to the dimension $\frac{M}{2}$, the subspaces of higher dimension are not used completely.

For COM-N/MFSK, we see, that the BER is shifted to the right for the higher ordered modulation scheme, i.e. the bandwidth efficiency is increased on the cost of the power efficiency. This effect is contrary to pure MFSK, where the BER performance increases for higher order modulation alphabets. The effect obtained for COM-N/MFSK is similar as for other modulation schemes like PSK or QAM, [31] and [24].

OFDM-4/8FSK and OFDM-COM-N/4FSK have the same bandwidth efficiency of 0.75 $\frac{\text{bit/s}}{\text{Hz}}$. If OFDM-4/8FSK in Fig. 4.1 and OFDM-COM-N/4FSK in Fig. 4.2 are compared, we can conclude, that in the region of 10^{-1}, the combined alphabet has significant less complexity and shows a better power efficiency. Note, that the sum energy is twice compared to 4/8FSK, since the FSK block size is $M = 4$. 7/16FSK and COM-N/8FSK have bandwidth efficiencies of 0.8125 $\frac{\text{bit/s}}{\text{Hz}}$ and 0.875 $\frac{\text{bit/s}}{\text{Hz}}$. However, for COM-N/8FSK the complexity of the system is low compared to 7/16FSK. For COM-N/8FSK, only 128 vectors/subspaces are needed, whereas for 7/16FSK 8196 vectors/subspaces are used to obtain a bandwidth efficiency, which is less than the one for COM-N/8FSK.

Fig. 4.3 and Fig. 4.4 show the simulation results for a transmission over the Rayleigh block fading channel, as introduced in Sec. 2.2. The detection rule used for all transmission schemes is the squared scalar product. Note, that in

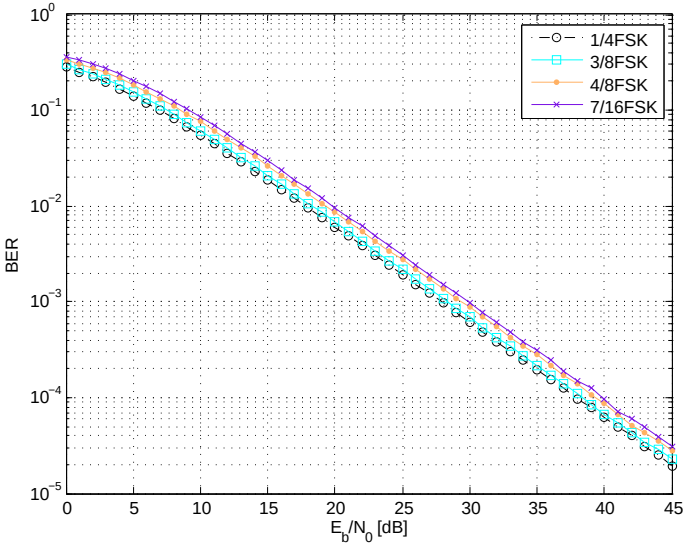

Figure 4.3: Performance comparison (BER vs. $\frac{E_b}{N_0}$) of uncoded OFDM-1/4FSK, OFDM-3/8FSK, OFDM-4/8FSK and OFDM-7/16FSK with noncoherent detection and transmission over the Rayleigh block fading channel, no cyclic prefix, no guard bands.

case of an FSK block size of $M = 4$, the fading coefficient is constant over 4 subcarriers, before it changes to a new independent realization. For a block size of $M = 8$, it is constant over 8 subcarriers, i.e. with an increasing FSK block size and therefore for higher order modulation schemes, the channel has to be constant for a larger number of subcarriers. The other possibility would be, to assume the channel to be constant over $M = 16$ subcarriers. Anyhow, this assumption is neglectable, since the decisions are made FSK block wise.

Additionally to Fig. 4.3 and Fig. 4.4, Table 4.2 shows the loss in $\frac{E_b}{N_0}$ in dB for the different modulation schemes. The loss in power efficiency for all multitone FSK alphabets and for all combined FSK alphabets compared to pure

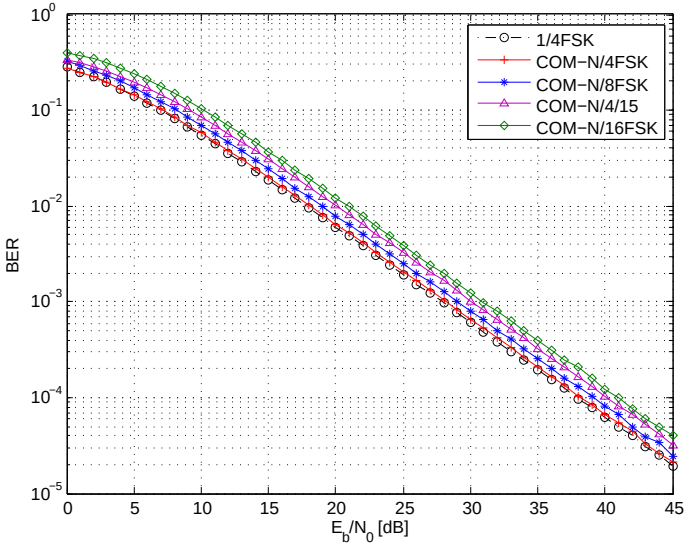

Figure 4.4: Performance comparison (BER vs. $\frac{E_b}{N_0}$) of uncoded OFDM-1/4FSK, OFDM-COM-N/4FSK, OFDM-COM-N/8FSK, OFDM-COM-N/16FSK and OFDM-COM-N/4FSK/15 with noncoherent detection and transmission over the Rayleigh block fading channel, no cyclic prefix, no guard bands.

1/4FSK is less, compared to the results obtained for the transmission over the AWGN channel. OFDM-COM-N/4FSK shows roughly the same performance compared to pure OFDM-1/4FSK. The difference between both curves is neglectable, in contrast to the gain in bandwidth efficiency of 50% for the combined alphabet. The loss between COM-N/4FSK and COM-N/8FSK is around 1 dB. For COM-N/8FSK seven bits are transmitted within one FSK block of size $M = 8$ performs better compared to 4/8FSK, where six bits are transmitted for the same FSK block size. COM-N/4FSK/15 plays a special role. It performs a bit worse, than COM-N/8FSK, but still better than COM-N/16FSK. The loss in power efficiency is due to the reason, that all subspaces except the null space are used for the transmission and the situation, that

Table 4.2: Loss in $\frac{E_b}{N_0}$ for different N/MFSK and COM-N/MFSK modulation schemes.

Modulation scheme		Loss [dB]
1/4FSK	- COM-N/4FSK	~ 0.4
COM-N/4FSK	- 3/8FSK	~ 0.1
3/8FSK	- COM-N/8FSK	~ 0.6
COM-N/8FSK	- 4/8FSK	~ 0.4
4/8FSK	- 7/16FSK	~ 0.5
7/16FSK	- COM-N/4FSK/15	~ 0.3
COM-N/4FSK/15	- COM-N/16FSK	~ 0.7

three or four subcarriers within a subspace can be used for transmission. As a consequence, these blocks are more sensitive towards the fading from the channel, compared to COM-N/8FSK, where the FSK block consists of eight subcarriers and at most four out of eight subcarriers are active.

The performance in terms of BER vs. $\frac{E_b}{N_0}$ [dB] for a transmission over a Rayleigh frequency selective fading channel, as proposed in Sec. 2.2, can be seen in Fig. 4.5 for N/MFSK and in Fig. 4.6 for COM-N/MFSK. Pure 1/4FSK is again used as a reference plot. For the Rayleigh frequency selective fading channel, each subcarrier is affected by a different independent fading coefficient. For 1/4FSK, either the squared scalar product or the squared Frobenius norm can be used for detection. For N/MFSK, the squared Frobenius norm is used for detection, whereas for the combined alphabets, the multivariate or the matrix variate PDF are used for detection. Both PDFs presume knowledge of the noise variance σ_n^2 and the channel covariance matrix $\mathbf{\Lambda}_h$ in the receiver. The simulations have been carried out with perfect knowledge of σ_n^2 and $\mathbf{\Lambda}_h$.

For COM-N/16FSK, 32768 subspaces are obtained. The ML detection us-

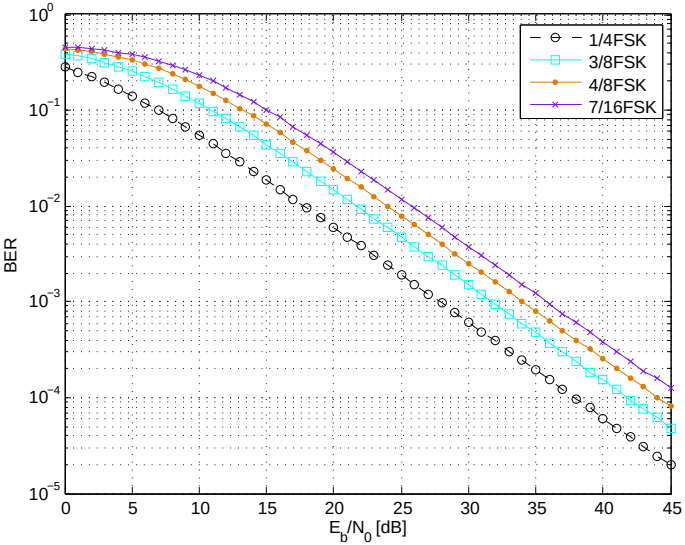

Figure 4.5: Performance comparison (BER vs. $\frac{E_b}{N_0}$) of uncoded OFDM-1/4FSK, OFDM-3/8FSK, OFDM-4/8FSK and OFDM-7/16FSK with noncoherent detection and transmission over the Rayleigh frequency selective fading channel, no cyclic prefix, no guard bands.

ing the PDF has a high complexity, since all 32768 possibilities have to be compared. Therefore, only COM-N/4FSK and COM-N/8FSK are used.

A higher ordered modulation alphabet leads in both cases, N/MFSK as well as COM-N/MFSK, to a shift to the right of the curves. Pure 1/4FSK still shows the best performance, having a worse bandwidth efficiency. COM-N/4FSK is located in between 3/8FSK and 4/8FSK, whereas COM-N/8FSK performs worse compared to 7/16FSK.

The effect of the frequency selective fading is, that each subcarrier is faded out independently from its neighbors, i.e. each basis vector of a subspace is

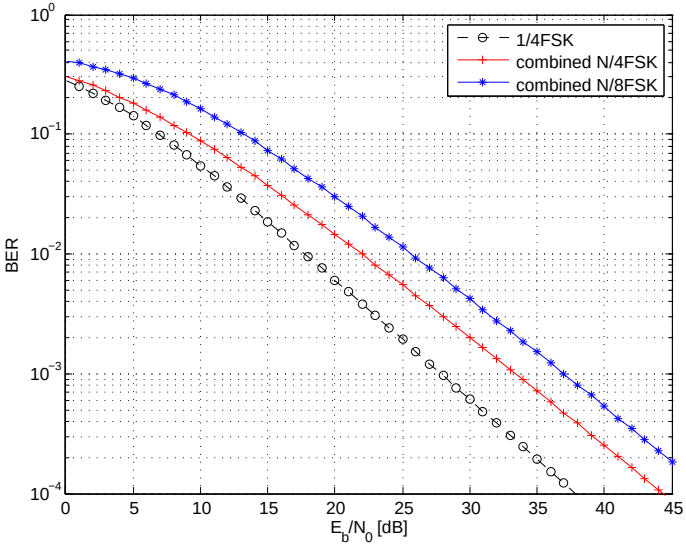

Figure 4.6: Performance comparison (BER vs. $\frac{E_b}{N_0}$) of uncoded OFDM-1/4FSK, OFDM-COM-N/4FSK and OFDM-COM-N/8FSK with noncoherent detection and a transmission over the Rayleigh frequency selective fading channel, no cyclic prefix, no guard bands.

scaled differently. This leads to a decreased performance in terms of BER over $\frac{E_b}{N_0}$ for N/MFSK as well as COM-N/MFSK. However, we have shown, that even for these scenarios, it is possible to increase the bandwidth efficiency. If OFDM multitone FSK is used, the PDF can be simplified to the squared Frobenius norm and an ML detection rule is obtained.

4.2 BICM and Iterative Detection

The performance of coded OFDM-N/MFSK and coded OFDM-COM-N/MFSK is compared in the following. An iterative receiver, c.f. Sec. 2.3.2, is used and

we optimize our mapping according to the optimization algorithm presented in [46], to achieve the maximum extrinsic information of the demapper, by applying a vector swapping algorithm, in conjunction with the cost function provided in [35]. For channel coding a convolutional code with code rate $r_c = \frac{1}{2}$, memory length 6 and generator polynomial $\begin{bmatrix}133 & 171\end{bmatrix}_8$ is used. Since we are interested in worse channel scenarios, the simulations were carried out for a transmission over the Rayleigh block fading channel. Neither guard bands nor a cyclic prefix were used.

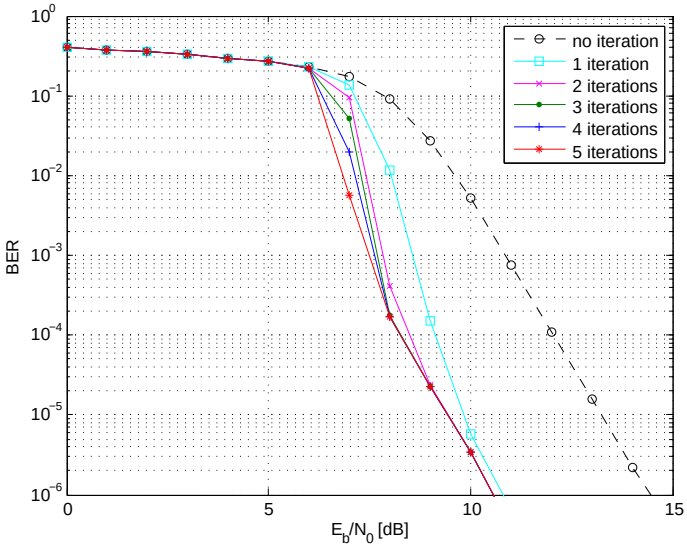

Figure 4.7: Performance comparison (BER vs. $\frac{E_b}{N_0}$) of coded OFDM-COM-N/4FSK with noncoherent detection and transmission over the Rayleigh block fading channel for different iteration steps. Simulation parameters: no cyclic prefix, no guard bands, $r_c = \frac{1}{2}$, memory 6 convolutional code with generator polynomial $[133\ 171]_8$.

Fig. 4.7 shows the BER over $\frac{E_b}{N_0}$ for coded OFDM-COM-N/4FSK. An iterative receiver with five iteration steps is used. No iteration corresponds to

soft decoding of the convolutional code with the BCJR, i.e. serial demapping and decoding. With an increasing number of iterations, a remarkable gain in power efficiency for iterative demapping and decoding is obtained. With decreasing noise power, less gain is achieved for a single iteration step. For the following simulations five iteration steps are used for having optimal results in the region of higher noise power.

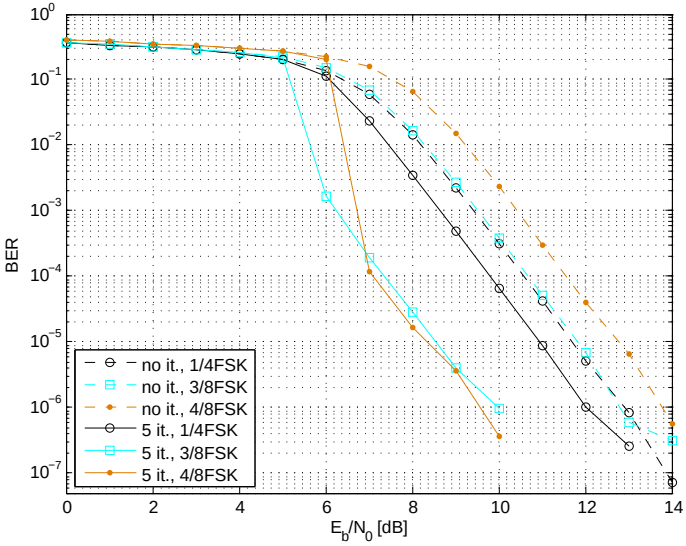

Figure 4.8: Performance comparison (BER vs. $\frac{E_b}{N_0}$) of coded OFDM-1/4FSK, OFDM-3/8FSK and OFDM-4/8FSK with noncoherent detection and a transmission over the Rayleigh block fading channel for different iteration steps. Simulation parameters: no cyclic prefix, no guard bands, $r_c = \frac{1}{2}$, memory 6 convolutional code with generator polynomial $[133\ 171]_8$.

Fig. 4.8 shows the performance of 1/4FSK, used again as reference plot, versus 3/8FSK and 4/8FSK and Fig. 4.9 shows the BER over $\frac{E_b}{N_0}$ for COM-N/4FSK and COM-N/8FSK. The system setup, presented in Table 4.1 is used and for coding a rate $r_c = \frac{1}{2}$ with memory 6 and generator polynomial

$\begin{bmatrix}133 & 171\end{bmatrix}_8$ is applied. Therefore the same data rate for all BER curves is obtained.

In Fig. 4.8, we observe, that for serial demapping and decoding, i.e. no iteration steps, 1/4FSK performs best. This is due to the fact, that the subspaces are orthogonal to each other and that the optimization algorithm is made for iterative detection. After five iteration steps, both 3/8FSK and 4/8FSK, perform better compared to 1/4FSK. In the region of large noise, 3/8FSK performs better than 4/8FSK. This is due to the fact, that in the uncoded case for the Rayleigh block fading channel, see Fig. 4.3, 3/8FSK is better in the region of a bit error probability of $P_b = 10^{-1}$ up to $P_b = 10^{-2}$. In this region, coding starts to improve the resulting BER. We can conclude for multitone FSK, that for large noise, subspaces of lower dimensions are beneficial. At around 7 dB, 3/8FSK and 4/8FSK intersect. 4/8FSK is better than 3/8FSK.

For COM-N/4FSK and COM-N/8FSK in Fig. 4.9, a similar result is obtained as for OFDM multitone FSK. However, for no iteration steps COM-N/8FSK is slightly better than COM-N/4FSK. After five iteration steps, this result is still obtained with a remarkable gain in power efficiency for both combined alphabets compared to 1/4FSK. For a bit error probability of $P_b = 10^{-6}$ for 1/4FSK $\frac{E_b}{N_0}$ is approximately 12 dB, whereas for COM-N/4FSK 1.5 dB less are needed to achieve the same BER and for COM-N/8FSK a gain of approximately 5 dB compared to pure 1/4FSK is obtained.

Besides the increased power efficiency for five iteration steps for the combined alphabets, the bandwidth efficiency is also larger compared to pure OFDM-1/4FSK and the multitone FSK alphabets. For OFDM-COM-N/8FSK, the waterfall region is at $\frac{E_b}{N_0} = 6\,\text{dB}$.

It is stressed again, that for the combined alphabets of higher dimension, i.e. for an increasing FSK block size M, two effects are obtained: The fading coefficient is constant for a larger number of frequencies, i.e. the channel becomes more “flat”. And the bits are spread over more subcarriers. Since we use a convolutional code with an interleaver, our coded bits are hugely spread over the whole OFDM block. These facts lead to the gain for the combined alphabets of higher dimension M.

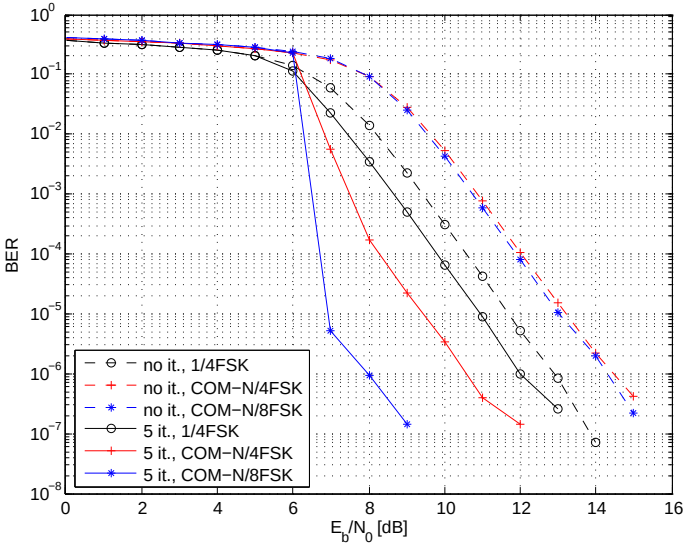

Figure 4.9: Performance comparison (BER vs. $\frac{E_b}{N_0}$) of coded OFDM-1/4FSK, OFDM-COM-N/4FSK and OFDM-COM-N/8FSK with noncoherent detection and a transmission over the Rayleigh block fading channel for different iteration steps. Simulation parameters: no cyclic prefix, no guard bands, $r_c = \frac{1}{2}$, memory 6 convolutional code with generator polynomial $[133\ 171]_8$.

4.3 Chapter Summary

Different simulation results for an uncoded transmission over the AWGN channel, the Rayleigh block fading channel and the Rayleigh frequency selective fading channel have been discussed. We have observed an interesting effect for COM-N/MFSK alphabets and for the multitone FSK alphabets for a transmission over the AWGN channel. A higher dimension of the space, i.e. an increasing FSK block size M, causes a shift of the BER curve to the right. For COM-N/MFSK, this effect tends to be stronger, than for the multitone FSK alphabets. This effect is well-known for modulation principles as QAM

or PSK. It can also be observed for the Rayleigh frequency selective fading channel.

However, for the uncoded transmission over the Rayleigh block fading channel, we have observed, that all results lie in the same region. OFDM-1/4FSK shows the best performance, directly followed by our new proposed OFDM-COM-N/4FSK. The difference in BER turned out to be neglectable, compared to the gain in bandwidth efficiency of 50 % for COM-N/4FSK.

For the coded simulation results with BICM and an iterative receiver, the main result obtained is, that the combined alphabets give a huge gain in power efficiency compared to pure 1/4FSK, which has been used as reference plot. To achieve this gain, an optimization algorithm for the mapping has been used.

Chapter 5

Extended Mapping for Transmission with Subspaces of Different Dimensions

So far, we have seen, that the bandwidth efficiency of OFDM-MFSK can be significantly increased by making use of our approach of combining subspaces of different dimensions or for the case of the vector-valued transmission by combining different FSK alphabets of the same FSK block size M. If not

mentioned otherwise, from now on we refer to vectors. Since channel coding is a must in today's transmission schemes, one could think about gaining an extra bit for channel coding by making use of extended mapping, as proposed by Clevron and Vary in [8] and by Henkel in [17]. This idea has been evaluated within the master thesis of George Yammine and results have been already published in [46].

In the following, the principles of extended mapping are briefly introduced. This is followed by an extended mapping for OFDM-COM-N/4FSK, also called symmetric extended mapping, and we will present the new idea of a non-symmetric extended mapping for the combined FSK alphabet.

For performance comparison, we compare coded OFDM-COM-N/4FSK with OFDM-1/4FSK with extended mapping for transmission over the Rayleigh block fading channel. Finally, the simulation results of the two extended mapping schemes, symmetric and non-symmetric extended mapping, for OFDM-COM-N/4FSK for transmission over the Rayleigh block fading channel are discussed.

5.1 Principles of Extended Mapping

Extended mapping, see [8] and [17], offers the possibility of gaining additional bits per FSK vector for coding. So far, the iterative demapper and decoder for BICM-ID, c.f. 2.6, have been interpreted in the following way: the mapping was an inner code with code rate $r_c = 1$, since no redundancy was added for the mapping, and the channel code was treated as an outer code. For 2^m N/MFSK vectors of the combined alphabet, which consisted of $\sum_{N=1}^{M/2} \binom{M}{N}$ vectors, $m = \left\lfloor \log_2 \left[\sum_{N=1}^{M/2} \binom{M}{N} \right] \right\rfloor$ bits have been assigned. Therefore each transmit vector was assigned an explicit bit mapping of length m.

Extended mapping is the process of assigning multiple bit labels to the transmit vectors (in general constellation points). This presents the possibility to gain extra coded bits, with the cost of introducing ambiguity in the mapping. This ambiguity can only be resolved with a turbo receiver, based

on the receiver for BICM-ID. By doing so, the information exchange between the demapper and decoder leads to the right decision over the ambiguous bit mappings after a sufficient number of iterations.

Table 5.1: Extended mapping for OFDM-COM-N/4FSK. The black colored bits are the same for each of the two combinations and the blue colored bits contain the ambiguity.

Transmit vectors	$\mathbf{x}_1$	$\mathbf{x}_2$	$\mathbf{x}_3$	$\mathbf{x}_4$	$\mathbf{x}_5$	$\mathbf{x}_6$	$\mathbf{x}_7$	$\mathbf{x}_8$
$\mathbf{x}_k$	$\begin{bmatrix}0\\0\\0\\1\end{bmatrix}$	$\begin{bmatrix}0\\0\\1\\0\end{bmatrix}$	$\begin{bmatrix}0\\1\\0\\1\end{bmatrix}$	$\begin{bmatrix}1\\0\\1\\0\end{bmatrix}$	$\begin{bmatrix}0\\1\\0\\0\end{bmatrix}$	$\begin{bmatrix}1\\0\\0\\1\end{bmatrix}$	$\begin{bmatrix}0\\1\\1\\0\end{bmatrix}$	$\begin{bmatrix}1\\0\\0\\0\end{bmatrix}$
Mapping	$\begin{bmatrix}0\\0\\0\\0\end{bmatrix}$	$\begin{bmatrix}0\\1\\0\\1\end{bmatrix}$	$\begin{bmatrix}0\\0\\0\\1\end{bmatrix}$	$\begin{bmatrix}0\\1\\0\\0\end{bmatrix}$	$\begin{bmatrix}0\\0\\1\\1\end{bmatrix}$	$\begin{bmatrix}0\\0\\1\\0\end{bmatrix}$	$\begin{bmatrix}0\\1\\1\\1\end{bmatrix}$	$\begin{bmatrix}0\\1\\1\\0\end{bmatrix}$
	$\begin{bmatrix}1\\1\\0\\0\end{bmatrix}$	$\begin{bmatrix}1\\0\\0\\1\end{bmatrix}$	$\begin{bmatrix}1\\1\\0\\1\end{bmatrix}$	$\begin{bmatrix}1\\0\\0\\0\end{bmatrix}$	$\begin{bmatrix}1\\1\\1\\1\end{bmatrix}$	$\begin{bmatrix}1\\1\\1\\0\end{bmatrix}$	$\begin{bmatrix}1\\0\\1\\1\end{bmatrix}$	$\begin{bmatrix}1\\0\\1\\0\end{bmatrix}$

Table 5.1 provides an extended mapping for COM-N/4FSK. Multiple bit labels are assigned to each FSK vector of length $M = 4$ and by doing so, one extra coded bit is obtained. There exists ambiguity for each of the eight vectors, since two possible bit combinations are assigned now to each of the eight transmit vectors. To visualize the two combinations, the bits in Table 5.1 are colored. The black colored bits are the same for each of the two combinations and the blue colored bits contain the ambiguity. To analyze the behaviour of the iterative system, we have discussed in [46] the EXIT charts [39] of the system. For the mapping, a vector swapping algorithm, see [46] was used.

We have shown in Chapter 3.2, that for the combination of subspaces of

different dimensions, an alphabet is obtained, where not all of the included subspaces are needed for transmission. If we go back to the vector-valued transmission model, the alphabet of OFDM-COM-N/4FSK contains ten possible transmit vectors.

Table 5.2: Non-symmetric extended mapping for OFDM-COM-N/4FSK. The black colored bits are the same for each of the two combinations and the blue colored bits contain the ambiguity.

Transmit vectors	$\mathbf{x}_1$	$\mathbf{x}_2$	$\mathbf{x}_3$	$\mathbf{x}_4$	$\mathbf{x}_5$	$\mathbf{x}_6$	$\mathbf{x}_7$	$\mathbf{x}_8$	$\mathbf{x}_9$	$\mathbf{x}_{10}$
$\mathbf{x}_k$	$\begin{bmatrix}0\\0\\0\\1\end{bmatrix}$	$\begin{bmatrix}0\\0\\1\\0\end{bmatrix}$	$\begin{bmatrix}0\\1\\0\\0\end{bmatrix}$	$\begin{bmatrix}1\\0\\0\\0\end{bmatrix}$	$\begin{bmatrix}1\\1\\0\\0\end{bmatrix}$	$\begin{bmatrix}0\\0\\1\\1\end{bmatrix}$	$\begin{bmatrix}1\\0\\1\\0\end{bmatrix}$	$\begin{bmatrix}0\\1\\0\\1\end{bmatrix}$	$\begin{bmatrix}1\\0\\0\\1\end{bmatrix}$	$\begin{bmatrix}0\\1\\1\\0\end{bmatrix}$
Mapping	$\begin{bmatrix}1\\1\\1\\0\end{bmatrix}$	$\begin{bmatrix}1\\1\\1\\1\end{bmatrix}$	$\begin{bmatrix}1\\0\\1\\1\end{bmatrix}$	$\begin{bmatrix}1\\0\\0\\1\end{bmatrix}$	$\begin{bmatrix}0\\1\\1\\0\end{bmatrix}$	$\begin{bmatrix}0\\0\\1\\1\end{bmatrix}$	$\begin{bmatrix}0\\1\\0\\1\end{bmatrix}$	$\begin{bmatrix}0\\1\\0\\0\end{bmatrix}$	$\begin{bmatrix}0\\0\\0\\0\end{bmatrix}$	$\begin{bmatrix}1\\1\\0\\0\end{bmatrix}$
	$\begin{bmatrix}1\\1\\0\\1\end{bmatrix}$	$\begin{bmatrix}0\\0\\0\\1\end{bmatrix}$	$\begin{bmatrix}0\\1\\1\\1\end{bmatrix}$	$\begin{bmatrix}1\\0\\0\\0\end{bmatrix}$			$\begin{bmatrix}1\\0\\1\\0\end{bmatrix}$	$\begin{bmatrix}0\\0\\1\\0\end{bmatrix}$		

If extended mapping is applied for any combined alphabet, it is possible to use all available vectors of the transmit vector alphabet. This results in a lower ambiguity for the bit assignment in the mapping. With an increased number of transmit vectors, single mappings can be assigned to a subset of the transmit vectors, whereas double mappings are assigned to the rest of the transmit vectors. This step leads to a reduced ambiguity for the mapping. The iterative receiver benefits now of an increase of the available a-priori information, which itself leads to an increase of the extrinsic information due to the decreased ambiguity of the multiple mappings.

The decision, which has to be made now, is to find the vectors, used for single bit mappings, and the ones for double bit mappings. We propose a

similar non-symmetric extended mapping as proposed by Clevron and Vary in [8]. The vectors with the largest separating angles are chosen for the double mappings, i.e. the 1/MFSK vectors, since they enclose an angle of 90°. Additional to these vectors, depending on the number of required vectors for double bit mappings, pairwise orthogonal vectors from the next higher-dimensional alphabet are chosen. The chosen transmit vectors are now optimized according to the optimization algorithm in [46]. Table 5.2 shows a non-symmetric extended mapping for OFDM-COM-N/4FSK. The blue colored bits highlight the ambiguous bits.

5.2 Simulation Results

Fig. 5.1 shows the performance comparison for the BER over $\frac{E_b}{N_0}$ for a coded transmission over the Rayleigh block fading channel for OFDM-1/4FSK, OFDM-1/4FSK with extended mapping and for OFDM-COM-N/4FSK without extended mapping. Guard intervals as well as guard bands are set to zero and the number of iteration steps for the iterative receiver was set to five. The transmit vectors are energy normalized. For OFDM-1/4FSK a $r_c = \frac{1}{2}$, memory 6 convolutional code with generator polynomial $[133\ 171]_8$ has been used. For the other two schemes, we found out in [46], that a $r_c = \frac{1}{3}$, memory 6 convolutional code with generator polynomial $[133\ 165\ 171]_8$ and a $r_c = \frac{1}{3}$, memory 3 convolutional code with generator polynomial $[13\ 15\ 17]_8$ are optimum. The code rates have been chosen in a way, that the data rate for all three systems is the same: 1 information bit per FSK vector. We can observe, that OFDM-COM-N/4FSK shows an earlier convergence point compared to OFDM-1/4FSK with extended mapping. A gain of approximately 2 dB is obtained. At $\frac{E_b}{N_0} \approx 9$ dB, OFDM-1/4FSK with extended mapping starts to perform better than OFDM-1/4FSK. Important is the fact, that our proposed combined alphabet shows a huge gain in power efficiency, compared to OFDM-1/4FSK with extended mapping. Additionally, our combined alphabet can be realized in an effective way, compared to setting up a scheme, using extended mapping.

Fig. 5.2 shows the simulation results for OFDM-COM-N/4FSK with sym-

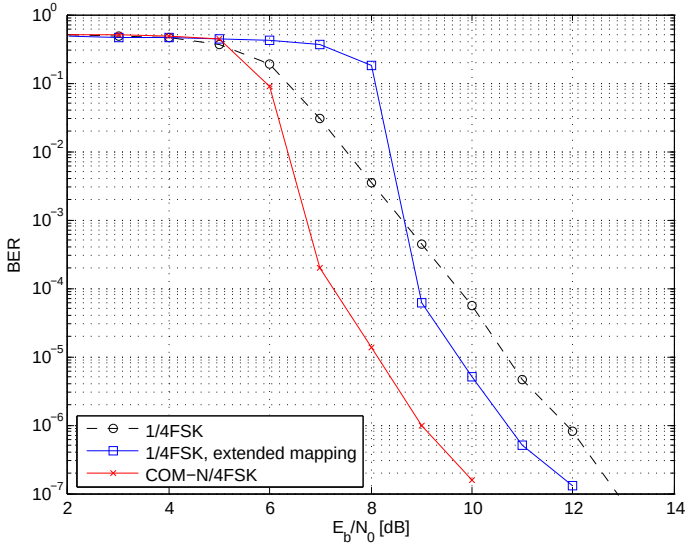

Figure 5.1: Performance comparison (BER vs. $\frac{E_b}{N_0}$) of a coded transmission over the Rayleigh block fading channel for OFDM-1/4FSK, OFDM-1/4FSK with extended mapping and OFDM-COM-N/4FSK.

metric extended mapping and OFDM-COM-N/4FSK with our new proposed non-symmetric extended mapping with a $r_c = \frac{1}{2}$, memory 2 convolutional code with generator polynomial $[5\ 7]_8$ for a transmission over a Rayleigh block fading channel. Uncoded OFDM-1/4FSK is used as reference plot and all three simulation results have the same information data rate. We observe, that using non-symmetric extended mapping leads to an improved power efficiency compared to OFDM-COM-N/4FSK with symmetric extended mapping. The gain obtained is approximately 1 dB. Note, that the LLR values are calculated bit-wise and therefore we have already taken into account the different symbol probabilities for the case of the non-symmetric extended mapping.

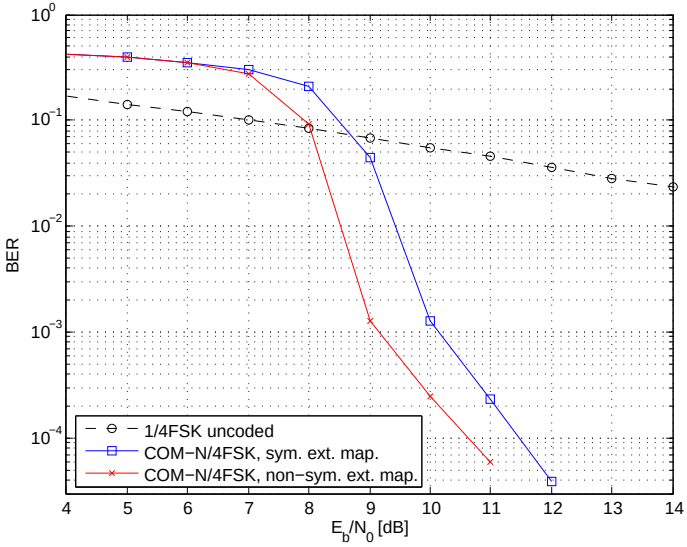

Figure 5.2: Performance comparison (BER vs. $\frac{E_b}{N_0}$) of uncoded OFDM-1/4FSK, OFDM-COM-N/4FSK with symmetric extended mapping and OFDM-COM-N/4FSK with non-symmetric extended mapping for a transmission over the Rayleigh block fading channel.

5.3 Chapter Summary

In this chapter, we

- used symmetric extended mapping for our combined alphabet,
- introduced non-symmetric extended mapping for COM-N/MFSK,
- and analyzed the performance of our proposed combined FSK alphabet without extended mapping versus pure OFDM-MFSK using extended mapping.

OFDM-COM-N/4FSK has shown a huge gain ($\approx$ 2 dB) versus OFDM-1/4FSK with extended mapping. Both transmission schemes had the same end to end

data rate. This shows again the low complexity of our approach to increase the bandwidth of OFDM-MFSK significantly.

We have shown that there is a gain of $\approx$ 1 dB when the non-symmetric extended mapping is used for COM-N/4FSK, compared to the simulation result for COM-N/4FSK with extended mapping.

Chapter 6

Summary and Conclusions

The starting point for this thesis was to consider noncoherent communication over fast fading channels, where OFDM-MFSK and its multitone variant, proposed by Wetz et al. and Linduska et al. in [45], [44] and [25], built our starting point and we tried to improve the bandwidth efficiency of OFDM-MFSK. The three new main contributions are:

- It was shown, that OFDM-MFSK and its multitone variant are a special case of noncoherent communication based on subspaces as proposed by Hochwald and Marzetta in [19].
- A new transmission scheme with subspaces of different dimensions was

proposed with an increase in bandwidth efficiency approaching the limit of 1 $\frac{\text{bit}}{\text{s Hz}}$, without a noteworthy increase of the complexity of the system. This new transmission scheme is named OFDM-COM-N/MFSK.

- The advantage of extended mapping together with non-symmetric extended mapping was shown for OFDM-COM-N/MFSK.

In Chapter 2, we presented the necessary fundamentals for understanding this thesis. We introduced the vector-valued transmission model [24], [11] for OFDM, followed by a brief description of the channel models of interest for this thesis. We presented OFDM-MFSK and its multitone variant, the transmission schemes our work is built on. Both are very robust in fast fading time-variant environments and can be detected noncoherently. However their bandwidth efficiency is low. We shortly addressed their noncoherent detection and described a coded transmission model with an iterative receiver. A short note on the capacity of multipath fading channels was given, since Telatar et al. [38] and Medard et al. [26], have shown for frequency selective fading channels, that for a large transmission bandwidth the channel capacity of the infinite bandwidth AWGN channel can be approached with "peaky" input signals. They proposed FSK and noncoherent detection to be a good basis. Finally, the basic principles for understanding a subspace based transmission were given.

In Chapter 3 we have characterized, that OFDM-MFSK is a special case of a noncoherent communication based on subspaces in the context of MIMO systems. The starting point built the vector-valued transmission model for OFDM-MFSK and the matrix-valued transmission model for the subspace based communication system. We have shown, that the FSK vectors of dimension $M \times 1$ can be transformed into matrices, by writing the frequency positions of an FSK vector on the main diagonal of an $M \times M$ dimensional matrix, where the off-diagonal elements have to be "artificial" zeros.

Being able to describe OFDM-MFSK as a noncoherent transmission based on subspaces, we developed a possibility how to combine subspaces of different dimensions. This was achieved by combining OFDM-MFSK and its multitone variant and we named the new transmission scheme OFDM-COM-N/MFSK.

The combination of subspaces of different dimensions for OFDM-MFSK and its multitone variant implicates an increase in bandwidth efficiency. This

result is one of the main results of this thesis. We compare different MFSK, multitone FSK and COM-N/MFSK modulation schemes with respect to their bandwidth efficiencies and show, that with our proposed combined alphabets the increase in bandwidth efficiency approaches $1\,\frac{\text{bit}}{\text{s Hz}}$. Noteworthy is the circumstance, that the increase in bandwidth efficiency for COM-N/MFSK can be realized in an effective way, since the complexity of the system does not increase remarkably.

We also addressed the noncoherent detection of the subspaces for COM-N/MFSK based on the matrix variate PDF and derived the conditional complex-valued matrix variate PDF for the Rayleigh block fading channel and the Rayleigh frequency selective fading channel. When possible, it was simplified to an ML detection rule. For the Rayleigh block fading channel, the squared scalar product turned out to be ML for the combination of subspaces of different dimensions. For the Rayleigh frequency selective fading channel and subspaces of the same dimension, we have derived the squared Frobenius norm for ML detection. This result is of interest, since it allows to increase the bandwidth efficiency of OFDM-MFSK under worse channel conditions, since for the Rayleigh frequency selective fading channel, each fading coefficient changes independently.

We discussed the principal angle as distance measure and stated that only subspaces up to the dimension $\frac{M}{2}$ should be combined.

Finally, we explained how to go back from subspaces to FSK vectors by making a comparison of the conditional matrix variate PDF and the conditional multi-variate PDF for the used channel models. Therefore, the results derived for the subspace based transmission model have been transferred to the vector-valued transmission model.

Detailed simulation results for uncoded transmission as well as coded transmission over different channel models have been discussed within Chapter 4. For transmission over the AWGN channel, we observed, that the combined alphabet shows a similar behaviour as it is known for QAM or PSK, since with an increasing FSK block size M, the resulting curve is shifted to the right. This is contrary to pure OFDM-MFSK. For the Rayleigh block fading channel, this behaviour relativizes, since OFDM-MFSK, its multitone variant and the combined alphabets show similar results. The loss in $\frac{E_b}{N_0}$ for COM-N/4FSK compared to 1/4FSK is only ≈ 0.4 dB with an increased bandwidth

efficiency of 50 %. We also presented simulation results for coded transmission using an iterative receiver. Multitone FSK as well as COM-N/MFSK benefit from the iterative demapper and decoder and show a huge gain compared to OFDM-1/4FSK. With an increasing FSK block size the combined alphabets have a larger gain in power efficiency after five iteration steps.

The third main contribution of this thesis was to investigate an extended mapping scheme within Chapter 5. We proposed a symmetric extended mapping for our COM-N/4FSK alphabet and developed a non-symmetric extended mapping scheme by making use of all available subspaces within the set of a transmit alphabet. This results in reduced ambiguity for the bit labels, which is also mirrored in the simulation results, where a gain of ≈ 1 dB for the non-symmetric extended mapping is obtained compared to the symmetric extended mapping. We also compared 1/4FSK with extended mapping and COM-N/4FSK without extended mapping, using the same code rate, such that the data rate of both systems was the same. We have seen, that for the Rayleigh block fading channel COM-N/4FSK shows a gain in power efficiency of ≈ 2 dB compared to 1/4FSK with extended mapping. Since it is easier to implement and realize COM-N/4FSK than 1/4FSK with extended mapping, our proposed combined alphabet turns out to be effective with respect to the increase in bandwidth efficiency and in power efficiency.

In this thesis, we characterized OFDM-MFSK and OFDM multitone FSK as a special case of noncoherent subspace based transmissions. Based on this subspace based transmission, we have shown as one of our key ideas, how subspaces of different dimensions can be combined. An outstanding result of this combination is the possibility to increase the bandwidth efficiency of OFDM-MFSK significantly without a substantial increase in complexity. The upper bound of $1\,\frac{\text{bit}}{\text{s Hz}}$ for the bandwidth efficiency is approached. By making use of extended mapping and non-symmetric extended mapping, we have gained an additional bit for either increasing the data rate or the redundancy. We propose OFDM-COM-N/MFSK being a very good candidate for the practical application of frequency hopping. There is no need of channel state information and it is very robust in fast fading environments.

Appendix $\mathcal{A}$

Unitary Space-Time Modulation: Noncoherent ML receiver

The stepwise derivation of the maximum-likelihood detection rule for the transmission of unitary subspace based matrices, as defined in [19], is

$$\hat{\mathbf{\Phi}}_l = \underset{\mathbf{\Phi}_l \in \{\mathbf{\Phi}_1, \cdots, \mathbf{\Phi}_L\}}{\operatorname{argmax}} p\left(\mathbf{Y}|\mathbf{\Phi}_l\right)$$

$$= \underset{\mathbf{\Phi}_l \in \{\mathbf{\Phi}_1, \cdots, \mathbf{\Phi}_L\}}{\operatorname{argmax}} \frac{\exp\left(-\operatorname{tr}\left\{\left[\mathbf{I} + \frac{\rho T}{M_{\mathrm{tx}}} \mathbf{\Phi}_l^H \mathbf{\Phi}_l\right]^{-1} \mathbf{Y}^H \mathbf{Y}\right\}\right)}{\pi^{TN} \det^{N_{\mathrm{rx}}}\left[\mathbf{I} + \frac{\rho T}{M_{\mathrm{tx}}} \mathbf{\Phi}_l^H \mathbf{\Phi}_l\right]} \tag{A.1}$$

$$= \underset{\mathbf{\Phi}_l \in \{\mathbf{\Phi}_1, \cdots, \mathbf{\Phi}_L\}}{\operatorname{argmax}} \frac{\exp\left(-\operatorname{tr}\left\{\left[\mathbf{I} - \frac{1}{1+\frac{M_{\mathrm{tx}}}{\rho T}} \mathbf{\Phi}_l^H \mathbf{\Phi}_l\right] \mathbf{Y}^H \mathbf{Y}\right\}\right)}{\pi^{TN} \left(1 + \frac{\rho T}{M_{\mathrm{tx}}}\right)^{M_{\mathrm{tx}} N_{\mathrm{rx}}}}. \tag{A.2}$$

For solving from (A.1) to (A.2) the following matrix formulas have to be applied [37]:

$$\det(\mathbf{I} + \mathbf{AB}) = \det(\mathbf{I} + \mathbf{BA})$$

and the matrix inversion lemma

$$(\mathbf{A} + \mathbf{BCD})^{-1} = \mathbf{A}^{-1} - \mathbf{A}^{-1}\mathbf{B}(\mathbf{C}^{-1} + \mathbf{DA}^{-1}\mathbf{B})^{-1}\mathbf{DA}^{-1}. \tag{A.3}$$

Rewriting Eq. (A.2) leads to

$$\begin{aligned}
\hat{\mathbf{\Phi}}_l &= \underset{\mathbf{\Phi}_l \in \{\mathbf{\Phi}_1, \cdots, \mathbf{\Phi}_L\}}{\operatorname{argmax}} \frac{\exp\left(-\operatorname{tr}\left\{\mathbf{I}_T \mathbf{Y}^H \mathbf{Y}\right\} + \operatorname{tr}\left\{\frac{1}{1+\frac{M_{\mathrm{tx}}}{\rho T}} \mathbf{\Phi}_l^H \mathbf{\Phi}_l \mathbf{Y}^H \mathbf{Y}\right\}\right)}{\pi^{TN} \left(1 + \frac{\rho T}{M_{\mathrm{tx}}}\right)^{M_{\mathrm{tx}} N_{\mathrm{rx}}}} \\
&= \underset{\mathbf{\Phi}_l \in \{\mathbf{\Phi}_1, \cdots, \mathbf{\Phi}_L\}}{\operatorname{argmax}} \frac{\exp(-\operatorname{tr}\{\mathbf{I}_T \mathbf{Y}^H \mathbf{Y}\}) \exp\left(\operatorname{tr}\left\{\frac{1}{1+\frac{M_{\mathrm{tx}}}{\rho T}} \mathbf{\Phi}_l^H \mathbf{\Phi}_l \mathbf{Y}^H \mathbf{Y}\right\}\right)}{\pi^{TN} \left(1 + \frac{\rho T}{M_{\mathrm{tx}}}\right)^{M_{\mathrm{tx}} N_{\mathrm{rx}}}} \\
&= \underset{\mathbf{\Phi}_l \in \{\mathbf{\Phi}_1, \cdots, \mathbf{\Phi}_L\}}{\operatorname{argmax}} \exp\left(\operatorname{tr}\left\{\frac{1}{1+\frac{M_{\mathrm{tx}}}{\rho T}} \mathbf{\Phi}_l^H \mathbf{\Phi}_l \mathbf{Y}^H \mathbf{Y}\right\}\right).
\end{aligned} \tag{A.4}$$

Based on the fact that a dependency on the transmitted matrix $\mathbf{\Phi}_l$ is only given in the second term of the exponential function, the maximum-likelihood detection rule has been simplified to Eq. (A.4).

According to the definition of Hochwald and Marzetta in [19] the number of time-slots T has to be greater than the number of transmit antennas M_{tx},

which leads to the following approximation of

$$\frac{1}{1+\frac{M_{\text{tx}}}{\rho T}} = \frac{1}{\frac{\rho T+M_{\text{tx}}}{\rho T}} = \frac{\rho T}{\rho T+M_{\text{tx}}} \underbrace{\approx}_{T>M_{\text{tx}}} 1. \tag{A.5}$$

Making use of this approximation yields

$$\begin{aligned} \hat{\mathbf{\Phi}}_l &= \underset{\mathbf{\Phi}_l\in\{\mathbf{\Phi}_1,\cdots,\mathbf{\Phi}_L\}}{\operatorname{argmax}} \operatorname{tr}\{\mathbf{\Phi}_l^H\mathbf{\Phi}_l\mathbf{Y}^H\mathbf{Y}\} \\ &= \underset{\mathbf{\Phi}_l\in\{\mathbf{\Phi}_1,\cdots,\mathbf{\Phi}_L\}}{\operatorname{argmax}} \operatorname{tr}\{\mathbf{Y}\mathbf{\Phi}_l^H\mathbf{\Phi}_l\mathbf{Y}^H\}. \end{aligned} \tag{A.6}$$

Note, that the trace of a product of matrices is invariant with respect to cyclic permutations of conformable matrices, [27].

The application of

$$\|\mathbf{A}\|_F^2 = \operatorname{tr}\left\{\mathbf{A}^H\mathbf{A}\right\} = \sum_{k=1}^{p}\sum_{l=1}^{q}|a_{kl}|^2, \tag{A.7}$$

where $\|\mathbf{A}\|_F^2$ is the squared Frobenius norm, is possible. For any matrix $\mathbf{A}$ of dimension $p\times q$, the squared Frobenius norm $\|\mathbf{A}\|_F^2$ of $\mathbf{A}$ leads to the same result as taking the trace of the hermitian of the matrix $\mathbf{A}$ times itself ($\operatorname{tr}\left\{\mathbf{A}^H\mathbf{A}\right\}$), resulting in a quadratic matrix of dimension $q\times q$.
Proof:

$$\begin{aligned} \operatorname{tr}\{\mathbf{A}^H\mathbf{A}\} &= \operatorname{tr}\left\{\begin{bmatrix} \sum_{k=1}^{p} a_{1k}^H a_{k1} & \cdots & \sum_{k=1}^{p} a_{1k}^H a_{kq} \\ \vdots & \ddots & \vdots \\ \sum_{k=1}^{p} a_{qk}^H a_{k1} & \cdots & \sum_{k=1}^{p} a_{qk}^H a_{kq} \end{bmatrix}\right\} \\ &= \sum_{k=1}^{p} a_{1k}^H a_{k1} + \cdots + \sum_{k=1}^{p} a_{qk}^H a_{kq} \\ &\underbrace{=}_{a_{1k}^H=a_{k1},\cdots,a_{qk}^H=a_{kq}} a_{11}^2 + \cdots + a_{1k}^2 + \cdots + a_{qk}^2 + \cdots + a_{qp}^2 \end{aligned}$$

$$= \sum_{k=1}^{p}\sum_{l=1}^{q}|a_{kl}|^2$$

$$= \|\mathbf{A}\|_F^2.$$

The ML detection becomes

$$\hat{\mathbf{\Phi}}_l = \underset{\mathbf{\Phi}_l \in \{\mathbf{\Phi}_1,\cdots,\mathbf{\Phi}_L\}}{\operatorname{argmax}} \|\mathbf{Y}\mathbf{\Phi}_l^H\|_F^2,$$

Appendix $\mathcal{B}$

Detection of Subspaces

The matrix variate Θ distribution of a matrix $\mathbf{Y}$ is defined by Gupta and Nagar in [14] and [15]

$$f(\mathbf{Y}) = \frac{1}{\left(2\Gamma\left(1+\frac{1}{\Theta}\right)\right)^{MM}\det(\mathbf{A})^{M}\det(\mathbf{B})^{M}} \exp\left\{-\sum_{i=1}^{M}\sum_{j=1}^{M}\left|\sum_{k=1}^{M}\sum_{l=1}^{M}A_{ik}^{-1}(Y_{kl}-E\left[Y_{kl}\right])B_{lj}^{-1}\right|^{\Theta}\right\}. \tag{B.1}$$

$\mathbf{Y}$ is the $M \times M$ receive matrix and $\mathbf{A}$ and $\mathbf{B}$ are constant and nonsingular $M \times M$ matrices. The definitions for them will follow within this section. For $\Theta = 2$, the PDF in Eq. (B.1) is the matrix variate normal distribution and [15] states for this case, that

$$\Gamma\left(1 + \frac{1}{2}\right) = \frac{1}{2}\sqrt{\pi}. \tag{B.2}$$

The term within the exponential function could be rewritten

$$\begin{aligned} &\sum_{i=1}^{M}\sum_{j=1}^{M}\left|\sum_{k=1}^{M}\sum_{l=1}^{M} A_{ik}^{-1}(Y_{kl} - E\left[Y_{kl}\right])B_{lj}^{-1}\right|^2 \\ &= \operatorname{tr}\left(\left(\mathbf{A}^{-1}(\mathbf{Y} - E\left[\mathbf{Y}\right])\mathbf{B}^{-1}\right)\left(\mathbf{A}^{-1}(\mathbf{Y} - E\left[\mathbf{Y}\right])\mathbf{B}^{-1}\right)^H\right), \end{aligned} \tag{B.3}$$

due to the properties, that the inner double sum corresponds to a matrix multiplication and the outer double sum corresponds to the squared Frobenius norm. The definition of the squared Frobenius norm is

$$\|\mathbf{X}\|_F^2 = \sum_{i=1}^{m}\sum_{j=1}^{n}|x_{ij}|^2 = \operatorname{tr}(\mathbf{X}\mathbf{X}^H)$$

for any $m \times n$ matrix $\mathbf{X}$, where x_{ij} denote the single elements of the matrix. Inserting $\Theta = 2$, Eq. (B.2) and Eq. (B.3) into Eq. (B.1), leads to

$$\begin{aligned} f(\mathbf{Y}) &= \frac{1}{(\pi)^{\frac{MM}{2}}\det(\mathbf{A})^M\det(\mathbf{B})^M} \\ &\qquad \exp\left\{-\operatorname{tr}\left[\left(\mathbf{A}^{-1}(\mathbf{Y} - E\left[\mathbf{Y}\right])\mathbf{B}^{-1}\right)\left(\mathbf{A}^{-1}(\mathbf{Y} - E\left[\mathbf{Y}\right])\mathbf{B}^{-1}\right)^H\right]\right\} \\ &= \frac{1}{(\pi)^{\frac{MM}{2}}\det(\mathbf{A})^M\det(\mathbf{B})^M} \\ &\qquad \exp\left\{-\operatorname{tr}\left[\left(\mathbf{A}^{-1}(\mathbf{Y} - E\left[\mathbf{Y}\right])\mathbf{B}^{-1}\right)\right.\right. \\ &\qquad\qquad \left.\left.\left((\mathbf{B}^{(-1)})^H(\mathbf{Y} - E\left[\mathbf{Y}\right])^H(\mathbf{A}^{-1})^H\right)\right]\right\} \\ &= \frac{1}{(\pi)^{\frac{MM}{2}}\det(\mathbf{A})^M\det(\mathbf{B})^M} \\ &\qquad \exp\left\{-\operatorname{tr}\left[\mathbf{A}^{-1}(\mathbf{Y} - E\left[\mathbf{Y}\right])(\mathbf{B}^{-1}(\mathbf{B}^{(-1)})^H\right)\right. \end{aligned}$$

$$
\begin{aligned}
& (\mathbf{Y} - E[\mathbf{Y}])^H (\mathbf{A}^{-1})^H \big] \big\} \\
= \quad & \frac{1}{(\pi)^{\frac{MM}{2}} \det(\mathbf{A})^M \det(\mathbf{B})^M} \\
& \exp\left\{ -\mathrm{tr}\left[\mathbf{A}^{-1} (\mathbf{Y} - E[\mathbf{Y}]) (\mathbf{B}^H \mathbf{B})^{-1} (\mathbf{Y} - E[\mathbf{Y}])^H (\mathbf{A}^{-1})^H \right] \right\}.
\end{aligned}
$$

So far we made us of mathematical applications of properties of the Hermitian and the inverse of a matrix, [1] and [6]. Since the trace of a matrix is invariant with respect to cyclic matrix permutations of conformable matrices [27], the $M \times M$ matrices for the present case can be rearranged

$$
\begin{aligned}
f(\mathbf{Y}) \quad = \quad & \frac{1}{(\pi)^{\frac{MM}{2}} \det(\mathbf{A})^M \det(\mathbf{B})^M} \\
& \exp\left\{ -\mathrm{tr}\left[(\mathbf{Y} - E[\mathbf{Y}])^H \mathbf{A}^{-1} (\mathbf{A}^{-1})^H (\mathbf{Y} - E[\mathbf{Y}]) (\mathbf{B}^H \mathbf{B})^{-1} \right] \right\} \\
= \quad & \frac{1}{(\pi)^{\frac{MM}{2}} \det(\mathbf{A})^M \det(\mathbf{B})^M} \\
& \exp\left\{ -\mathrm{tr}\left[(\mathbf{Y} - E[\mathbf{Y}])^H (\mathbf{A}\mathbf{A}^H)^{-1} (\mathbf{Y} - E[\mathbf{Y}]) (\mathbf{B}^H \mathbf{B})^{-1} \right] \right\}.
\end{aligned}
$$

Following the derivations in [15], we can now define positive definite $M \times M$ matrices $\mathbf{\Phi} = \mathbf{B}^H \mathbf{B}$ and $\mathbf{\Sigma} = \mathbf{A}\mathbf{A}^H$, such that $\mathbf{A} = \mathbf{\Sigma}^{\frac{1}{2}}$ and $\mathbf{B} = \mathbf{\Phi}^{\frac{1}{2}}$.

$$
\begin{aligned}
f(\mathbf{Y}|E[\mathbf{Y}], \mathbf{\Sigma}, \mathbf{\Phi}) \quad = \quad & \frac{1}{(\pi)^{\frac{MM}{2}} \det(\mathbf{\Sigma})^{\frac{M}{2}} \det(\mathbf{\Phi})^{\frac{M}{2}}} \\
& \exp\left\{ -\mathrm{tr}\left[(\mathbf{Y} - E[\mathbf{Y}])^H \mathbf{\Sigma}^{-1} (\mathbf{Y} - E[\mathbf{Y}]) \mathbf{\Phi}^{-1} \right] \right\}
\end{aligned} \tag{B.4}
$$

The matrix-valued transmission model Eq. (2.19) is

$$
\mathbf{Y} = \mathbf{H}\mathbf{X} + \mathbf{N},
$$

where the diagonal entries of the channel matrix $\mathbf{H}$ contain the fading coefficients in the frequency domain. For a finite set of equiprobable transmit matrices $\mathbf{X}$, the mean of the received matrix $\mathbf{Y}$ is the expected value of $\mathbf{Y}$, i.e. $\mathbf{E}[\mathbf{Y}]$, and it is defined by

$$
E[\mathbf{Y}] = E[\mathbf{H}\mathbf{X} + \mathbf{N}] = E[\mathbf{H}]E[\mathbf{X}] + E[\mathbf{N}] = E[\mathbf{H}]\mathbf{X} + E[\mathbf{N}].
$$

The complex-valued additive white Gaussian noise has zero mean and two sided noise power spectral density of $\frac{N_0}{2}$ and the complex-valued fading coefficients in case of a Rayleigh block fading channel or Rayleigh frequency selective fading channel, respectively, are normal distributed with mean μ_h and variance σ_h^2.

Gupta and Varga state in [14] and [15], that $\mathbf{\Sigma} \otimes \mathbf{\Phi}$, is a covariance matrix, where $\otimes$ denotes the Kronecker product between the matrices $\mathbf{\Sigma}$ and $\mathbf{\Phi}$. $\mathbf{\Sigma}$ denotes the amongst row covariance matrix and $\mathbf{\Phi}$ the amongst column covariance matrix, see [10] and therefore it is possible to calculate them by

$$\mathbf{\Sigma} = E\left[(\mathbf{Y} - E[\mathbf{Y}])(\mathbf{Y} - E[\mathbf{Y}])^H\right] \tag{B.5}$$

$$\mathbf{\Phi} = E\left[(\mathbf{Y} - E[\mathbf{Y}])^H(\mathbf{Y} - E[\mathbf{Y}])\right] \tag{B.6}$$

The lemmas we used for the derivation of $\mathbf{\Sigma}$ and $\mathbf{\Phi}$ can be found amongst others in [13] and [22]. The amongst row covariance matrix becomes

$$\begin{aligned}
\mathbf{\Sigma} &= E\left[(\mathbf{Y} - E[\mathbf{Y}])(\mathbf{Y} - E[\mathbf{Y}])^H\right] \\
&= E\left[(\mathbf{HX} + \mathbf{N} - E[\mathbf{H}]\mathbf{X} - \underbrace{E[\mathbf{N}]}_{=0})(\mathbf{HX} + \mathbf{N} - E[\mathbf{H}]\mathbf{X} - \underbrace{E[\mathbf{N}]}_{=0})^H\right] \\
&= E\left[(\mathbf{HX} + \mathbf{N} - E[\mathbf{H}]\mathbf{X})(\mathbf{X}^H\mathbf{H}^H + \mathbf{N}^H - \mathbf{X}^H E[\mathbf{H}]^H)\right] \\
&= \underbrace{E\left[\mathbf{HX}\mathbf{X}^H\mathbf{H}^H\right]}_{\substack{= E[\mathbf{HX}(\mathbf{HX})^H] \\ = E[|\mathbf{HX}|^2] \\ = E[|H|^2]E[|X|^2] \\ = \sigma_h^2 \frac{E_s}{M}\mathbf{I}}} + \underbrace{E\left[\mathbf{HX}\mathbf{N}^H\right]}_{\substack{= E[\mathbf{HX}]E[\mathbf{N}] \\ = 0}} - E\left[\mathbf{HX}\mathbf{X}^H E[\mathbf{H}]^H\right] \\
&\quad + E\left[\mathbf{N}\mathbf{X}^H\mathbf{H}^H\right] + \underbrace{E\left[\mathbf{N}\mathbf{N}^H\right]}_{= \sigma_n^2\mathbf{I}} - E\left[\mathbf{N}\mathbf{X}^H E[\mathbf{H}]^H\right] - E\left[E[\mathbf{H}]\mathbf{X}\mathbf{X}^H\mathbf{H}^H\right] \\
&\quad - E\left[E[\mathbf{H}]\mathbf{X}\mathbf{N}^H\right] + E\left[E[\mathbf{H}]\mathbf{X}\mathbf{X}^H E[\mathbf{H}]^H\right] \\
&= \left[\frac{E_s}{M}\sigma_h^2 + \sigma_n^2\right]\mathbf{I} - E\left[\mathbf{HX}\mathbf{X}^H E[\mathbf{H}^H]\right] - E\left[E[\mathbf{H}]\mathbf{X}\mathbf{X}^H\mathbf{H}^H\right]
\end{aligned}$$

$$
\begin{aligned}
&+ \underbrace{E\left[E[\mathbf{H}]\mathbf{X}\mathbf{X}^H E[\mathbf{H}]^H\right]}_{\substack{= E[E[\mathbf{H}]]E[\mathbf{X}\mathbf{X}^H]E[E[\mathbf{H}^H]] \\ = \mu_h \mathbf{I} E[\mathbf{X}\mathbf{X}^H]\mu_h \mathbf{I} \\ = \mu_h^2 \frac{E_s}{M}\mathbf{I}}} \\
= &\left[\frac{E_s}{M}\sigma_h^2 + \sigma_n^2 - \mu_h^2\frac{E_s}{M}\right]\mathbf{I} \\
= &\left[\frac{E_s}{M}(\sigma_h^2 - \mu_h^2) + \sigma_n^2\right]\mathbf{I}. \qquad \text{(B.7)}
\end{aligned}
$$

Note that $E[\mathbf{X}\mathbf{X}^H]$ is equal to the symbol energy E_s divided by the FSK block size M, i.e. it is the average energy per subcarrier within an FSK block of size M.

The amongst column covariance matrix $\mathbf{\Phi}$ is defined by

$$
\begin{aligned}
\mathbf{\Phi} &= E\left[(\mathbf{Y} - E[\mathbf{Y}])^H(\mathbf{Y} - E[\mathbf{Y}])\right] \\
&= E\left[(\mathbf{H}\mathbf{X} + \mathbf{N} - E[\mathbf{H}]\mathbf{X} - \underbrace{E[\mathbf{N}]}_{=0})^H(\mathbf{H}\mathbf{X} + \mathbf{N} - E[\mathbf{H}]\mathbf{X} - \underbrace{E[\mathbf{N}]}_{=0})\right] \\
&= E\left[(\mathbf{X}^H\mathbf{H}^H + \mathbf{N}^H - \mathbf{X}^H E[\mathbf{H}]^H)(\mathbf{H}\mathbf{X} + \mathbf{N} - E[\mathbf{H}]\mathbf{X})\right] \\
&= E\left[\mathbf{X}^H\mathbf{H}^H\mathbf{H}\mathbf{X}\right] + E\left[\mathbf{X}^H\mathbf{H}^H\mathbf{N}\right] - E\left[\mathbf{X}^H\mathbf{H}^H E[\mathbf{H}]\mathbf{X}\right] + E\left[\mathbf{N}^H\mathbf{H}\mathbf{X}\right] \\
&\quad + E\left[\mathbf{N}^H\mathbf{N}\right] - E\left[\mathbf{N}^H E[\mathbf{H}]\mathbf{X}\right] - E\left[\mathbf{X}^H E[\mathbf{H}]^H\mathbf{H}\mathbf{X}\right] \\
&\quad - E\left[\mathbf{X}^H E[\mathbf{H}]^H\mathbf{N}\right] + E\left[\mathbf{X}^H E[\mathbf{H}]^H E[\mathbf{H}]\mathbf{X}\right] \\
&= \mathbf{X}^H\mathbf{\Lambda}_h\mathbf{X} + \sigma_n^2\mathbf{I} - \mu_h^2\mathbf{X}^H\mathbf{X}, \qquad \text{(B.8)}
\end{aligned}
$$

where $\mathbf{\Lambda}_h$ denotes the covariance matrix of the channel.

The conditional matrix variate PDF for maximum-likelihood detection for a received matrix $\mathbf{Y}$, given a transmitted matrix $\mathbf{X}$, is

$$
p(\mathbf{Y}|\mathbf{X}) = \frac{1}{(\pi)^{\frac{MM}{2}}\det(\mathbf{\Sigma})^{\frac{M}{2}}\det(\mathbf{\Phi})^{\frac{M}{2}}}\exp\left\{-\mathrm{tr}\left[\mathbf{Y}^H\mathbf{\Sigma}^{-1}\mathbf{Y}\mathbf{\Phi}^{-1}\right]\right\}. \qquad \text{(B.9)}
$$

Appendix C

List of Frequently Used Acronyms, Operators and Symbols

Acronyms

AA-LP	anti aliasing lowpass filter
ASK	amplitude shift keying
AWGN	additive white Gaussian noise
BCJR	Bahl, Cocke, Jelinek and Raviv

BER	bit error rate
BICM	bit-interleaved coded modulation
BICM-ID	BICM with iterative detection
BIC-OFDM	bit-interleaved coded OFDM
CDMA	code division multiple access
CSI	channel state information
DAB	digital audio broadcasting
DET	detection
DFT	discrete Fourier transform
DVB-T	digital video broadcasting - terrestrial
FDM	frequency division multiplexing
FFT	fast Fourier transform
IDFT	inverse discrete Fourier transform
IP-LP	interpolation lowpass filter
LLR	log likelihood ratio
LTE	long term evolution
LTI	linear time invariant
MAP	mapper
ML	maximum likelihood
MFSK	M-ary Frequency Shift Keying
MIMO	multiple input multiple output
OFDM	Orthogonal Frequency Division Multiplexing
OFDM-MFSK	OFDM and MFSK
OFDM-N/MFSK	OFDM multitone FSK
OFDM-COM-N/MFSK	OFDM combined N/MFSK
PDF	probability density function
P/S	parallel to serial conversion
QAM	quadrature amplitude modulation
SISO	single input single output
SNR	signal-to-noise ratio
S/P	serial to parallel conversion

TDM	time division multiplexing
WLAN	wireless local area network

Operators

$\mathbf{A}^*$	complex conjugate of the matrix $\mathbf{A}$
$\mathbf{A}^{\mathrm{H}}$	complex conjugate transpose of the matrix $\mathbf{A}$
$\mathbf{A}^{\mathrm{T}}$	transpose of the matrix $\mathbf{A}$
$\mathbf{A}^{-1}$	inverse of the matrix $\mathbf{A}$
$[\mathbf{A}]_{mn}$	the mn-th entry of a matrix $\mathbf{A}$
$\lvert \cdot \rvert$	absolute value
$\det(\mathbf{A})$	determinant of the matrix $\mathbf{A}$
$\mathrm{diag}(\mathbf{x})$	transform the vector $\mathbf{x}$ into a diagonal matrix $\mathbf{X}$
$E[\cdot]$	expected value
exp(x)	exponential function of argument x
$\in$	element of a set or a field
$\lfloor \cdot \rfloor$	floor function, largest integer smaller or equal than the argument
$\otimes$	Kronecker product
$\leq$	less or equal
log	logarithm
$\arg\max_k p(k)$	value of k, that maximizes p
$\lVert \cdot \rVert$	norm
$\lVert \cdot \rVert_F^2$	squared Frobenius norm
$\mathbf{u}^T\mathbf{v}$	scalar product between two column vectors $\mathbf{u}$ and $\mathbf{v}$
$\sum_{k=1}^{n} a_k$	sum of elements a_k, $k = 1, \ldots, n$
$\mathrm{tr}(\mathbf{A})$	trace of matrix $\mathbf{A}$
$\mathcal{A} \cup \mathcal{B}$	union of two sets $\mathcal{A}$ and $\mathcal{B}$

Symbols

$\mathbf{1}$	all ones matrix
A	transmit vector or transmit matrix alphabet
$\mathbb{C}$	set of complex-valued numbers
δ	Kronecker delta

E_b	average energy per transmitted bit
E_s	symbol energy
$\mathbf{\Sigma}$	among row covariance matrix
f_c	carrier frequency
f_Δ	subcarrier spacing
f_k	k-th subcarrier frequency
$g(t)$	received signal
$h(\tau, t)$	time-variant channel impulse response
H	channel transfer function
$\lvert H \rvert$	absolute value of the transfer function H
$\mathbf{H}$	channel matrix
$\mathbf{I}$	identity matrix, size according to context
$\mathbf{\Lambda}$	covariance matrix
$\mathbf{\Lambda}_h$	covariance matrix of the channel
M	FSK block size
M_{tx}	number of transmit antennas
m	number of transmitted bits per transmit symbol/vector/matrix
N	number of active subcarriers per FSK block of size M
N_0	noise power spectral density
$\mathbf{N}$	AWGN matrix
N_f	number of subcarriers of an OFDM transmission system
N_g	number of subcarriers for guard interval
N_{rx}	number of receive antennas
$n(t)$	additive white Gaussian noise process in time-domain
$\mathbf{n}$	noise vector
η	bandwidth efficiency
$\mathbf{\Phi}$	unitary transmit matrix, or among column covariance matrix
φ	phase
$q(k)$	digital source bits
$\mathbb{R}$	set of real-valued numbers
r_c	code rate

ρ	expected SNR at each receiver antenna
$s(t)$	transmit signal
σ^2	variance
σ_h^2	variance of the channel
σ_n^2	noise variance
T	number of time-slots
T_G	duration of the guard interval
t	absolute time
τ	delay time
μ	mean value
$\mathbf{X}$	transmit matrix
$\mathbf{x}$	transmit vector
$\mathbf{Y}$	receive matrix
$\mathbf{y}$	receive vector

Bibliography

[1] *Teubner-Taschenbuch der Mathematik Teil II*. Stuttgart, Leipzig: Teubner, 1995. ISBN 3-8154-2100-4.

[2] A. Ashikhmin and A. R. Calderbank. Grassmannian packings from operator reed-muller codes. *Information Theory, IEEE Transactions on*, 56(11):5689–5714, November 2010.

[3] L.R. Bahl, J. Cocke, F. Jelinek, and J. Raviv. Optimal decoding of linear codes for minimizing symbol error rate. *Information Theory, IEEE Transactions on*, 20:284–287, March 1974.

[4] J. A. C. Bingham. Multicarrier modulation for data transmission: an idea whose time has come. *Communications Magazine, IEEE*, 48(5):5–14, May 1990.

[5] M. Bossert. *Channel Coding for Telecommunications*. John Wiley & Sons Ltd, 1999.

[6] I. N. Bronstein, K. A. Semendjajew, G. Musiol, and H. Mühlig. *Taschenbuch der Mathematik*. Frankfurt am Main: Harri Deutsch, 1995. ISBN 3-8171-2002-8.

[7] C. Caire, G. Taricco, and E. Biglieri. Bit-interleaved coded modulation. *Information Theory, IEEE Transactions on*, 44(3):927–946, May 1998.

[8] T. Clevron and P. Vary. Iterative decoding of bicm with non-regular signal constellation sets. In *5th International ITG Conference on Source and Channel Coding (SCC 2004)*, volume 2, Erlangen, Germany, January 2004.

[9] D. Divsalar and M. K. Simon. Maximum-likelihood differential detection of uncoded and trellis coded amplitude phase modulation over awgn and fading channels-metrics and performance. *Communications, Transactions on*, 42(1):76–89, January 1994.

[10] P. Dutilleul. The mle algorithm for the matrix normal distribution. *Statistical Computation and Simulation, Journal of*, 64:105–123, 1999.

[11] A. Engelhart. *Vector Detection Techniques with Moderate Complexity.* PhD thesis, Ulm University, 2003. ISBN 3-18-372410-3.

[12] G. H. Golub and C. F. van Loan. *Matrix Computations.* The John Hopkins University Press, 1996. ISBN 0-8018-5414-8.

[13] R. M. Gray. *Probability, Random Processes, and Ergodic Processes.* Springer Verlag, 2009. ISBN 978-1441910899.

[14] A. K. Gupta and D. K. Nagar. *Matrix Variate Distributions.* Chapman & Hall/Crc, 2000. ISBN 1-58488-046-5.

[15] A. K. Gupta and T. Varga. Matrix variate θ-generalized normal distribution. *American Mathematical Society, Transactions of*, 347(4):1429–1437, April 1995.

[16] J. Hagenauer, E. Offer, and L.Papke. Iterative decoding of binary block and convolutional codes. *Information Theory, IEEE Transactions on*, 42(2):429–445, March 1996.

[17] P. Henkel. Extended mappings for bit-interleaved coded modulation. In *IEEE 17th International Symposium on Personal, Indoor and Mobile Radio Communications (PIMRC'06)*, Helsinki, Finland, September 2006.

[18] B. M. Hochwald and T. L. Marzetta. Capacity of a mobile multiple-antenna communication link in rayleigh flat fading. *Information Theory, IEEE Transactions on*, 45(1):139–157, January 1999.

[19] B. M. Hochwald and T. L. Marzetta. Unitary space-time modulation for multiple-antenna communications in rayleigh flat fading. *Information Theory, IEEE Transactions on*, 46(2):543–564, March 2000.

[20] K. Jänich. *Lineare Algebra*. Springer Lehrbuch, 11th edition, 2008. ISBN 978-3-540-75501-2.

[21] S. M. Kay. *Fundamentals of Statistical Signal Processing - Estimation Theory*. Prentice Hall PTR, 1993. ISBN 0-13-345711-7.

[22] S. M. Kay. *Intuitive Probability and Random Processes Using MATLAB*. Springer, 2006. ISBN 978-0-387-24157-9.

[23] X. Li and J. A. Ritcey. Bit-interleaved coded modulation with iterative decoding. *IEEE Communication Letters*, 1(6):169–171, November 1997.

[24] J. Lindner. *Informationsübertragung. Grundlagen der Kommunikationstechnik*. Springer, Berlin, first edition, 2004. ISBN 3540214003.

[25] A. Linduska, M. Wetz, W. G. Teich, and J. Lindner. Analysis of ofdm multitone fsk schemes in frequency selective fast fading channels. In *9th International Symposium on Communication Theory and Applications (ISCTA)*, Ambleside, England, July 2009.

[26] M. Médard and R. G. Gallager. Bandwidth scaling for fading multipath channels. *Information Theory, IEEE Transactions on*, 48(4):840–852, April 2002.

[27] C. Meyer. *Matrix Analysis and Applied Linear Algebra*. Society for Industrial and Applied Mathematics, 2000. ISBN 978-0898714548.

[28] E. Peiker, G. Yammine, W. G. Teich, and J. Lindner. Increasing the bandwidth efficiency of ofdm-n/mfsk. In *Proc. 18th International OFDM Workshop 2014 (InOWo'14)*, Essen, Germany, August 2014.

[29] E. Peiker-Feil, M. Wetz, W. G. Teich, and J. Lindner. Ofdm-mfsk as a special case of noncoherent communication based on subspaces. In *Proc. 17th International OFDM Workshop 2012 (InOWo'12)*, pages 1–5, Essen, Germany, August 2012.

[30] A. Peled and A. Ruiz. Frequency domain data transmission using reduced computational complexity algorithms. In *Acoustic, Speech, and Signal Processing, IEEE International Conference on ICASSP '80*, volume 5, pages 964–967, April 1980.

[31] J. G. Proakis. *Digital Communications*. New York, McGraw-Hill Book Company, third edition, 1995. ISBN 0-07-051726-6.

[32] J. G. Proakis and M. Salehi. *Communication Systems Engineering*. Prentice Hall, second edition, 2002. ISBN 0-13-061793-8.

[33] J. G. Proakis, M. Salehi, and G. Bauch. *Modern Communication Systems Using MATLAB®*. Cengage Learning, third edition, 2013, 2004. ISBN-13 978-1-111-99017-6.

[34] M. Russel and G. L. Stüber. Interchannel interference analysis of ofdm in a mobile environment. In *Vehicular Technology Conference, 1995 IEEE 45th*, volume 2, pages 820–824, Chicago, IL, July 1995.

[35] F. Schreckenbach, N. Gortz, J. Hagenauer, and G. Bauch. Optimization of symbol mappings for bit-interleaved coded modulation with iterative decoding. *Communications Letter, IEEE*, 7(12):593–595, December 2003.

[36] G. F. Simmons. *Topology and Modern Analysis*. McGraw-Hill BOOK COMPANY, INC., 1963.

[37] T. Söderström and P. Stoica. *System Identification*. Prentice Hall, 1995. ISBN 0-13-881236-5.

[38] I. E. Telatar and D. N. C. Tse. Capacity and mutual information of wideband multipath fading channels. *Information Theory, IEEE Transactions on*, 46(4):1384–1400, July 2000.

[39] S. ten Brink. Convergence of iterative decoding. *Electronic Letters*, 35:806–808, May 1999.

[40] S. ten Brink. Designing iterative decoding schemes with the extrinsic information transfer chart. *AEU, International Journal of Electronic Communications*, 54(6):389–398, 2000.

[41] Z. Utkovski. *Non-coherent Communication in Wireless Point-to-Point and Relay Channels: A Geometric Approach*. PhD thesis, Ulm University, 2010. ISBN 978-3-86247-091-4.

[42] R. van Nee and R. Prasad. *OFDM for Wireless Multimedia Communications*. Artech House Publishers, 2000. ISBN 0-89006-530-6.

[43] S. B. Weinstein and P. M. Ebert. Data transmission by frequency-division multiplexing using the discrete fourier transform. *Communications Technology, IEEE Transactions on*, 19(5):628–634, October 1971.

[44] M. Wetz. *Transmission Methods for Wireless Multi Carrier Systems in Time-Varying Environments*. PhD thesis, Ulm University, 2011. ISBN 978-3-86247-201-7.

[45] M. Wetz, I. Periša, W. G. Teich, and J. Lindner. Robust transmission over fast fading channels on the basis of ofdm-mfsk. *Wireless Personal Communications*, 47(1):113–123, October 2008.

[46] G. Yammine, E. Peiker, W.G. Teich, and J. Lindner. Improved performance of coded ofdm-mfsk using combined alphabets and extended mapping. In *8th International Symposium on Turbo Codes and Iterative Informations Processing (ISTC)*, Bremen, Germany, August 2014.

[47] L. Zheng and D. N. C. Tse. Communication on the grassmann manifold: A geometric approach to the noncoherent multiple-antenna channel. *Information Theory, IEEE Transactions on*, 48(2):359–383, February 2002.

Lebenslauf

For the reasons of data privacy, the curriculum vitae has been removed.

For the reasons of data privacy, the curriculum vitae has been removed.

Publikationsliste

- Eva Peiker, Jan Dominicus, Werner G. Teich, Jürgen Lindner: Reduction of Inter-Carrier Interference in OFDM Systems through Application of Windowing in the Receiver. *In Proc. 13th International OFDM Workshop (InOWo'08)*, pp. 133-137, Hamburg, Germany, 27-28 August, 2008.

- Eva Peiker, Jan Dominicus, Werner G. Teich, Jürgen Lindner: Improved Performance of OFDM Systems for Fast Time-Varying Channels. *In Proc. 2nd International Conference on Signal Processing and Communication Systems (ICSPCS)*, Goldcoast, Queensland, Australia, 15-17 December, 2008.

- Eva Peiker, Werner G. Teich, Jürgen Lindner: Windowing in the Receiver for OFDM Systems in High-Mobility Scenarios. *In Proc. Multi-Carrier Systems and Solutions 2009*, pp. 57-65, Herrsching, Germany, May 2009.

- Eva Peiker, Werner G. Teich, Jürgen Lindner: OFDM-MFSK with Windowing in the Rx: A Robust Tx Scheme for Fast Fading Channels. *In Proc. 9th International Symposium on Communication Theory and Applications (ISCTA)*, Ambleside, England, July 2007.

- Eva Peiker, Nicolas Schneckenburger, Werner G. Teich, Jürgen Lindner: Turbo Equalization in OFDM Systems for Fast Fading Channels. *In Proc. 14th International OFDM Workshop (InOWo'09)*, Hamburg, Germany, September 2009.

- Eva Peiker-Feil, Nicolas Schneckenburger, Werner G. Teich, Jürgen Lindner: Improving SC-FDMA Performance by Time Domain Equalization for UTRA LTE Uplink. *In Proc. 15th International OFDM Workshop (InOWo'10)*, Hamburg, Germany, September 2010.

- Nardine Farah, Eva Peiker-Feil, Werner G. Teich, Jürgen Lindner: Comparison of CDD and MC-CAFS for the MIMO-OFDM DL in LTE. *In Proc. 16th International OFDM Workshop (InOWo'11)*, Hamburg, Germany, August/September 2011.

- Eva Peiker-Feil, Matthias Wetz, Werner G. Teich, Jürgen Lindner: OFDM-MFSK as a Special Case of Noncoherent Communication Based on Subspaces. *In Proc. 17th International OFDM Workshop (InOWo'12)*, Essen, Germany, August 2012.

- George Yammine, Eva Peiker, Werner G. Teich, Jürgen Lindner: Improved Performance of Coded OFDM-MFSK Using Combined Alphabets and

Extended Mapping. *In Proc. 8th International Symposium on Turbo Codes and Iterative Information Provessing (ISTC)*, Bremen, Germany, August 2014.

- Eva Peiker, George Yammine, Werner G. Teich, Jürgen Lindner: Increasing the Bandwidth Efficiency of OFDM-MFSK. *In Proc. 18th International OFDM Workshop (InOWo'14)*, Essen, Germany, August 2014.